

12378
Z
'1996)



This is to certify that the
dissertation entitled
Theoretical Study of Neutron Scattering
from Mott Insulators

presented by

Hyunju Chang

has been accepted towards fulfillment
of the requirements for

Ph.D. degree in Physics

Thomas A. Kaplan S.D. Mahanti
T.A. Kaplan and S.D. Mahanti
Major professor

Date August 25, 1995

**LIBRARY
Michigan State
University**

**PLACE IN RETURN BOX to remove this checkout from your record.
TO AVOID FINES return on or before date due.**

DATE DUE	DATE DUE	DATE DUE
_____	_____	_____
_____	_____	_____
_____	_____	_____
_____	_____	_____
_____	_____	_____
_____	_____	_____
_____	_____	_____

ABSTRACT

THEORETICAL STUDY OF NEUTRON SCATTERING FROM MOTT INSULATORS

By

Hyunju Chang

Even though many theoretical works have been done in La_2CuO_4 and $\text{YBa}_2\text{Cu}_3\text{O}_6$, the insulating parents of the high- T_c superconductors, there is no satisfactory theory to describe the low-temperature neutron scattering experiments in these materials. This dissertation addresses our theoretical study of the neutron scattering of the copper compounds, La_2CuO_4 , $\text{YBa}_2\text{Cu}_3\text{O}_6$ and $\text{Sr}_2\text{CuO}_2\text{Cl}_2$, and the related nickel compounds, La_2NiO_4 , KNiF_3 , and NiO .

We develop a theory of the spin density which incorporates quantum spin fluctuations (QSF) and covalence effects (COV) simultaneously. We found the spin density, to a good approximation, to be a product of a site spin expectation value which incorporates QSF and a form factor which takes COV into account. The ordered moment is also defined from the spin density, and is found to be affected by both the QSF and COV.

We have calculated the magnetic form factor with various theoretical tools and the calculated form factors are compared with experiments.

As a simple procedure to obtain the form factor for La_2NiO_4 , we follow the model which was developed by Hubbard and Marshall. The Hubbard and Marshall procedure failed to explain the observed large covalence in La_2NiO_4 .

We have carried out *ab initio* cluster calculations of the form factor in a solid using a cluster approximation based on quantum chemistry technique. We have used restricted Hartree-Fock (RHF) and unrestricted Hartree-Fock (UHF) procedures with correlation corrections via a restricted multi-configuration self-consistent-field (MCSCF) approach to obtain the ground state cluster wave functions needed in the neutron form factor calculations.

We find that the *ab initio* cluster calculations describe the experimental form factor in KNiF_3 and NiO extremely well, but fail badly in La_2NiO_4 . We applied the same method to the cuprate materials, La_2CuO_4 , $\text{YBa}_2\text{Cu}_3\text{O}_6$ and $\text{Sr}_2\text{CuO}_2\text{Cl}_2$. The calculated form factors for these cuprates turn out to agree reasonably well with experiments, although there are other indications that the degree of covalence is underestimated in our calculations.

To My Mother

ACKNOWLEDGEMENTS

I would like to express my deep gratitude to my thesis advisors Professor T. A. Kaplan and Professor S. D. Mahanti for their physical insights to guide me to understand physics during my graduate research years. I greatly appreciate their constant support and the sharing of their enthusiasm for physics with me. I also would like to greatly thank Professor J. F. Harrison for helping me to understand *ab initio* quantum chemistry techniques. I have always considered him as one of my advisors.

I am also grateful to Professors J. Cowen and P. Danielewicz for serving on my guidance committee. I would like to thank Ms. Janet King for making my life in this department so much simpler and easier.

I wish to thank Randy Rencsok and Dr. R. Boehm for helping me to solve the problems encountered in using quantum chemistry computational codes. I also would like to thank all my friends in the department for making my life here more easier and enjoyable. Especially I want to thank Dr. Hyangsuk Seong for being a mentor in my graduate life.

I owe a great debt to my dear husband, Jaeyong Yee. This work could not have been completed without his endless help and encouragement. I also hope this work would be a little reward to my precious daughter, Lily, for the time she had to spend without mommy. I also would like to thank my parents-in-law for their support and encouragement in many ways. Finally, I would like to dedicate this thesis to my dear mother who has been always patient and supportive during my studies.

Financial support from the Natural Science Foundation and the Center for Fundamental Materials Research of MSU, without which this thesis could not have been done, is also greatly acknowledged.

Contents

Abstract	i
Acknowledgments	iv
1 Introduction	1
2 Theory of the spin density in an antiferromagnetic insulator including covalence and quantum spin fluctuations	8
2.1 Introduction	8
2.2 Effective spin hamiltonian	10
2.3 Spin density	13
2.3.1 Formalism	13
2.3.2 Relation to the Hubbard-Marshall theory	18
2.3.3 Correction term from $\mathcal{H}^{(4)}$ using the spin wave approximation	22
2.3.4 Estimation of the correction terms in spin density	24
2.4 Ordered moment	25
2.5 Summary	26
3 Hubbard-Marshall model calculation	28

3.1	Introduction	28
3.2	Hubbard-Marshall theory	29
3.3	Hubbard-Marshall model calculation for La_2NiO_4	34
3.4	Discussion	38
4	Ab initio cluster calculation of neutron scattering form factor	41
4.1	Introduction	41
4.2	General theory of <i>ab initio</i> calculation methods	42
4.2.1	Hartree-Fock(HF) Self-Consistent-Field (SCF) method	43
4.2.2	Beyond the Hartree-Fock approximation	46
4.2.3	Natural orbitals	48
4.3	Theoretical form factor	50
4.4	Cluster and environment	53
4.4.1	Cluster	53
4.4.2	Point charge model	54
4.4.3	Effective core potential(ECP)	54
5	Neutron scattering form factor of the nickel compounds	58
5.1	Introduction	58
5.2	KNiF_3	59
5.2.1	Experimental form factor	60
5.2.2	$(\text{NiF}_6)^{4-}$ cluster	63

5.2.3	Environment	64
5.2.4	Comparison with experiment	65
5.3	NiO	67
5.3.1	Cluster	69
5.3.2	Environment	69
5.3.3	Comparison with experiment	70
5.4	La ₂ NiO ₄	74
5.4.1	Cluster	76
5.4.2	Environment	76
5.4.3	Comparison with experiment	79
5.5	Summary	79
6	Neutron scattering form factor of the cuprate compounds	83
6.1	Introduction	83
6.2	Cu ²⁺ ion	84
6.2.1	Ionic form factor	85
6.3	YBa ₂ Cu ₃ O ₆	88
6.3.1	Cluster	90
6.3.2	Environment	92
6.3.3	Calculated form factor	93
6.3.4	Comparison with experiment	98

6.4	La_2CuO_4	101
6.4.1	Cluster	102
6.4.2	Environment	103
6.4.3	Calculated form factor	103
6.4.4	Comparison with experiment	105
6.5	$\text{Sr}_2\text{CuO}_2\text{Cl}_2$	106
6.5.1	Cluster	108
6.5.2	Environment	108
6.5.3	Comparison with experiment	108
6.6	Conclusions	110
A	Perturbation calculation of the contribution of the 4-spin hamiltonian $\hat{\mathcal{H}}^{(4)}$	113
B	Construction of natural orbitals in MCSCF	117
B.1	Development of programs	118
C	Failure of the Mulliken Charge Population Analysis	122
D	Crystal field splitting in KNiF_3 and NiO	125

List of Tables

5.1	Experimental values of $\langle S_z \rangle f(\bar{q}_M)$ in KNiF_3	62
5.2	Madelung potential value at the origin of the cluster in KNiF_3	64
5.3	Madelung potential value at the origin of the cluster in NiO	69
6.1	Total energies (eV) of various calculations for Cu^{2+} ion	87
6.2	Comparison of total energies (eV) of clusters	96
6.3	Covalence factors obtained from the cluster calculations	110
C.1	Mulliken charge population values for different basis sets for Ni	123
D.1	$10Dq$ values for KNiF_3 and NiO	126

List of Figures

3.1	Orbitals of a linear chain antiferromagnet.	31
3.2	Antiferromagnetically ordered NiO ₂ plane	35
3.3	Schematic diagram of antibonding wave function in NiO ₂ plane . . .	36
3.4	Comparison of Hubbard-Marshall model calculation with the ex- periment for La ₂ NiO ₄	39
4.1	Effective core potentials for La ³⁺	57
5.1	Crystal structure of KNiF ₃	61
5.2	Form factor of KNiF ₃	66
5.3	Crystal structure of NiO	68
5.4	RHF Form Factor of NiO	71
5.5	UHF Form Factor of NiO	72
5.6	Crystal structure of La ₂ NiO ₄ and La ₂ CuO ₄	75
5.7	Form factor of La ₂ NiO ₄ with different ECP environment	78
5.8	Form factor of La ₂ NiO ₄ compared with experiment	80
6.1	Form factor of Cu ²⁺ ion with various calculation methods.	86

6.2	Comparison of form factor of free Cu^{2+} ion, Cu^{2+} ion with point charge distribution, and $(\text{CuO}_5)^{8-}$ cluster form factor	89
6.3	Crystal structure of $\text{YBa}_2\text{Cu}_3\text{O}_6$	91
6.4	Bilayer structure of CuO_2 planes in $\text{YBa}_2\text{Cu}_3\text{O}_6$	94
6.5	Form factor of $\text{YBa}_2\text{Cu}_3\text{O}_6$ with various calculation methods. . .	97
6.6	Comparison of form factor of $\text{YBa}_2\text{Cu}_3\text{O}_6$ with experiment	99
6.7	Form factor of La_2CuO_4 with various calculation methods.	104
6.8	Comparison of form factor of La_2CuO_4 with experiment.	107
6.9	Comparison of form factor of $\text{Sr}_2\text{CuO}_2\text{Cl}_2$ with experiment. . . .	109
B.1	Structure of program sets to construct NO's	121

Chapter 1

Introduction

Since the discovery of high- T_c superconductivity in $\text{La}_{2-x}\text{Sr}_x\text{CuO}_4$ and $\text{YBa}_2\text{Cu}_3\text{O}_{6+x}$, there have been many theoretical and experimental works in La_2CuO_4 and $\text{YBa}_2\text{Cu}_3\text{O}_6$, the insulating parents of the high- T_c superconductors[chak90]. It is widely believed that the electronic structure of these insulators is well understood [chak90]. However there are fundamental problems associated with the interpretation of the low-temperature neutron scattering experiments in these insulating parents as discussed below [kapl91, kapl92, maha93].

Neutron Bragg scattering experiments found the *ordered moment* (to be defined later) to be in the range $0.60 \sim 0.66\mu_B$ [yama87, tran88B, burl88] (this value itself is still controversial as discussed in Chap.6). This result was interpreted [tran88B] in terms of the spin 1/2 antiferromagnetic Heisenberg model for spins on a square net (which corresponds to Cu^{2+} ions (d^9 configuration) sitting at the Cu sites on the CuO_2 planes). It was noted [tran88B] that this result agreed closely with the spin wave theory, and the large reduction from the nominal $1.1\mu_B$ (taking $g = 2.2$) is due to quantum spin fluctuations [ande52]. The excellent

agreement with the spin wave theory was taken [tran88B] to signify negligible contribution of covalence to the reduction of the ordered moment (the existence of this covalent reduction had been noted by Hubbard and Marshall many years ago [hubb65]). Moreover, recent Monte Carlo calculations [rege88, gros89] agree with the spin wave result, thereby reinforcing the idea of small covalent reduction of the antiferromagnetic moment discussed above. The conclusion of negligible covalence was recently questioned[kapl91] since these oxides are expected to have extremely large covalence. The latter view was supported by a recent neutron diffraction experiment in La_2NiO_4 , (structurally same as La_2CuO_4), which apparently showed a very large covalent contribution to the form factor with a covalent reduction of the ordered moment by $\sim 50\%$! [wang91, wang92] The obvious intuitive notion that *both* effects, spin fluctuations and covalence, should contribute to the reduction of the ordered moment clearly leads to a contradiction in the cuprates.

Previous theories considered spin fluctuations without covalence, or covalence without spin fluctuations, whereas these two should be treated simultaneously. Here, in this work we consider these two effects simultaneously via the 1-band Hubbard model in the $\frac{1}{2}$ -filled narrow band regime. In particular, we calculate the neutron scattering cross section, that is a measurable quantity experimentally, allowing a unified theory of these two effects on the ordered moment[kapl92].

As a consequence of this theory, we [kapl92] were able to detect two errors in the interpretation [tran88B] of the neutron scattering data. The interpretational errors made by the experimentalists [tran88B] are (i) they interpreted the site spin incorrectly as the ordered moment rather than the site spin in the Heisenberg model ground state and (ii) they used the form factor of K_2CuF_4 to substitute for that of the cuprate materials ; since K_2CuF_4 is a *ferromagnet*, its form factor

contains no momentum reduction which is expected in an *antiferromagnet*. In order to resolve this situation, we have decided to calculate the form factor.

As a simple procedure to obtain the form factor, we follow the model calculation which was developed by Hubbard and Marshall [hubb65] for La_2NiO_4 . The Hubbard and Marshall procedure failed to explain the data in La_2NiO_4 . This motivated us to carry out a proper calculation of the form factor using an *ab initio* cluster method based on quantum chemistry techniques. As far as we know, it is the first time modern quantum chemistry methods have been used to calculate the form factor in a solid. In order to justify the adequacy of the method, we have carried out the cluster calculation for several Mott insulators including the insulating parents of the high T_C superconductors. The *ab initio* cluster calculation method describes the experimental form factor in KNiF_3 and NiO extremely well. It is noted that this is the first satisfactory *ab initio* calculation of the form factor in KNiF_3 and NiO . However the same cluster method fails badly in La_2NiO_4 [chan94, kapl94]

We applied the same method to the cuprate materials, La_2CuO_4 , $\text{YBa}_2\text{Cu}_3\text{O}_6$ and $\text{Sr}_2\text{CuO}_2\text{Cl}_2$, which we were originally interested in. The calculated form factor for these cuprates turns out to agree reasonably with experiments.

The organization and the basic results of this thesis are as follows. First, in Chapter 2, we describe our theory of the spin density which incorporates quantum spin fluctuations and covalence effect simultaneously [kapl91, kapl92]. We work with the 1-band Hubbard hamiltonian for the 1/2-filled regime and formulate the expectation value of the spin density in the ground state using a perturbation theory. The spin density is found to be a product of a site spin expectation value

i
n
th
tw
pri
ing

and the form factor, plus some correction terms. We calculate the correction terms and show they are negligible for the type of the materials being considered. Thus the spin density is a simple product of the site spin and the form factor. The site spin expectation value is calculated from the Heisenberg spin hamiltonian, which includes quantum spin fluctuations but no covalence, and the form factor includes the covalence effect but no quantum spin fluctuations. The ordered moment is defined from the expectation value of the spin density, and is affected by both quantum spin fluctuations and covalence. The expectation value the of site spin can be estimated by the spin wave approximation[ande52], which agrees with recent Monte Carlo calculations[rege88, gros89]. The reduction from its mean field value is about 40% (caused by quantum spin fluctuations only). The rest of this dissertation is concerned with calculating the form factor to investigate the covalence effect.

In Chapter 3, we calculate the form factor for La_2NiO_4 using Hubbard-Marshall(HM) theory [hubb65]. The experimental form factor of La_2NiO_4 shows about 50% reduction in the ordered moment which was claimed to be due to the covalence in the form factor by Wang et. al.[wang91]. The HM analysis of the ordered moment was first tried by Wang et. al. [wang91] to understand their experiment. In the HM model, the wave function is a linear combination of the ionic orbitals of one magnetic ion and neighboring ligands of the system. The moment in the Ni^{2+} ion comes from the triple state where two d electrons are in the e_g state and have parallel spins. The choice of the same wave function for the two parallel spin electrons (made by Wang et. al. [wang91]) violates the Pauli principle. Hence we decided to calculate the form factor with a physically meaningful choice of the wave function in the e_g states in Ni^{2+} . Our results disagreed

with experiment and moreover they were spoiling the excellent agreement that had been obtained with that unjustified model by Wang et. al.'s. Wang et. al [wang92] also came to a similar conclusion in their later work. We were therefore led to find more accurate methods, namely *ab initio* cluster methods based on the Hartree-Fock (HF) self-consistent-field (SCF) technique, with correlation corrections to calculate the form factor.

We introduce the *ab initio* cluster method in Chapter 4. First we review the general concepts of the Hartree-Fock (HF) self-consistent-field (SCF) method. Then we introduce the configuration interaction (CI) and multi-configuration self-consistent-field (MCSCF) methods to include the correlation effects (which go beyond the HF method). We derive expressions for the form factor within HF or MCSCF approximations. We then describe our cluster approach and how we treat the environment outside the cluster.

In Chapter 5, we describe the cluster calculations and results for the nickel compounds, KNiF_3 , NiO , and La_2NiO_4 [chan94, kapl94]. First we apply our cluster method to a rather simple antiferromagnet, KNiF_3 by choosing the $(\text{NiF}_6)^{4-}$ cluster. The ground state wave function of this cluster is calculated using the restricted Hartree-Fock (RHF) and unrestricted Hartree-Fock (UHF) approximations. The calculated UHF form factor for KNiF_3 agrees very well with the experiment. Moreover we could estimate the quantum spin fluctuations quantitatively by comparing our calculation with the experiment, where the absolute value of the intensities of the Bragg peaks are available. The site spin expectation value, obtained from the experiment using our theoretical form factor, agrees very well with the value obtained using the spin wave approximation to the Heisenberg model.

We then apply the RHF and UHF method to NiO taking $(\text{NiO}_6)^{10-}$ as a basic cluster. The calculated form factor agrees with the experiment [alpe61] with some small corrections from orbital contribution. Unfortunately absolute experimental values are not available in NiO, hence we could not determine the site spin value. However the very complicated shape of the form factor agrees very well with the experiment over the whole range of scattering vectors, \vec{q} studied in the experiment, giving further support to the accuracy of our procedure to obtain the ground state wave function. We apply the same method to La_2NiO_4 where the experiment showed the large covalence. But our cluster method is in seriously disagreement with the observed form factor in La_2NiO_4 .

In Chapter 6, we address the calculation of the form factor in La_2CuO_4 , $\text{Sr}_2\text{CuO}_2\text{Cl}_2$, and $\text{YBa}_2\text{Cu}_3\text{O}_6$ taking clusters, $(\text{CuO}_6)^{10-}$, $(\text{CuO}_4\text{Cl}_2)^{8-}$ and $(\text{CuO}_5)^{8-}$, respectively. We show the results of RHF and UHF calculations. We found that the calculated form factor *shape* agrees reasonably well with the experiments. Especially, within a family of \vec{q} values characterized by increasing only q_z , the slope of $f(\vec{q})$ vs $|\vec{q}|$ is found to be nearly flat. It led us to conclude that the spin density of the cuprate material is confined in the CuO_2 plane. We have also improved our results by including correlation effect via multi-configuration self-consistent field (MCSCF) procedure and introducing additional effective core potentials (ECP) for environment. Unfortunately, the changes in the form factor by these efforts turned out to be within the experimental errors.

Finally we discuss the difference between La_2CuO_4 and La_2NiO_4 , and try to explain the failure of the cluster method in La_2NiO_4 and its success in KNiF_3 , NiO, and other cuprate materials. We also discuss the covalence quantitatively which we found in our cluster calculations and compare our results with an in-

dependent study on the covalence by Martin and Hay [mart93] using the similar cluster methods for La_2CuO_4 . There is an indication of deficiency in our MCSCF approach that the degree of covalence found in our MCSCF results was appreciably less than that of very extensive CI calculation by Martin and Hay. We suggest that these additional correlation effect may explain the discrepancy in La_2NiO_4 .

Chapter 2

Theory of the spin density in an antiferromagnetic insulator including covalence and quantum spin fluctuations

2.1 Introduction

As we pointed out in Chap.1, earlier theoretical studies of the ordered magnetic moment in antiferromagnetic (AF) insulators considered spin fluctuations without covalence, or covalence without spin fluctuations. The theories of quantum or zero-point spin fluctuations [kapl92, rege88, gros89] were based on the Heisenberg spin model, and therefore contained no covalence effects on the antiferromagnetic ordered moment. On the other hand, the theory of covalence effects on the ordered moment [hubb65, akim76] were based on Hartree-Fock theory which contains no quantum spin fluctuations. The effects, quantum spin fluctuations (QSF) and covalence (COV) are conceptually different. Covalence is a *local* effect: it can occur in one molecule with a magnetic ion bonded to diamagnetic ions; whereas the existence of QSF in an antiferromagnet requires long range order and therefore

involves all the spins.

Here, in this chapter, in order to unify these two conceptually disparate effects, we considered the 1-band Hubbard model in the $\frac{1}{2}$ -filled narrow band regime, employing the mapping from a multi-band to the one-band model of Hybertson et. al. [hybe90]. For the purpose of understanding ground and low-lying excited state properties, the transition metal oxides with which we are concerned here can be represented by a multi-band Hubbard hamiltonian, multiple bands corresponding to d -orbitals of the transition metal ion and p -orbitals of the ligands. Furthermore, when p -orbitals are filled, the multi-band hamiltonian can be mapped into a one-band (or two-band) Hubbard hamiltonian [hybe90] where the active bands correspond to effective d -orbitals. For the cuprates, one has to deal with the singly occupied e_g orbital which results in a $\frac{1}{2}$ -filled one-band Hubbard hamiltonian.

We obtain the expectation value of the spin density in the ground state of this one-band Hamiltonian. Then we show that the Fourier transform of the spin density can be expressed as a product of an expectation value of the site spin incorporating QSF effect and a form factor including COV, with some additional correction terms. The expectation value of the site spin is obtained with an effective spin hamiltonian which is described below. We calculate the correction terms and show that they are negligible in the $\frac{1}{2}$ -filled narrow band regime. As we shall show, the calculation of the spin density also allows a discussion of the ordered moment.

2.2 Effective spin hamiltonian

The one-band Hubbard Hamiltonian is given by

$$\mathcal{H} = U \sum_i n_{i\uparrow} n_{i\downarrow} + \sum_{ij\sigma} t_{ij} a_{i\sigma}^\dagger a_{j\sigma}, \quad (2.1)$$

where $a_{i\sigma}^\dagger$ creates a fermion in the one-particle state $w_{i\sigma} = w_i(\vec{r})\alpha_\sigma$ and $n_{i\sigma}$ is the corresponding number operator. $w_i(\vec{r}) = w(\vec{r} - \vec{R}_i)$ is a Wannier function associated with the magnetic ion of transition metal at site \vec{R}_i and α_σ is the spin state ($\sigma = \pm 1$). The $w_i(\vec{r})$'s are real and form an orthonormal set. U is the Coulomb repulsion between two on-site electrons ($U > 0$) and t_{ij} is the hopping parameter which is assumed to be non-zero, $t_{ij} = t$, for only nearest neighbor pairs i and j . We consider the case where the hopping parameter t is very small compared to U and the band is half filled, i.e. (the number of electrons) = (the number of sites). In this spirit, we write Eq.(2.1) as

$$\mathcal{H} = \mathcal{H}_o + V, \quad (2.2)$$

where $\mathcal{H}_o = U \sum_i n_{i\uparrow} n_{i\downarrow}$ and $V = \sum_{ij\sigma} t_{ij} a_{i\sigma}^\dagger a_{j\sigma}$, treating V as the perturbation.

The Schrödinger equation of the system is written as

$$\mathcal{H}\Psi = E\Psi. \quad (2.3)$$

We define $P\Psi$ with an effective hamiltonian \mathcal{H}_{eff} , satisfying the relation of

$$\mathcal{H}_{eff}P\Psi = EP\Psi, \quad (2.4)$$

where E and Ψ are the same as in Eq. (2.3), and P is the projection operator which projects Ψ on to the ground state manifold of \mathcal{H}_o . This manifold, called the

P -manifold, is characterized by one electron per each site and has dimensionality (degeneracy) of 2^N .

The ground state of Eq. (2.3) can be written as

$$\Psi = P\Psi + Q\Psi, \quad (2.5)$$

where $Q = 1 - P$.

Rewrite Eq. (2.3) using Eq. (2.5)

$$\mathcal{H}(P + Q)\Psi = E(P + Q)\Psi, \quad (2.6)$$

and apply P on both sides of Eq. (2.6), then we obtain

$$\begin{aligned} P\mathcal{H}(P + Q)\Psi &= PE(P + Q)\Psi \\ &= EP\Psi, \end{aligned} \quad (2.7)$$

because of $P = 1 - Q$.

If we apply Q on both sides of Eq. (2.6), then

$$Q\mathcal{H}(P + Q)\Psi = QE(P + Q)\Psi \quad (2.8)$$

Using $Q^2 = Q$ and $QP = 0$ (which follows from $Q + P = 1$), Eq. (2.8) becomes

$$Q[Q(\mathcal{H} - E)Q\Psi + \mathcal{H}P\Psi] = 0. \quad (2.9)$$

Then we obtain

$$Q\Psi = -\frac{1}{Q(\mathcal{H} - E)Q}\mathcal{H}P\Psi. \quad (2.10)$$

where $\frac{1}{Q(\mathcal{H} - E)Q}$ is the inverse of $Q(\mathcal{H} - E)Q$, assumed to exist.

By plugging Eq. (2.10) into Eq. (2.7), we find

$$P\mathcal{H}P\Psi - P\mathcal{H}\frac{1}{Q(\mathcal{H}-E)Q}\mathcal{H}P\Psi = EP\Psi.$$

Using $P^2 = P$,

$$P\left(P\mathcal{H}P - P\mathcal{H}\frac{1}{Q(\mathcal{H}-E)Q}\mathcal{H}P\right)P\Psi = EP\Psi. \quad (2.11)$$

Then we obtain \mathcal{H}_{eff} by comparing Eq. (2.11) and Eq. (2.4), as

$$\mathcal{H}_{eff} = P\mathcal{H}P - P\mathcal{H}\frac{1}{Q(\mathcal{H}-E)Q}\mathcal{H}P. \quad (2.12)$$

We can write $\mathcal{H} - E = \mathcal{H}_o - E_o + V - \delta E$ and expand $\frac{1}{Q(E-\mathcal{H})Q}$ in terms of small $(V - \delta E)$. Note that $E_o = 0$, $\mathcal{H}_o Q = UQ$, and $PHQ = PVQ$. In the half-filled narrow band regime, which is characterized by small $|\frac{t}{U}|$, \mathcal{H}_{eff} can be reduced to a spin hamiltonian

$$\mathcal{H}_{eff} = \sum_{ij} J_{ij} \vec{S}_i \cdot \vec{S}_j + \mathcal{H}^{(4)} + O\left(\frac{t^6}{U^5}\right), \quad (2.13)$$

where $S_i^x = \frac{1}{2}(a_{i\uparrow}^\dagger a_{i\downarrow} + a_{i\downarrow}^\dagger a_{i\uparrow})$, $S_i^y = \frac{1}{2i}(a_{i\uparrow}^\dagger a_{i\downarrow} - a_{i\downarrow}^\dagger a_{i\uparrow})$, and $S_i^z = \frac{1}{2}(a_{i\uparrow}^\dagger a_{i\uparrow} - a_{i\downarrow}^\dagger a_{i\downarrow})$. Here, the first term is the well-known Heisenberg Hamiltonian with $J_{ij} = (t_{ij}^2/U)$ and the second term, $\mathcal{H}^{(4)}$, is of order (t^4/U^3) and includes 4-spin operators. These latter terms have been discussed in detail by Takahashi [taka77].

$P\Psi$ is obtained from the lowest eigenfunction, $\Phi(s_1, s_2, \dots)$, of \mathcal{H}_{eff} through the relation

$$P\Psi = \mathcal{A}\Pi_n w_n(\vec{r}_n)\Phi(s_1, s_2, \dots), \quad (2.14)$$

where \vec{r}_n is the space coordinate of the n-th electron, s_i is the site spin coordinate, and \mathcal{A} is the antisymmetrizer operator.

To the leading order in the hopping integral, $Q\Psi$ in Eq. (2.10), is given by

$$Q\Psi = -\frac{1}{U}Q\mathcal{H}P\Psi. \quad (2.15)$$

Note that $Q\mathcal{H}P = QVP$.

2.3 Spin density

2.3.1 Formalism

The Fourier transform of the spin density in the ground state Ψ of the Hubbard hamiltonian is

$$\langle s(\vec{q}) \rangle_{\Psi} = \frac{\langle (P\Psi + Q\Psi) | s(\vec{q}) | (P\Psi + Q\Psi) \rangle}{1 + \langle Q\Psi | Q\Psi \rangle}. \quad (2.16)$$

Since Ψ is in the space of Slater determinants, we can use the spin density operator $s(\vec{q})$ in the form [kapl91, kapl92]

$$s(\vec{q}) = \frac{1}{2} \sum_{ij\sigma} f_{ij}(\vec{q}) \sigma a_{i\sigma}^{\dagger} a_{j\sigma} \quad (2.17)$$

$$= s_D(\vec{q}) + s_{OD}(\vec{q}), \quad (2.18)$$

where $f_{ij}(\vec{q}) = \int e^{i\vec{q}\cdot\vec{r}} w_i(\vec{r}) w_j(\vec{r}) d\vec{r}$. The first term of Eq. (2.18), s_D comes from $i = j$ and the second term, s_{OD} comes from $i \neq j$ terms. In the narrow band regime, the overlap of the Wannier functions for $i \neq j$ is small ; so we assume f_{ij} to be order of t for $i \neq j$. In this spirit, we calculate the expectation value of the spin density to $O(t^2)$.

The leading term , of $O(t^0)$, in Eq. (2.16) is

$$\begin{aligned} \langle s(\vec{q}) \rangle_0 &= \langle P\Psi | s_D(\vec{q}) | P\Psi \rangle \\ &= f_w(\vec{q}) \sum_j e^{i\vec{q}\cdot\vec{R}_j} \langle S_j^z \rangle, \end{aligned} \quad (2.19)$$

where $f_w(\vec{q}) = \int e^{i\vec{q}\cdot\vec{r}} w(\vec{r})^2 d\vec{r}$, and the angular bracket means an average in the $P\Psi$ space.

The contribution from s_{OD} , $\langle P\Psi|s_{OD}(\vec{q})|P\Psi\rangle$ in Eq. (2.16) is $O(t^1)$. It identically vanishes because s_{OD} contains intersite terms which takes one out of the P -manifold.

The terms of $O(t^2)$ in Eq. (2.16) are

$$\begin{aligned} \langle s(\vec{q}) \rangle_2 &= \langle Q\Psi|s_D(\vec{q})|Q\Psi\rangle - \langle P\Psi|s_D(\vec{q})|P\Psi\rangle \langle Q\Psi|Q\Psi\rangle \\ &\quad + \langle P\Psi|s_{OD}(\vec{q})|Q\Psi\rangle + \langle Q\Psi|s_{OD}(\vec{q})|P\Psi\rangle. \end{aligned} \quad (2.20)$$

Here, the physically interesting quantity for us is the Fourier transform of the spin density at \vec{q} values corresponding to the Bragg peaks. So we are interested in the values of $\vec{q} = \vec{q}_A$, in Eq. (2.16), where \vec{q}_A corresponds to the antiferromagnetic Bragg wave vectors. The first two terms in Eq. (2.20), that is the contribution from s_D , upon using Eq. (2.15), can be written as

$$\begin{aligned} &\langle Q\Psi|s_D(\vec{q})|Q\Psi\rangle - \langle P\Psi|s_D(\vec{q})|P\Psi\rangle \langle Q\Psi|Q\Psi\rangle \\ &= f_w(\vec{q}) \left(\frac{t^2}{U^2} \right) \sum_j \sum_{\langle mn \rangle \sigma \sigma'} e^{i\vec{q}\cdot\vec{R}_j} [\langle a_{m\sigma}^\dagger a_{n\sigma} S_j^z a_{n\sigma'}^\dagger a_{m\sigma'} \rangle \\ &\quad - \langle S_j^z \rangle \langle a_{m\sigma}^\dagger a_{n\sigma} a_{n\sigma'}^\dagger a_{m\sigma'} \rangle], \end{aligned} \quad (2.21)$$

where the angular bracket means an average in the $P\Psi$ space and the sum $\langle mn \rangle$ is over nearest neighbor pairs m, n and it is noted that m, n should be counted differently from n, m .

The contribution from the third term in Eq. (2.20), s_{OD} , is

$$\langle P\Psi|s_{OD}(\vec{q})|Q\Psi\rangle = -\frac{t}{U} \frac{1}{2} \sum_{\langle mn \rangle \sigma \sigma'} f_{mn}(\vec{q}) \langle a_{m\sigma}^\dagger a_{n\sigma} \sigma a_{n\sigma'}^\dagger a_{m\sigma'} \rangle. \quad (2.22)$$

Since $f_{mn}(\vec{q}) = f_{nm}(\vec{q})$ and $\sum_{\sigma\sigma'} \langle a_{m\sigma}^\dagger a_{n\sigma} \sigma a_{n\sigma'}^\dagger a_{m\sigma'} \rangle = -\sum_{\sigma\sigma'} \langle a_{n\sigma}^\dagger a_{m\sigma} \sigma a_{m\sigma'}^\dagger a_{n\sigma'} \rangle$, Eq. (2.22) is identically zero. Similarly, the last term of Eq. (2.20), the another contribution from s_{OD} , vanishes.

Now let's carry out the summations on X_{jmn} in Eq. (2.21) where

$$X_{jmn} \equiv \langle a_{m\sigma}^\dagger a_{n\sigma} S_j^z a_{n\sigma'}^\dagger a_{m\sigma'} \rangle - \langle S_j^z \rangle \langle a_{m\sigma}^\dagger a_{n\sigma} a_{n\sigma'}^\dagger a_{m\sigma'} \rangle. \quad (2.23)$$

First, one can divide the summation $\sum_j \sum_{\langle mn \rangle}$ into two types of terms (1) where $j = m$ or $j = n$ and (2) where $j \neq m$ and $j \neq n$, i.e.

$$\sum_j \sum_{\langle mn \rangle} \longrightarrow 2 \sum_{\langle jn \rangle} + \sum_j \sum_{\langle mn \rangle \neq j}. \quad (2.24)$$

In the case (1),

$$2 \sum_{\langle jn \rangle} \sum_{\sigma\sigma'} X_{jjn} = 2 \sum_{\langle jn \rangle} \sum_{\sigma\sigma'} \left(\langle a_{j\sigma}^\dagger a_{n\sigma} S_j^z a_{n\sigma'}^\dagger a_{j\sigma'} \rangle - \langle S_j^z \rangle \langle a_{j\sigma}^\dagger a_{n\sigma} a_{n\sigma'}^\dagger a_{j\sigma'} \rangle \right). \quad (2.25)$$

The first term of Eq. (2.25) vanishes since $S_j^z a_{j\sigma'} P = 0$ and the second term $\sum_{\sigma\sigma'} \langle a_{j\sigma}^\dagger a_{n\sigma} a_{n\sigma'}^\dagger a_{j\sigma'} \rangle$ can be reduced to $(\frac{1}{2} - 2\vec{S}_j \cdot \vec{S}_n)$ after summation over σ, σ' .

Thus Eq. (2.25) is reduced to

$$2 \sum_{\langle jn \rangle} \sum_{\sigma\sigma'} X_{jjn} = -2 \sum_j Z \left(\frac{1}{2} - 2\langle \vec{S}_j \cdot \vec{S}_n \rangle \right) \quad (2.26)$$

where n is a particular nearest neighbor of j (n can be any one of the nearest neighbors), and Z is number of the nearest neighbors.

In the case (2), the summation over X_{jmn} can be written as

$$\begin{aligned} \sum_j \sum_{\langle mn \rangle \neq j} \sum_{\sigma\sigma'} X_{jmn} &= \sum_j \sum_{\langle mn \rangle \neq j} \sum_{\sigma\sigma'} \left(\langle S_j^z a_{m\sigma}^\dagger a_{n\sigma} a_{n\sigma'}^\dagger a_{m\sigma'} \rangle \right. \\ &\quad \left. - \langle S_j^z \rangle \langle a_{m\sigma}^\dagger a_{n\sigma} a_{n\sigma'}^\dagger a_{m\sigma'} \rangle \right) \\ &= \sum_j \sum_{\langle mn \rangle \neq j} \left(\langle S_j^z \vec{S}_m \cdot \vec{S}_n \rangle - \langle S_j^z \rangle \langle \vec{S}_m \cdot \vec{S}_n \rangle \right). \quad (2.27) \end{aligned}$$

Now let's rewrite the summation $\sum_j \sum_{\langle mn \rangle \neq j}$ as (see Eq. (2.24)),

$$\sum_j \sum_{\langle mn \rangle \neq j} \longrightarrow \sum_j \sum_{\langle mn \rangle} -2 \sum_{\langle jn \rangle} \quad (2.28)$$

Using Eq. (2.28) in Eq. (2.27), we find that the first sum becomes

$$\sum_j \langle S_j^z \sum_{\langle mn \rangle} \vec{S}_m \cdot \vec{S}_n \rangle - \langle S_j^z \rangle \sum_{\langle mn \rangle} \langle \vec{S}_m \cdot \vec{S}_n \rangle. \quad (2.29)$$

Noting that $P\Psi$ is the ground state (eigenstate) of $\sum_{\langle mn \rangle} (\frac{1}{2} - 2\vec{S}_m \cdot \vec{S}_n)$, Eq. (2.29) vanishes.

The second sum becomes

$$-2 \sum_{\langle jn \rangle} [\langle S_j^z \vec{S}_j \cdot \vec{S}_n \rangle - \langle S_j^z \rangle \langle \vec{S}_j \cdot \vec{S}_n \rangle]. \quad (2.30)$$

The first term of Eq. (2.30) can be written as

$$\sum_{\langle jn \rangle} \langle S_j^z \vec{S}_j \cdot \vec{S}_n \rangle = \sum_{\langle jn \rangle} \left[\frac{1}{4} \langle S_n^z \rangle + i \langle (S_j^y S_n^x - S_j^x S_n^y) \rangle \right], \quad (2.31)$$

using the relations $\vec{S}_m \cdot \vec{S}_n = S_j^z S_n^z + S_j^x S_n^x + S_j^y S_n^y$ and $S_j^z S_j^x = i S_j^y$. The 2nd term of Eq. (2.31) vanishes because of symmetry on the summation of $\langle jn \rangle$ and the first term becomes $\sum_{\langle jn \rangle} (1/4) \langle S_n^z \rangle$. Eq. (2.30) then reduces to

$$-2 \sum_{\langle jn \rangle} \left[\frac{1}{4} \langle S_n^z \rangle - \langle S_j^z \rangle \langle \vec{S}_j \cdot \vec{S}_n \rangle \right]. \quad (2.32)$$

Using the relation $\langle S_n^z \rangle = -\langle S_j^z \rangle$ for the nearest neighbor pair $\langle jn \rangle$ when there is antiferromagnetic ordering, Eq. (2.32) becomes

$$Z \sum_j \left[\frac{1}{2} + 2 \langle \vec{S}_j \cdot \vec{S}_n \rangle \right] \langle S_j^z \rangle. \quad (2.33)$$

Combining (2.26) and (2.33), Eq. (2.20), the second leading term of Eq. (2.16) becomes

$$\langle s(\vec{q}) \rangle_2 = -2\gamma Z f_w(\vec{q}) \left(\frac{t^2}{U^2} \right) \sum_j e^{i\vec{q} \cdot \vec{R}_j} \langle S_j^z \rangle \quad (2.34)$$

where

$$\gamma \equiv 1/4 - 3\langle \vec{S}_n \cdot \vec{S}_m \rangle. \quad (2.35)$$

Then we obtain a simple expression for the Fourier transform of the spin density in Eq. (2.16), from Eq. (2.34) and Eq. (2.19), at Bragg peaks as,

$$\langle s(\vec{q}) \rangle = [1 - 2\gamma Z(\frac{t^2}{U^2})] f_w(\vec{q}) \langle S_j^z \rangle F(\vec{q}), \quad (2.36)$$

where $F(\vec{q}) = \sum_j e^{i(\vec{q}-\vec{q}_A)\cdot\vec{R}_j}$, is the geometric structure factor that gives Bragg peaks at the antiferromagnetic wave vector \vec{q}_A .

In Eq. (2.36), $\langle S_j^z \rangle$ is the average site spin in the ground state of \mathcal{H}_{eff} . After keeping terms of $O(t^4)$ in \mathcal{H}_{eff} [taka77], we obtain $\langle S_j^z \rangle$ to order of t^2

$$\langle S_j^z \rangle = \langle S_z \rangle_{Heis} (1 + \xi \frac{t^2}{U^2}), \quad (2.37)$$

where $\langle S_z \rangle_{Heis}$ is the magnitude of the sublattice spin per site in the ground state of the Heisenberg Hamiltonian and ξ is a correction term coming from $\mathcal{H}^{(4)}$ in Eq. (2.13). The details of estimating ξ will be discussed in Sec. (2.3.3).

Substituting the values of $\langle S_j^z \rangle$ from Eq. (2.37) in Eq. (2.36), we obtain the spin density $\langle s(\vec{q}) \rangle$ as

$$\langle s(\vec{q}) \rangle = \langle S_z \rangle_{Heis} \left[1 - (2\gamma Z - \xi) \left(\frac{t^2}{U^2} \right) \right] f_w(\vec{q}) F(\vec{q}). \quad (2.38)$$

Eq. (2.38) is the *central* result of our calculations in this section. It gives the Fourier transform of the spin density at the Bragg wave vectors as a product of $\langle S_z \rangle_{Heis}$, the form factor of the magnetic site, and a moment reduction factor $\left[1 - (2\gamma Z - \xi) \left(\frac{t^2}{U^2} \right) \right]$ arising from the hopping term of the one-band Hubbard

Hamiltonian. In the next section we will discuss how our results reduce to the earlier theory of covalent reduction of the spin density given by Hubbard and Marshall [hubb65].

2.3.2 Relation to the Hubbard-Marshall theory

To apply Eq. (2.38) to neutron Bragg scattering experiments, we need to know explicitly the Wannier functions, $w(\vec{r})$ associated with the magnetic ions. This Wannier function can be expanded in the basis of Bloch functions,

$$w(\vec{r}) = \frac{1}{\sqrt{N}} \sum_{\vec{k}} \psi_{\vec{k}}, \quad (2.39)$$

where N is number of sites. The Bloch function $\psi_{\vec{k}}$ can be expanded again in the basis of unit cell functions $u(\vec{r} - \vec{R})$ which are not generally orthogonal. The point is that the function $u(\vec{r})$ is available explicitly from atomic calculations.

$$\psi_{\vec{k}} = \sqrt{\frac{C_{\vec{k}}}{N}} \sum_{\vec{R}} e^{i\vec{k} \cdot \vec{R}} u(\vec{r} - \vec{R}), \quad (2.40)$$

$C_{\vec{k}}$ can be determined by the normalization condition of the Bloch function,

$$\begin{aligned} \langle \psi_{\vec{k}} | \psi_{\vec{k}} \rangle &= 1 \\ &= \frac{C_{\vec{k}}}{N} \sum_{\vec{R}} \sum_{\vec{R}'} e^{i\vec{k} \cdot (\vec{R} - \vec{R}')} \int u(\vec{r} - \vec{R}) u(\vec{r} - \vec{R}') d\vec{r}, \end{aligned} \quad (2.41)$$

where we assume we can neglect the overlap beyond nearest neighbors :

$$\begin{aligned} \int u(\vec{r} - \vec{R}) u(\vec{r} - \vec{R}') d\vec{r} &= 1 & \vec{R} - \vec{R}' = 0, \\ &= \Delta & \vec{R} - \vec{R}' = \vec{\tau}, \\ &= 0 & \text{otherwise}, \end{aligned} \quad (2.42)$$

where $\vec{\tau}$ is a vector connecting nearest-neighbor magnetic ions. From Eq. (2.41)

and Eq. (2.42), we obtain

$$\sqrt{C_{\vec{k}}} = \left(\frac{1}{1 + \Delta \sum_{\vec{\tau}} e^{i\vec{k} \cdot \vec{\tau}}} \right)^{1/2}. \quad (2.43)$$

For small Δ , $\sqrt{C_{\vec{k}}}$ becomes

$$\sqrt{C_{\vec{k}}} = 1 - \frac{1}{2}\Delta\gamma_k Z + \frac{3}{8}\Delta^2\gamma_k^2 Z^2 + \dots, \quad (2.44)$$

where $\gamma_k Z \equiv \sum_{\vec{r}} e^{i\vec{k}\cdot\vec{r}}$.

We can rewrite $w(\vec{r})$ using $\sqrt{C_{\vec{k}}}$ from Eq. (2.44) as

$$\begin{aligned} w(\vec{r}) &= \frac{1}{N} \sum_{\vec{k}, \vec{R}} \left(1 - \frac{1}{2}\Delta\gamma_k Z + \frac{3}{8}\Delta^2\gamma_k^2 Z^2 + \dots \right) e^{i\vec{k}\cdot\vec{R}} u(\vec{r} - \vec{R}) \\ &= u(\vec{r}) + \frac{1}{N} \sum_{\vec{k}, \vec{R}} \left(-\frac{1}{2}\Delta\gamma_k Z \right) e^{i\vec{k}\cdot\vec{R}} u(\vec{r} - \vec{R}) \\ &\quad + \frac{1}{N} \sum_{\vec{k}, \vec{R}} \left(\frac{3}{8}\Delta^2\gamma_k^2 Z^2 \right) e^{i\vec{k}\cdot\vec{R}} u(\vec{r} - \vec{R}) + \dots \end{aligned} \quad (2.45)$$

The form factor in the Wannier function basis is then written, keeping terms up to $O(\Delta^2)$ which we are interested in,

$$\begin{aligned} f_w(\vec{q}) &\approx \int u^2(\vec{r}) e^{i\vec{q}\cdot\vec{r}} d\vec{r} \\ &\quad - 2 \times \frac{1}{2} \frac{\Delta}{N} \sum_{\vec{k}, \vec{R}} (\gamma_k Z) \int u(\vec{r} - \vec{R}) u(\vec{r}) e^{i\vec{k}\cdot\vec{R} + i\vec{q}\cdot\vec{r}} d\vec{r} \\ &\quad + \frac{1}{4} \frac{\Delta^2}{N^2} \sum_{\vec{k}, \vec{R}} \sum_{\vec{k}', \vec{R}'} (\gamma_k Z) (\gamma_{k'} Z)^* \int u(\vec{r} - \vec{R}') u(\vec{r} - \vec{R}) e^{i\vec{k}\cdot\vec{R} - i\vec{k}'\cdot\vec{R}' + i\vec{q}\cdot\vec{r}} d\vec{r} \\ &\quad + 2 \times \frac{3}{8} \frac{\Delta^2}{N} \sum_{\vec{k}, \vec{R}} (\gamma_k Z)^2 \int u(\vec{r} - \vec{R}) u(\vec{r}) e^{i\vec{k}\cdot\vec{R} + i\vec{q}\cdot\vec{r}} d\vec{r}. \end{aligned} \quad (2.46)$$

Let's consider the form factor $f_w(\vec{q})$ term by term in Eq. (2.46) at $\vec{q} = \vec{q}_A$, using $\gamma_k Z \equiv \sum_{\vec{r}} e^{i\vec{k}\cdot\vec{r}}$.

The first term of Eq. (2.46) becomes

$$\begin{aligned} f_w^{(1)}(\vec{q}_A) &= \int u^2(\vec{r}) e^{i\vec{q}_A\cdot\vec{r}} d\vec{r} \\ &= f_u(\vec{q}_A). \end{aligned} \quad (2.47)$$

The second term becomes

$$f_{\omega}^{(2)}(\vec{q}) = -\Delta \frac{1}{N} \sum_{\vec{k}, \vec{R}} \sum_{\vec{\tau}} \int u(\vec{r} - \vec{R}) u(\vec{r}) e^{i\vec{k} \cdot (\vec{\tau} + \vec{R}) + i\vec{q} \cdot \vec{r}} d\vec{r}. \quad (2.48)$$

Using $\frac{1}{N} \sum_{\vec{k}} e^{i\vec{k} \cdot (\vec{\tau} + \vec{R})} = \delta_{\vec{\tau} + \vec{R}, 0}$,

$$\begin{aligned} f_{\omega}^{(2)}(\vec{q}) &= -\Delta \sum_{\vec{\tau}} \int u(\vec{r} + \vec{\tau}) u(\vec{r}) e^{i\vec{q} \cdot \vec{r}} d\vec{r}, \\ &= -\Delta \sum_{\vec{\tau}} e^{i\vec{q} \cdot \frac{\vec{\tau}}{2}} f(\vec{q}, \vec{\tau}), \end{aligned} \quad (2.49)$$

where $f(\vec{q}, \vec{\tau}) = \int e^{i\vec{q} \cdot \vec{r}} u(\vec{r} + \frac{\vec{\tau}}{2}) u(\vec{r} - \frac{\vec{\tau}}{2}) d\vec{r}$. Since $f(\vec{q}, \vec{\tau}) = f(\vec{q}, -\vec{\tau})$ the summation on $\vec{\tau}$ can be written as $\sum_{|\vec{\tau}|} (e^{i\vec{q} \cdot \frac{\vec{\tau}}{2}} + e^{-i\vec{q} \cdot \frac{\vec{\tau}}{2}}) f(\vec{q}_A, \vec{\tau})$. Then $f^{(2)}(\vec{q}_A)$ vanishes by $e^{\pm i\vec{q}_A \cdot \frac{\vec{\tau}}{2}} = \pm i$.

Similarly the third term becomes

$$f_{\omega}^{(3)}(\vec{q}) = \frac{\Delta^2}{4} \sum_{\vec{\tau}} \sum_{\vec{\tau}'} \int u(\vec{r} + \vec{\tau}') u(\vec{r} + \vec{\tau}) e^{i\vec{q} \cdot \vec{r}} d\vec{r}. \quad (2.50)$$

If $\tau \neq \tau'$, $f_{\omega}^{(3)}(\vec{q})$ vanishes by Eq. (2.42), so we keep terms only when $\tau = \tau'$. Then $f_{\omega}^{(3)}(\vec{q}_A)$ reduces to

$$\begin{aligned} f_{\omega}^{(3)}(\vec{q}_A) &= \frac{\Delta^2}{4} \sum_{\vec{\tau}} e^{i\vec{q}_A \cdot \vec{\tau}} f_u(\vec{q}_A) \\ &= \frac{\Delta^2}{4} (-Z) f_u(\vec{q}_A). \end{aligned} \quad (2.51)$$

One can obtain the fourth term by a similar way

$$f_{\omega}^{(4)}(\vec{q}) = \frac{3}{4} \Delta^2 \sum_{\vec{\tau}} \sum_{\vec{\tau}'} \int u(\vec{r} + \vec{\tau} - \vec{\tau}') u(\vec{r}) e^{i\vec{q} \cdot \vec{r}} d\vec{r}. \quad (2.52)$$

Keeping terms up to $O(\Delta^2)$ again, i.e. only keeping $\tau = \tau'$ terms, we obtain

$$f_{\omega}^{(4)}(\vec{q}_A) = \frac{3}{4} \Delta^2 Z f_u(\vec{q}_A). \quad (2.53)$$

From the above equations, the total $f_w(\vec{q}_A)$ is given as

$$\begin{aligned} f_w(\vec{q}_A) &= f_w^{(1)}(\vec{q}_A) + f_w^{(2)}(\vec{q}_A) + f_w^{(3)}(\vec{q}_A) + f_w^{(4)}(\vec{q}_A) \\ &= f_u(\vec{q}_A) \left(1 + Z \frac{\Delta^2}{2} \right). \end{aligned} \quad (2.54)$$

Using Eq. (2.54) and keeping terms to order of t^2 , we can rewrite Eq. (2.38) in the form

$$\langle s(\vec{q}) \rangle = \langle S_z \rangle_{\text{Heis}} f_u(\vec{q}) \left[1 + Z \frac{\Delta^2}{2} - (2Z\gamma - \xi) \frac{t^2}{U^2} \right] F(\vec{q}). \quad (2.55)$$

Hubbard and Marshall[hubb65] considered a physical situation similar to the CuO_2 plane in La_2CuO_4 and $\text{YBa}_2\text{Cu}_3\text{O}_6$ compounds, where the paramagnetic cations involving 3d electrons are surrounded by diamagnetic anions with filled p-shells. They chose the unit cell function $u(\vec{r})$ as

$$u(\vec{r}) = C[d(\vec{r}) - A \sum_j p_j(\vec{r})], \quad (2.56)$$

where $d(\vec{r})$ and $p_j(\vec{r})$ are atomic wave functions associated with cations and surrounding anions respectively. C is a normalization constant and A is the d-p covalence parameter. For our system, i.e. a CuO_2 plane, $d(\vec{r})$ is a particular 3d wave function of Cu^{2+} and $p_j(\vec{r})$'s are the 2p wave functions of the surrounding O^{2-} .

We assume small A (weak covalence) and neglect overlap between anion orbitals and find that for arbitrary \vec{q} , the form factor $f_u(\vec{q})$ is obtained approximately by

$$\begin{aligned} f_u(\vec{q}) \approx & f_d(\vec{q})(1 - ZA^2) - 2A \sum_j [f_{dp_j}(\vec{q}) - f_{dp_j}(0)f_d(\vec{q})] \\ & + A^2 \sum_j f_{p_j}(\vec{q}). \end{aligned} \quad (2.57)$$

A complete expression without any approximation is given in Chap. 3. In Eq. (2.57), Z is the number of anions surrounding a cation ; for our system, $Z = 4$, and $f_d(\vec{q})$, $f_p(\vec{q})$ and $f_{dp}(\vec{q})$ are the Fourier transforms of $d^2(\vec{r})$, $p^2(\vec{r})$ and $d(\vec{r})p(\vec{r})$, respectively. For $\vec{q} = \vec{q}_A$, the contribution to the Bragg scattering from the last term of Eq. (2.57) involving $p^2(\vec{r})$ can be seen to vanish. Thus only the d^2 and the overlap ($d - p$) terms contribute to the form factor at magnetic Bragg scattering.

If we take the square-bracketed term in Eq. (2.55) as 1. and $\langle S_z \rangle_{Heis}$ as the mean field value, i.e. $\langle S_z \rangle_{Heis} = 0.5$, and plug Eq. (2.57) into Eq. (2.55), we obtain the Hubbard and Marshall result, described in Chap. 3. However, Eq. (2.55) clearly has both the effects of quantum spin fluctuations (in $\langle S_z \rangle_{Heis}$) and covalence (in $f_u(\vec{q})$), with some additional correction terms. According to our formalism, we should consider both these effects simultaneously and take account of the additional terms of $O(t^2)$. In the next sections, Sec.(2.3.3) and Sec.(2.3.4), we will show that the correction terms are negligible for the systems under study and the major sources of reduction of the spin density come from quantum spin fluctuations and the ($p - d$) covalence effect.

2.3.3 Correction term from $\mathcal{H}^{(4)}$ using the spin wave approximation

To calculate $\langle S_j^z \rangle$ in Eq. (2.37), we take \mathcal{H}_{eff} up to $O(\frac{t^4}{U^3})$ in Eq. (2.13). The term of \mathcal{H}_{eff} is well discussed by Takahashi[taka77]. We also follow Takahashi's method [taka77] and use the spin wave approximation, which is an expansion in inverse powers of the spin quantum number S . Our derivation of $\mathcal{H}^{(4)}$ agrees with Takahashi's result and we calculate $\langle S_j^z \rangle$ using perturbation method with

the ground state of \mathcal{H}_{eff} including $\mathcal{H}^{(4)}$.

From Eq. (2.12), the effective Hamiltonian can be written as

$$\mathcal{H}_{eff} = \mathcal{H}_o + \mathcal{H}^{(4)}, \quad (2.58)$$

where \mathcal{H}_o is the Heisenberg Hamiltonian, \mathcal{H}_{Heis} , as given by

$$\mathcal{H}_o = -\frac{t^2}{U} \sum_{\langle mn \rangle} \left(\frac{1}{2} - 2\vec{S}_m \cdot \vec{S}_n \right), \quad (2.59)$$

and

$$\mathcal{H}^{(4)} = \frac{1}{U^3} PVQVPVQVP - \frac{1}{U^3} PVQVQVQVP. \quad (2.60)$$

Then we treat $\mathcal{H}^{(4)}$ as perturbation to \mathcal{H}_o . The perturbation method is applicable because $\mathcal{H}^{(4)}$ is $O(\frac{t^4}{U^3})$ whereas \mathcal{H}_o is $O(\frac{t^2}{U})$ in the narrow band regime ($t \ll U$). $\mathcal{H}^{(4)}$ including 4-spin operators can be written in the form shown in Eq. (A.1) of Appendix A.

The expectation value of the site spin operator, S_j^z , is given by

$$\langle S_j^z \rangle = \langle \Psi | S_j^z | \Psi \rangle. \quad (2.61)$$

By the perturbation method, writing $\Psi = \Psi_o + \delta\Psi$, we obtain $\langle S_j^z \rangle$ up to the first correction

$$\langle S_j^z \rangle = \langle \Psi_o | S_j^z | \Psi_o \rangle + 2\langle \Psi_o | S_j^z | \delta\Psi \rangle \quad (2.62)$$

Using the spin wave approximation described in Appendix A, one finds $\langle \Psi_o | S_j^z | \Psi_o \rangle = \langle S_j^z \rangle_{Heis} = 0.30362$ and $2\langle \Psi_o | S_j^z | \delta\Psi \rangle = 1.2839 \frac{t^2}{U^2}$. If we rewrite Eq. (2.62) as

$$\langle S_j^z \rangle = \langle S_j^z \rangle_{Heis} \left[1 + \frac{1.2839}{0.30362} \left(\frac{t^2}{U^2} \right) \right], \quad (2.63)$$

then we obtain the correction term $\xi = 4.23$ in Eq. (2.37).

2.3.4 Estimation of the correction terms in spin density

In this section, we analyze the correction terms in the square-bracket of Eq. (2.55). First, we easily find γ in Eq. (2.35) from the known ground state energy (in unit of J) [gros89, rege88], because $\langle \vec{S}_n \cdot \vec{S}_m \rangle$ is proportional to the ground state eigenvalue of the Heisenberg Hamiltonian. The value of γ is 1.26. It is interesting to note that γ is greater than its mean field value of 1. In the Neel state (mean field), only the z-components of spins are antiparallel while the x- and y- components are not correlated. On the other hand, in the exact ground state of \mathcal{H}_{eff} , the spin fluctuations can cause an increase in the probability of *antiparallelism* of all the three components of the spin thus providing a plausible explanation why γ is greater than 1.

For ξ in Eq. (2.55), we obtain $\xi = 4.23$ from the previous section.

The next correction term we are concerned with is value Δ which is defined in Sec. (2.3.2). If we choose the unit cell function in the form of Eq. (2.56), we find $\Delta = 2AS - A^2$, where $S = \int p(\vec{r})d(\vec{r})d^3r > 0$. From Wang et. al.'s Hubbard-Marshall model calculation [wang91], $A = 0.35$ and $S = 0.175$, for these values Δ accidentally vanishes. This suggests Δ should be extremely small. We take (t/U) in Eq. (2.55), as $(\frac{t}{U}) = \frac{0.43}{5.4} = 0.08$, from Hybertsen et. al. [hybe90] who mapped the three-band Hubbard model onto a one-band model.

Using the above values of γ, ξ , etc., we find the square-bracketed term in Eq. (2.55) is about 0.96. Thus our results suggest that these corrections can be safely neglected compared to the well-known reduction (about 40% of $\langle S_z \rangle$ from its mean field value) due to spin fluctuations. We expect similar or smaller values for other materials we are interested in. So, we obtain a simple form for Eq. (2.55)

(we drop the subscript u for simplicity from now on), as

$$\langle s(\vec{q}_A) \rangle = \langle S_z \rangle_{Heis} f(\vec{q}_A), \quad (2.64)$$

where

$$f(\vec{q}_A) = f_d(\vec{q}_A)(1 - ZA^2) - 2A \sum_j [f_{dp_j}(\vec{q}_A) - f_{dp_j}(0)f_d(\vec{q}_A)]. \quad (2.65)$$

when we assume small A and neglect the overlap between anions.

Here we define $f_A(\vec{q})$ from Eq. (2.57) without the last terms, i.e. without p^2 terms,

$$f_A(\vec{q}) = f_d(\vec{q})(1 - ZA^2) - 2A \sum_j [f_{dp_j}(\vec{q}) - f_{dp_j}(0)f_d(\vec{q})]. \quad (2.66)$$

Note that $f_A(\vec{q}_A) = f(\vec{q}_A)$ for non-zero \vec{q}_A .

2.4 Ordered moment

We are interested in the ordered moment of these AF insulators including the effects of both spin fluctuations and covalence. The ordered moment, M_{ord} is determined from the spin density $\langle s(\vec{q}_A) \rangle$ times $g\mu_B$ by extrapolation i.e. by putting $\vec{q}_A = 0$ in Eq. (2.65). When $\vec{q}_A = 0$, the 2nd term in Eq. (2.65) vanishes, and the ordered moment is

$$M_{ord} = g\mu_B \langle S_z \rangle_{Heis} (1 - ZA^2). \quad (2.67)$$

This agrees with Hubbard and Marshall who argued that the ordered moment (they called it the effective moment) will be reduced from the Heisenberg value

$g\mu_B\langle S_z \rangle_{Heis}$ (which they obtained in the mean field theory) by the *covalence reduction factor*, $(1 - ZA^2)$.

In general, without the approximation of small A and S , the covalence reduction factor, R_{cov} , can be defined as

$$R_{cov} = \frac{f_A(0)}{f(0)}, \quad (2.68)$$

where $f(0)$ is normalized to 1 from the definition of $f(\vec{q})$, but $f_A(0)$ is less than 1 because $f_A(\vec{q})$ does not contain the contribution from the p_j^2 terms associated with the ligands which identically vanishes at $\vec{q} = \vec{q}_A$ due to antiferromagnetic ordering (corresponding to the ordering of nearest-neighbor magnetic ions).

The ordered moment, M_{ord} is in general given in the form

$$M_{ord} = g\mu_B\langle S_z \rangle_{Heis} f_A(0). \quad (2.69)$$

2.5 Summary

In this chapter, we showed how the two concepts, namely covalence (COV) and quantum spin fluctuations (QSF), are unified in the spin density in a simple form given in Eq. (2.64). We also showed that other correction terms in $\langle s(\vec{q}_A) \rangle$ up to $O(t^2/U^2)$ are negligible and the main contributions to the reduction of $\langle s(\vec{q}_A) \rangle$ from the non-interacting AF ordered spins are QSF in $\langle S_z \rangle_{Heis}$ and COV in $f_A(\vec{q})$.

The experimentally measured quantity is the magnetic moment density $m(\vec{q}_A)$ which is

$$\begin{aligned} m(\vec{q}_A) &= g\mu_B\langle s(\vec{q}_A) \rangle \\ &= g\mu_B\langle S_z \rangle_{Heis} f(\vec{q}_A). \end{aligned} \quad (2.70)$$

Here only $f(\vec{q}_A)$ has \vec{q} -dependence and the other factors being constants. If we calculate $f(\vec{q}_A)$ and compare it with the experimental $m(\vec{q}_A)$, we can directly determine $\langle S_z \rangle_{Heis}$ from the experiment. The rest of this thesis is devoted to the calculation of the form factor $f(\vec{q}_A)$. The form factor carries information about not only COV but also QSF if the absolute experimental values of $m(\vec{q}_A)$ are available. The shape of the form factor reflects the spin distribution in real space. Therefore the form factor calculation is critical to an understanding of the magnetism in the antiferromagnetical systems in which we are interested this thesis.

Chapter 3

Hubbard-Marshall model calculation

3.1 Introduction

The effect of covalence in the neutron scattering form factor was first discussed by Hubbard and Marshall [hubb65]. Hubbard-Marshall (HM) theory takes the wave function for a system as a linear combination of atomic orbitals, thus allowing charge and spin transfer from the paramagnetic ion to the nearby diamagnetic ions. The covalence is a measure of the degree of this spin transfer. Akimitsu and Ito [akim76] calculated the neutron scattering form factor for K_2CuF_4 following HM theory and their calculated result agreed very well with the experiment.

Recently a HM model calculation for La_2NiO_4 was reported by Wang et. al. [wang91] and their calculation for the form factor also agreed very well with the experiment. These authors claimed that the large reduction of the ordered moment in their experiment was due to the covalence effect (see Chapter 2 regarding a discussion of the effect of covalence on the antiferromagnetic ordered moment). However the wave function for the system they used was rather unphysical. They took one spherically symmetric d orbital for the two parallel electrons instead of

2 different orbitals of e_g symmetry as is appropriate for the Ni^{2+} ion in a cubic field. This violates the Pauli principle that prohibits two parallel electrons from being in the same spatial orbital. We have calculated the form factor for La_2NiO_4 taking 2 e_g orbitals, $d_{x^2-y^2}$ and $d_{3z^2-r^2}$, and compared our result with the experiment [chan91]. Wang et. al. also reported a similar calculation in their later paper [wang92]. However, this physically meaningful choice for the wave function turned out to spoil the excellent agreement with experiment obtained with one spherical orbital. Considering the success of the HM model calculation in K_2CuF_4 , the failure of the similar method for La_2NiO_4 is somewhat surprising, since La_2NiO_4 has the same structure as K_2CuF_4 . This failure contributed our motivation to initiate *ab initio* calculations of the neutron scattering form factor.

In this chapter, we introduce HM theory for covalence in the neutron scattering form factor, and then describe our calculation for La_2NiO_4 within the HM theory, and compare with experiment. It should be noted that the concept of covalence in the form factor within HM theory is still valid in our *ab initio* calculation discussed in the later chapters because it also starts from a linear combination of atomic orbitals called basis functions.

3.2 Hubbard-Marshall theory

Hubbard and Marshall considered the transition metal compounds, which consists of a transition metal ion with unpaired electrons in d orbitals, and ligand ions of either F^- or O^{2-} , each of which has the configuration $1s^2 2s^2 2p^6$. In this system, a transfer of electrons is allowed from the ligand to the magnetic ion. This transfer is mainly p -electron transfer to the singly occupied $3d$ -orbitals, creating

an unpaired spin density on the ligand ions. Because of Pauli principle, the spin of the transferred electrons must be opposite to that of the electron in the singly occupied $3d$ state. Hence the spin density, created in the ligand orbitals, is parallel to that of the $3d$ orbital. The electron transfer from the ligand ion to the magnetic ion results in the spin transfer from the magnetic ion to the ligand ions. In this instance the moment of the magnetic ion is decreased as a consequence of the covalence. When the neighboring magnetic ions are antiferromagnetically ordered, the net spin density created in the intervening ligand ion can be cancelled, depending on the symmetry of the crystal structure. For ferromagnets, of course, there is no cancellation of the spin density created in the ligand ions.

The cross section for magnetic Bragg scattering is proportional to the square of the magnetic form factor associated with the magnetic ions and the form factor reflects the spatial distribution of spin density. In an antiferromagnet, when a ligand is shared equally by two antiferromagnetically ordered magnetic ions, the form factor is reduced from a purely ionic value, because a certain amount of the spin density, which is transferred to the ligands and is cancelled there, does not contribute to the peak intensity.

For an illustration of the covalence effect, let us consider an antiferromagnetic linear chain consisting of alternate single magnetic and ligand orbitals shown in Fig. 3.1. Each d orbital contains just one electron, and these are taken to be antiferromagnetically ordered in 1-dimension, while each p orbital contains 2 electrons. In Fig. 3.1, the antibonding orbital associated with the ion M is

$$\psi(\vec{r}) = N [d(\vec{r}) - Ap(\vec{r}) + Ap'(\vec{r})] \quad (3.1)$$

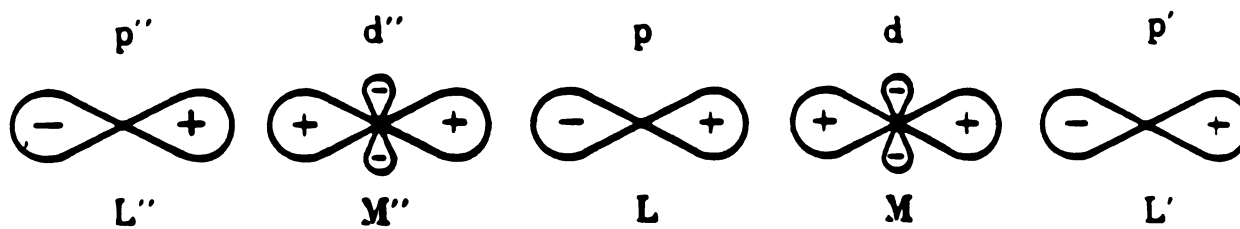


Figure 3.1: Orbitals of a linear chain antiferromagnet. M and M'' are the magnetic ions with antiparallel spins.

where the normalization constant N is given as

$$N^{-2} = 1 - 4AS + 2A^2 \quad (3.2)$$

and S is the magnitude of the overlap integral between p and d orbitals.

The spin density associated with M is

$$\begin{aligned} D(\vec{r}) &= \psi(\vec{r})^2 \\ &\approx N^2 \left[d(\vec{r})^2 - 2Ad(\vec{r})\{p(\vec{r}) - p'(\vec{r})\} + A^2\{p(\vec{r})^2 + p'(\vec{r})^2\} \right] \end{aligned} \quad (3.3)$$

where we have neglected the overlap between p and p' .

The first term of Eq. (3.3) involves $d(\vec{r})^2$ and is rather confined to the parent magnetic ion M ; the second term is an overlap density and is also confined to the immediate vicinity of M ; but the third term gives a density entirely on the ligands and is equally distant from the other magnetic ion, M'' . The spin density given by M'' is similar to that by M , but is of opposite sign in an antiferromagnet. In particular, we notice that for the moment density $A^2p(\vec{r})^2$ due to M , there is an equal and opposite contribution from M'' .

The total spin density in a crystal, associated with a N -magnetic ion system, can be written as

$$\mathcal{D} = \frac{1}{N} \sum_{\mathbf{n}} \sigma_{\mathbf{n}} D(\vec{r} - n\vec{R}), \quad (3.4)$$

where \vec{R} is the nearest neighbor vector connecting M and M'' , and $\sigma_{\mathbf{n}}$ is the site spin corresponding to antiferromagnetic ordering. It is noted that for an antiferromagnetic system $\sigma_{\mathbf{n}} = e^{i\vec{q}_A \cdot n\vec{R}}$ for an antiferromagnetic wave vector \vec{q}_A . In (3.4), the contribution $A^2p(\vec{r})^2$ due to M is cancelled by the $-A^2p(\vec{r})^2$ due to M'' ; in fact all the $p(\vec{r})^2$ terms cancel in the same way.

The form factor, which is the Fourier transform of the spin density of Eq. (3.4), can be written as

$$\begin{aligned} f(\vec{q}) &= \frac{1}{N} \sum_{\mathbf{n}} e^{i\vec{q}_A \cdot n\vec{R}} \int D(\vec{r} - n\vec{R}) e^{i\vec{q} \cdot \vec{r}} d\vec{r} \\ &= \frac{1}{N} \sum_{\mathbf{n}} e^{-i(\vec{q} - \vec{q}_A) \cdot n\vec{R}} \int D(\vec{r}) e^{i\vec{q} \cdot \vec{r}} d\vec{r} \end{aligned} \quad (3.5)$$

At $\vec{q} = \vec{q}_A$, Eq. (3.5) becomes

$$f(\vec{q}_A) = \int D(\vec{r}) e^{i\vec{q}_A \cdot \vec{r}} d\vec{r}. \quad (3.6)$$

It is noted that the contributions from $p(\vec{r})^2$ and $p'(\vec{r})^2$ terms in Eq. (3.3) to the form factor in Eq. (3.6) vanish because of $\int p'(\vec{r})^2 e^{i\vec{q}_A \cdot \vec{r}} d\vec{r} = e^{i\vec{q}_A \cdot \vec{R}} \int p(\vec{r})^2 e^{i\vec{q}_A \cdot \vec{r}} d\vec{r}$ and $e^{i\vec{q}_A \cdot \vec{R}} = -1$. Thus there is no contribution of $p(\vec{r})^2$ or $p'(\vec{r})^2$ term to the form factor. This reflects the above explanation that the spin density of ligand site associated with M , to the right of M , cancelled by the corresponding contribution associated with M'' .

When A and S are small, we can rewrite $D(\vec{r})$ in Eq. (3.3) using Eq. (3.2) up to second order,

$$D(\vec{r}) \approx d(\vec{r})^2(1 + 4AS - 2A^2) - 2Ad(\vec{r})\{p(\vec{r}) - p'(\vec{r})\} \quad (3.7)$$

without the third term of Eq. (3.3).

After rearranging Eq. (3.7) in the form

$$D(\vec{r}) = d(\vec{r})^2(1 - 2A^2) + 2A[2Sd(\vec{r})^2 - d(\vec{r})p(\vec{r}) + d(\vec{r})p'(\vec{r})], \quad (3.8)$$

it is noted that when we integrate $D(\vec{r})$ in Eq. (3.8), the second term (the terms inside the square bracket) vanishes. This results in the reduction of the ordered moment by the factor $(1 - 2A^2)$. When we calculate the form factor taking the

Fourier transform of Eq. (3.8), the second term of Eq. (3.8) contributes to the form factor as a positive value (although small) at $\vec{q} \neq 0$, that passes through a maximum as q increases. This makes the form factor appear flatter in the small $|q|$ region compared to the pure ionic form factor, which is given by the Fourier transfer of $d(\vec{r})^2$.

3.3 Hubbard-Marshall model calculation for La_2NiO_4

The experimental form factor of La_2NiO_4 [wang91] showed a plateau in the small $|q|$ region, as expected within HM theory described in the previous section. Therefore we applied Hubbard-Marshall theory to La_2NiO_4 taking two different d orbitals. These were chosen to be of e_g symmetry, in accordance with expectations from crystal field theory. We took the basic cluster consisting of one magnetic Cu^{2+} ion and 4 ligand O^{2-} ions in the NiO_2 plane where Ni^{2+} ordered antiferromagnetically as shown in Fig. 3.2.

In order to construct a wave function of the type given in Eq. (3.1), we used Hartree-Fock atomic orbitals for both Cu^{2+} and O^- ions, which were obtained from the restricted Hartree-Fock (RHF) method using COLUMBUS code [colu88]. For $p(\vec{r})$ atomic orbitals of O^{2-} , we scaled the O^- atomic orbital in the $|\vec{r}|$ space, to give the same overlap integral value, $S = 0.175$, for d_{r^2} and p_x of Wang et. al. [wang91]. Since the ground state of Ni^{2+} is spin triplet state, we considered two e_g orbitals, $d_{x^2-y^2}$ and $d_{3z^2-r^2}$, for each magnetic ion.

The spin density $D(\vec{r})$ is given as

$$D(\vec{r}) = \psi_{x^2-y^2}(\vec{r})^2 + \psi_{3z^2-r^2}(\vec{r})^2. \quad (3.9)$$

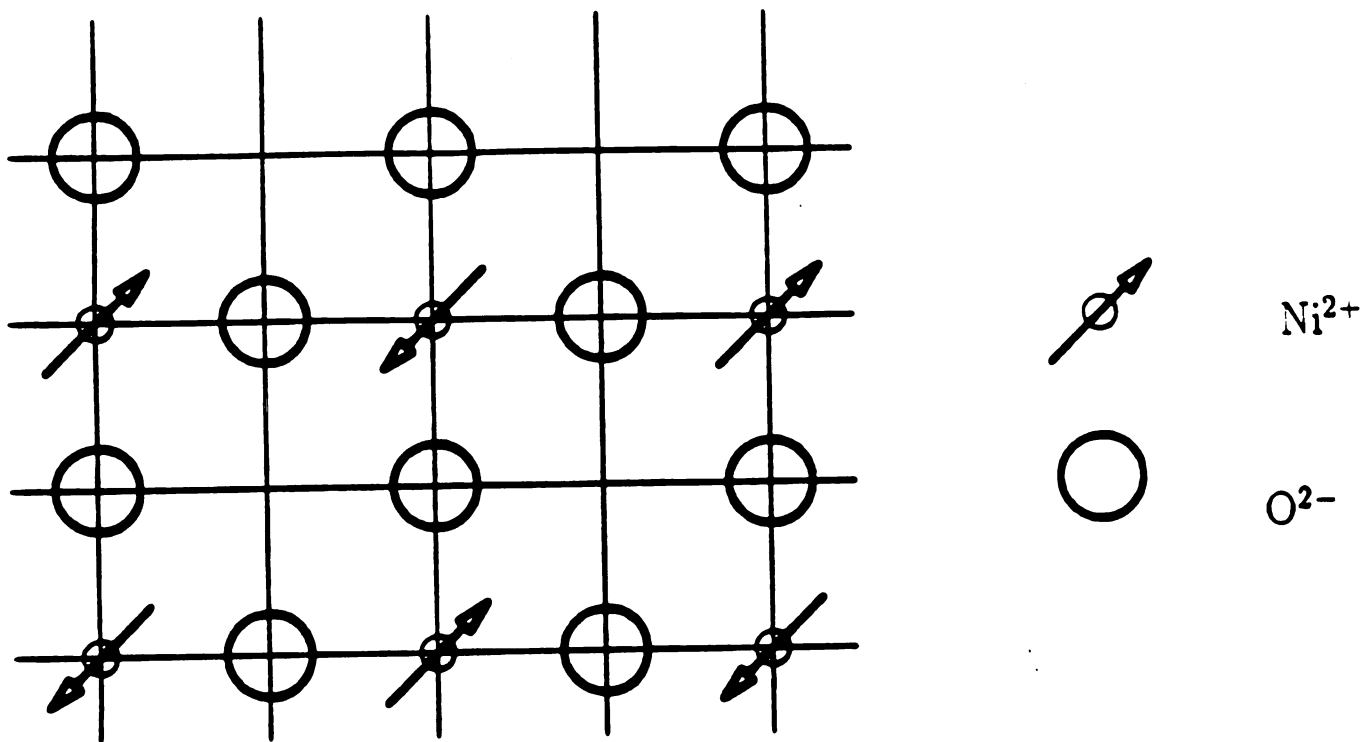


Figure 3.2: Antiferromagnetically ordered NiO_2 plane. The arrows represent spin up or down.

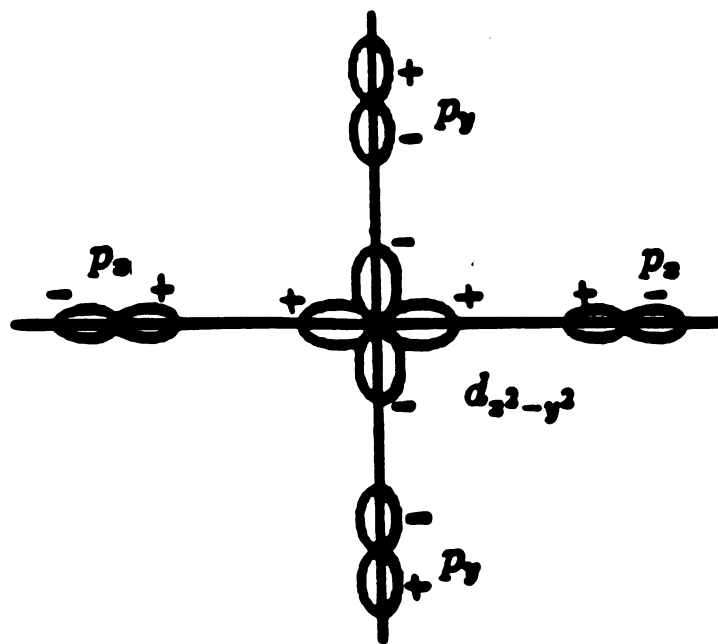


Figure 3.3: Schematic diagram of the antibonding wave function associated with the $d_{x^2-y^2}$ orbital in NiO_2 plane

The wave function $\psi_{x^2-y^2}(\vec{r})$ and $\psi_{3z^2-r^2}(\vec{r})$ can be written in a general form

$$\psi_k(\vec{r}) = N_k \left(d_k(\vec{r}) - A_k \sum_j p_{kj}(\vec{r}) \right), \quad (3.10)$$

where $k = 1$ and $k = 2$ represent $d_{x^2-y^2}$ and $d_{3z^2-r^2}$ respectively and the j index corresponds to the j -th ligand. The orientations of the p_{kj} 's are chosen to produce antibonding orbitals with d_k , with positive *covalence parameter* A_k as shown in Fig. 3.3.

The normalization constant N_k , when the nearest neighbor $p-p'$ overlap, $S_{pp'}$, is included, is given as

$$N_k^{-2} = 1 - 2ZA_kS + ZA_k^2(1 + 2S_{pp'}) \quad (3.11)$$

where $Z = 4$, the number of neighboring ligands.

The form factor associated with ψ_k is

$$\begin{aligned} f_k(\vec{q}) = & N_k^2 \int [d_k^2(\vec{r}) - 2A_k \sum_j d_k(\vec{r})p_{kj}(\vec{r}) \\ & + A_k^2 \sum_{i,j} p_{ki}(\vec{r})p_{kj}(\vec{r})] e^{i\vec{q}\cdot\vec{r}} d\vec{r}. \end{aligned} \quad (3.12)$$

For $\vec{q} = \vec{q}_A$,

$$f_k(\vec{q}_A) = f_d(\vec{q}_A) - 2A_k f_{dp}(\vec{q}_A) + 2A_k^2 f_{pp'}(\vec{q}_A), \quad (3.13)$$

where

$$\begin{aligned} f_d(\vec{q}_A) &= N_k^2 \int d_k^2(\vec{r}) e^{i\vec{q}_A \cdot \vec{r}} d\vec{r}, \\ f_{dp}(\vec{q}_A) &= N_k^2 \int \sum_j d_k(\vec{r}) p_{kj}(\vec{r}) e^{i\vec{q}_A \cdot \vec{r}} d\vec{r}, \\ f_{pp'}(\vec{q}_A) &= N_k^2 \int \sum_{\langle ij \rangle} p_{ki}(\vec{r}) p_{kj}(\vec{r}) e^{i\vec{q}_A \cdot \vec{r}} d\vec{r}. \end{aligned} \quad (3.14)$$

The $\sum_{(ij)}$ in Eq. (3.14) means summation over the pairs of nearest neighbors, because the $i = j$ case of the last term in Eq. (3.12) is cancelled by antiferromagnetic ordering, and because the 2nd-neighbor $p - p$ overlap is very small.

The total form factor is written as

$$f(\vec{q}_A) = \sum_k f_k(\vec{q}_A) \quad (3.15)$$

Note that $f_k(0) = 1$ when we use (3.12) (whereas $f_k(0) < 1$ if we use (3.13)). In Fig. 3.4, this $f(\vec{q}_A)$ is compared with the experiment [wang91] by choosing the covalence parameters, A_1 and A_2 , to give the best fit to the experiment.

3.4 Discussion

In Fig. 3.4, our more realistic model calculation shows worse agreement with the experiment than Wang et. al.'s model calculation [wang91], even though we chose physically meaningful wave functions. Our choice of A_1 and A_2 turned out to be rather big because the fitting procedure tried to reproduce the large reduction of the moment (by about 50%) which was seen in the experiment. Considering the fact that HM theory starts from the ionic limit, which presumes small A 's, La_2NiO_4 might be too covalent to be treated within HM theory.

When we compare our HM model calculation for La_2NiO_4 with a similar calculation in K_2CuF_4 where the HM model calculation agreed well with experiment [akim76], we have to take account of the difference between Cu^{2+} and Ni^{2+} . The ground state of Cu^{2+} has a singly occupied $d_{x^2-y^2}$ orbital. Hence the spin density distribution is confined in the CuO_2 plane and spin transfer mainly occurs within the plane. But both $d_{x^2-y^2}$ and $d_{3z^2-r^2}$ are singly occupied for Ni^{2+} . The spin distribution of $d_{3z^2-r^2}$ is 3-dimensional, so the model we have considered here

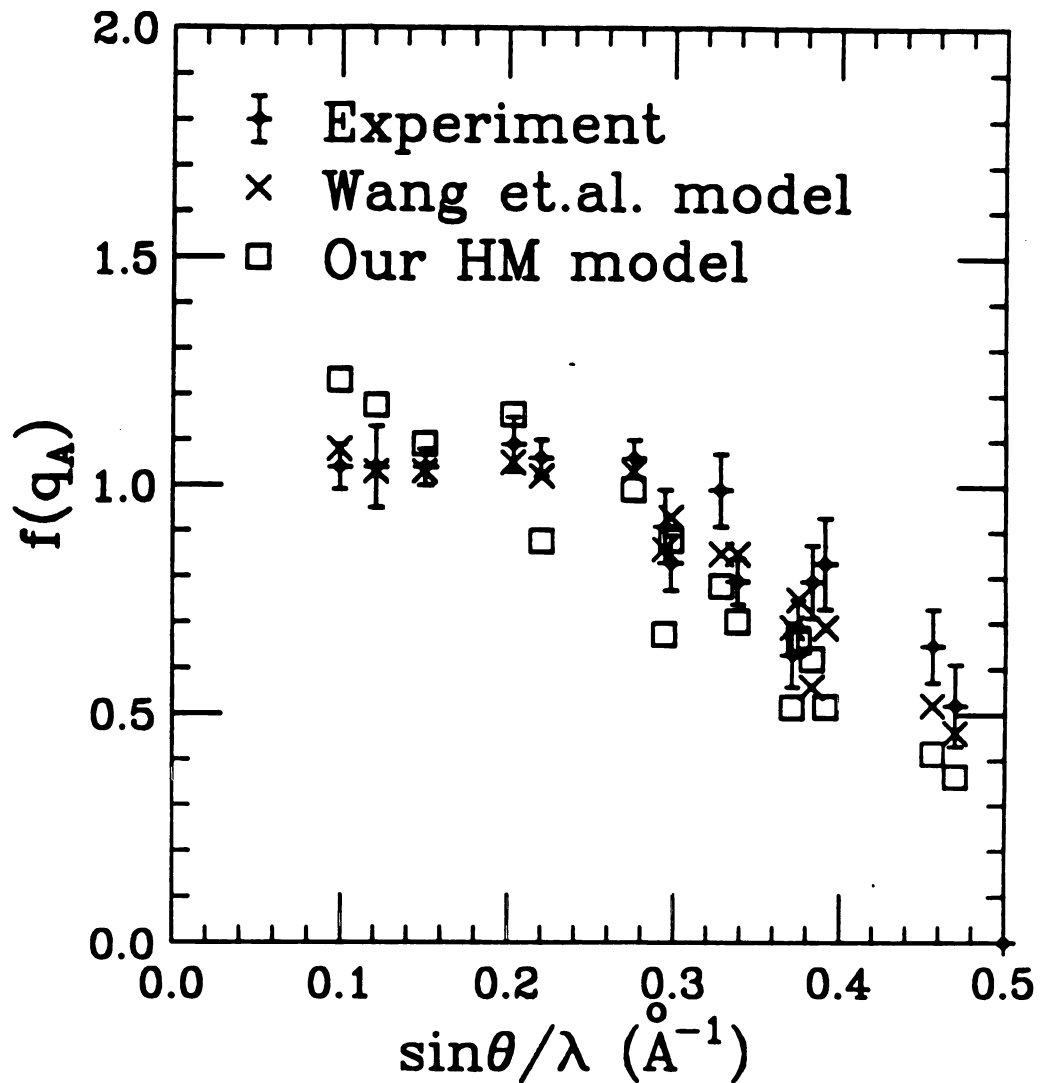


Figure 3.4: Comparison of Hubbard-Marshall model calculation with the experiment for La_2NiO_4 [wang91]. The square symbols are our HM model calculation with 2 e_g orbitals and the diagonal cross symbols are Wang. et. al.'s model calculation [wang91] using spherical d orbitals (see the text for details). It is noted that the total form factor is normalized to 2 in this case. The covalence parameters, A_1 and A_2 , in our form factor calculation, were chosen to be 0.40 and 0.30 respectively by least square fit to the experiment.

where there are one Ni^{2+} ion and 4 ligand O^{2-} ions in the NiO_2 plane, might not be appropriate for La_2NiO_4 . We have to allow for out of plane spin transfer for the Ni compounds. It is noted that the out of plane spin transfer is not cancelled because the out of plane oxygen is not shared by two antiferromagnetically ordered Ni^{2+} 's. There is another possibility where there is a spin transfer to the 2s orbitals of the ligands, which were not included in our model calculation.

In order to overcome this deficiency of our form factor model calculations, we have carried out *ab initio* cluster calculations of form factors that start from molecular orbitals which are linear combinations of basis functions including all the possible orbitals in the ligands as well as in the magnetic ion. In the cluster we take into account the out of plane oxygens also. The next three chapters are about the *ab initio* cluster calculations of the form factor of transition metal compounds including La_2NiO_4 .

Chapter 4

Ab initio cluster calculation of neutron scattering form factor

4.1 Introduction

In order to resolve the puzzle about the degree of covalence in the ordered moment of the cuprate materials discussed in Chap.1, we had to find a more accurate theory to calculate the form factor. The Hubbard-Marshall model does not seem to be a good model to get correct covalence because it failed to give the form factor for La_2NiO_4 correctly as discussed in Chap.[3].

A band calculation of the form factor of La_2NiO_4 using the local-spin-density approximation (LSDA) was reported by Wang et. al. [wang92]. However their calculated magnetic moment was found to be far too small, $0.45 \mu_B$ for each Ni^{2+} , which is much smaller than the observed value, namely about $1.0 \mu_B$. When they compared the shape of the form factor with experiment, the agreement was rather poor[wang92]. The case of La_2CuO_4 was found to be even worse. LSDA did not give the observed antiferromagnetic ordering for La_2CuO_4 [pick89]; i.e. it gave zero for the ordered moment. In $\text{Sr}_2\text{CuO}_2\text{Cl}_2$, Wang et. al. [wang90] using LSDA also got a very small moment and the agreement of the shape of the form factor

with experiment was as poor as in La_2NiO_4 . Poor agreement between LSDA (or LDA) results with experiment suggests that these approximations do not give a correct description of the ground state wave function of the system because of the strong intra-atomic correlation in LSDA .

At this point we decided to use quantum chemical *ab initio* methods to calculate the ground state wave function and the neutron form factor. There were some *ab initio* cluster calculations for La_2CuO_4 and $\text{YBa}_2\text{Cu}_3\text{O}_6$ reported [mart91, sula90] in the literature. But none of them studied the magnetic form factor.

In this chapter, I give a brief review of the quantum chemical *ab initio* methods: the Hartree-Fock (HF) approximation, and multi-configuration self-consistent-field (MCSCF) and configuration interaction (CI) approaches beyond HF. I describe how we calculate the form factor from the wave function obtained by *ab initio* methods. Then I address how we choose the cluster and how we treat the environment outside the cluster.

4.2 General theory of *ab initio* calculation methods

In this section, I review various *ab initio* methods to obtain the ground state wave function of a cluster using quantum chemistry technique. This review is based on Prof. J. F. Harrison's lecture notes and some reference books [levi91, mcwe89, lowe78].

In general an *ab initio* calculation via the variation method rigorously involves the following steps.

(1) Write down the hamiltonian operator $\hat{\mathcal{H}}$ for the system.

(2) Select some mathematical functional form ψ as a trial wave function with variable parameters.

(3) Minimize $E = \langle \psi | \hat{\mathcal{H}} | \psi \rangle$ with respect to the parameters.

The term *ab initio* is used to describe calculations in which the three steps listed above are all explicitly performed. In this section, we describe a certain kind of *ab initio* calculation called the self-consistent-field (SCF) method.

4.2.1 Hartree-Fock(HF) Self-Consistent-Field (SCF) method

In the non-relativistic limit, the electronic hamiltonian, $\hat{\mathcal{H}}$, for an N electron system can be written as follows, (We use atomic units.)

$$\hat{\mathcal{H}} = \sum_i \hat{f}_i + \sum_{j>i} \sum_i \hat{g}_{ij} \quad (4.1)$$

where

$$\hat{f}_i = -\frac{1}{2}\nabla_i^2 - \sum_{\alpha} \frac{Z_{\alpha}}{r_{i\alpha}}, \quad (4.2)$$

$$\hat{g}_{ij} = \frac{1}{r_{ij}}, \quad (4.3)$$

where the indices i, j refer to the electrons and α refers to the nuclei of the system. In atomic units, the electron charge, e , is 1 and the Bohr radius a_o is 1, the atomic unit (a.u.) of energy is $e^2/a_o = 27.2114eV$ and the atomic unit of length is $a_o = 0.52916\text{\AA}$.

The total hamiltonian for the system is the sum of the above electronic hamiltonian $\hat{\mathcal{H}}$ and the nuclear repulsion term, $V_{NN} = \frac{1}{2} \sum_{\alpha} \sum_{\beta \neq \alpha} (Z_{\alpha} Z_{\beta} / r_{\alpha\beta})$, which gives a constant contribution to the total energy.

We seek the solution of $\hat{\mathcal{H}}\psi = E\psi$, via the variational method. The most widely used form of the trial wave function of a many electron system is a Slater determinant.

A Slater determinant can be written with antisymmetrizer operator \mathcal{A} on the product of spin orbitals,

$$\psi = \mathcal{A}|\phi_1(1)\dots\phi_N(N)\rangle. \quad (4.4)$$

Here the $\phi_i(\vec{r}_j) \equiv \phi_i(j)$'s are one-electron functions, called spin orbitals which is a product of a space and a spin function.

For a simple illustration, consider a closed shell of an N electron system, where any single spatial orbital, ϕ_i , is occupied by an up (α) and a down (β) electron. (See the reference [mcwe89] for the open shell case.) The Slater determinant for a closed shell becomes

$$\psi = \mathcal{A}|\phi_{1\alpha}(1)\phi_{1\beta}(2)\dots\phi_{N/2\alpha}(N-1)\phi_{N/2\beta}(N)\rangle. \quad (4.5)$$

The electronic energy is

$$E = \langle\psi|\hat{\mathcal{H}}|\psi\rangle \quad (4.6)$$

$$= 2 \sum_i^{N/2} f_i + \sum_{i<j}^{N/2} (2J_{ij} - K_{ij}) \quad (4.7)$$

where

$$J_{ij} \equiv \langle\phi_i(1)\phi_j(2)|\frac{1}{r_{12}}|\phi_i(1)\phi_j(2)\rangle \quad (4.8)$$

$$K_{ij} \equiv \langle\phi_i(1)\phi_j(2)|\frac{1}{r_{12}}|\phi_i(2)\phi_j(1)\rangle \quad (4.9)$$

The minimization of E with respect to the functions ϕ_i leads to the Hartree-Fock (HF) equations,

$$\hat{\mathcal{F}}(1)\phi_i(1) = \varepsilon_i\phi_i(1) \quad i = 1, 2, \dots, N/2 \quad (4.10)$$

where $\hat{\mathcal{F}}$ is the Fock operator defined as

$$\hat{\mathcal{F}}(1) = \hat{f}(1) + \sum_{j=1}^{N/2} (2\hat{J}_j(1) - \hat{K}_j(1)), \quad (4.11)$$

where the Coulomb operator \hat{J}_j and the exchange operator \hat{K}_j are defined by

$$\hat{J}_j(1) = \int dv_2 \phi_j(2) \hat{g}(1,2) \phi_j(2) \quad (4.12)$$

$$\hat{K}_j(1) = \int dv_2 \phi_j(2) \hat{g}(1,2) \hat{P}_{12} \phi_j(2). \quad (4.13)$$

Here \hat{P}_{12} is the permutation operator that exchanges the pair of electrons, 1 and 2.

In general, an orbital, ϕ_i , called a molecular orbital (MO) for a molecule, is written as a linear combination of one-electron atomic basis function χ_μ

$$\phi_i = \sum_{\mu} C_{\mu i} \chi_{\mu}. \quad (4.14)$$

The basis functions χ_μ could be Gaussian type or Slater type centered on the atomic positions in a molecule. Substitution of the expansion of Eq. (4.14) into the HF equation, Eq. (4.10), gives

$$\sum_{\mu} C_{\mu i} \hat{\mathcal{F}} \chi_{\mu} = \varepsilon_i \sum_{\mu} \chi_{\mu} C_{\mu i}. \quad (4.15)$$

Multiplying Eq. (4.15) by χ_{ν}^* and integrating over the electronic coordinate gives

$$\sum_{\mu} C_{\mu i} (F_{\nu\mu} - \varepsilon_i \Delta_{\nu\mu}) = 0, \quad (4.16)$$

where $F_{\nu\mu} = \langle \chi_{\nu} | \hat{\mathcal{F}} | \chi_{\mu} \rangle$ is the Fock matrix and $\Delta_{\nu\mu} = \langle \chi_{\nu} | \chi_{\mu} \rangle$ is the overlap matrix. Eq. (4.16) is called the Hartree-Fock-Roothan equation. Requiring a non-trivial solution leads to a secular equation $\det(F_{\nu\mu} - \varepsilon_i \Delta_{\nu\mu}) = 0$. Eq. (4.16) is usually solved by an iterative process; the $F_{\nu\mu}$ integrals depend on the orbitals ϕ_i which depend on the unknown coefficients $C_{\mu i}$'s.

The eigenvalues of the HF equation, ε_i 's, are called orbital energies or one-electron energies of the corresponding MO ϕ_i 's. The total electronic energy of the system is given as

$$E = 2 \sum_i^{N/2} \varepsilon_i - \frac{1}{2} \sum_{i,j}^{N/2} (2J_{ij} - K_{ij}). \quad (4.17)$$

The total HF energy is given as

$$E_{HF} = E + V_{NN}, \quad (4.18)$$

where V_{NN} is the nuclear repulsion.

In a real implementation of the SCF procedure, the computer program looks for the $C_{\mu i}$'s to give the minimum E_{HF} , for fixed nuclear positions. Then one often optimizes this total energy to find the best nuclear positions (although we will not be concerned with the latter).

When the molecular orbitals, ϕ_i , are treated as spin-independent such as $\phi_{i,\alpha} = \phi_{i,\beta}$, as we did above, this procedure is called the restricted Hartree-Fock (RHF). On other hand, if we allow $\phi_{i,\alpha}$ and $\phi_{i,\beta}$ to differ, it is called the unrestricted Hartree-Fock (UHF) procedure.

4.2.2 Beyond the Hartree-Fock approximation

The Hartree-Fock energy of Eq. (4.18) will be lowered as the basis set is improved, approaching a limiting value as the basis set approaches a mathematical completeness. This limiting energy value is called the Hartree-Fock energy. This HF energy is however not as low as the exact energy of the system. This is because the Fock operator $\hat{\mathcal{F}}$ in Eq. (4.10) treats each electron moving in the *average* potential field due to the other electrons in the system. Since the electrons repel each other, in

reality the movement of one electron affects the movement of the other remaining electrons, i.e. their motions are correlated. The HF energy is higher than the true energy because the HF wavefunction, which is a single Slater determinant, is formally incapable of describing this correlated motion. The energy difference between the HF energy and the exact energy of a system is referred to as the *correlation energy*.

In order to overcome the restriction of a single determinant, we can introduce some mathematical flexibility by allowing ψ to contain many determinants. This leads to one of the techniques, called configuration interaction (CI). The basic idea of CI is simply to take the wavefunction ψ as a linear combination of many Slater determinants:

$$\psi = \sum_{I=1}^{N_{CSF}} C_I |I\rangle, \quad (4.19)$$

where $|I\rangle$, called a configuration state function (CSF), is a linear combination of determinants,

$$|I\rangle = \sum_{j=1}^{N_I} |D_j\rangle c_{jI}. \quad (4.20)$$

The $|D_j\rangle$'s are single determinants with different occupation schemes. In order to form $|D_j\rangle$, one starts from the SCF occupied and virtual (unoccupied) MO's. The CSF, $|I\rangle$, is formed from $|D_j\rangle$'s to be an eigenstate of the spin operator \hat{S}^2 and \hat{S}_z and classified as singly excited, doubly excited and triply excited according to whether 1,2,3 electrons are excited from occupied to unoccupied (virtual) orbitals. The most common type of CI calculation includes the singly and doubly excited CSF, usually designated as CISD. After constructing CSF's from SCF MO's, we minimize $E = \langle \psi | \hat{\mathcal{H}} | \psi \rangle$ with the new ψ of Eq. (4.19) with respect to CI the coefficients, C_I .

In order to increase the efficiency of a CI calculation (fast convergence and less computing effort), one can construct CSF's from non-SCF MO's, in contrast to the CI which starts from SCF MO's. The multi-configuration SCF (MCSCF) [shep88] is one way to do that and we have used MCSCF to investigate correlation effects in our cluster calculation. In an MCSCF calculation, the CSF's are constructed in the same way as in CI, but in the MCSCF, the configuration state function (CSF) is allowed to vary in addition to the CI coefficients, C_I 's. The CSF can be optimized by varying the MO coefficients, $C_{\mu i}$, of MO, ϕ_i 's in Eq. (4.14). (It is noted that the determinant, $|D_j\rangle$, is constructed from these MO's.)

For a simple 2-electron illustration of showing the difference between CI and MCSCF, one can consider ψ as

$$\psi = C_1|1\rangle + C_2|2\rangle \quad (4.21)$$

where

$$\begin{aligned} |1\rangle &= |D_1\rangle = \mathcal{A}|\phi_1\phi_2\rangle \\ |2\rangle &= |D_2\rangle = \mathcal{A}|\phi_3\phi_4\rangle. \end{aligned} \quad (4.22)$$

ϕ_1 and ϕ_2 are occupied SCF MO's and ϕ_3 and ϕ_4 are unoccupied SCF MO's, which form a doubly excited CI calculation. Each ϕ_i is expanded in basis functions, $\phi_i = \sum_{\mu} C_{\mu i}\chi_{\mu}$. In the CI calculation one varies only C_1 and C_2 , while in MCSCF one varies the CI coefficients, C_1 and C_2 , and the molecular orbital coefficients, $C_{\mu i}$'s, simultaneously to optimize the wavefunction ψ .

4.2.3 Natural orbitals

We will now introduce the idea of natural orbitals (NO). These turn out to be convenient for calculating physical quantities such as charge density and spin

1

is
de

density in terms of the one-particle density matrix in the basis of NO's.

From a MCSCF (or CI) wavefunction, $\psi(1, 2, \dots, N)$, the one particle density matrix is defined as

$$\gamma(1'|1) = N \int \psi^*(1', 2, \dots, N) \psi(1, 2, \dots, N) d\tau(2, \dots, N), \quad (4.23)$$

which satisfies

$$\int \gamma(1|1) d\tau(1) = N. \quad (4.24)$$

The electron density $\rho(\vec{x}_1)$ is given as

$$\rho(\vec{x}_1) = \gamma(1|1) \quad (4.25)$$

When $\psi(1, 2, \dots, N)$ is expressed in terms of MO's, Eq. (4.23) is written as

$$\gamma(1'|1) = \sum_i \sum_j \phi_i^*(1') \phi_j(1) A_{ij}, \quad (4.26)$$

where A_{ij} is defined in Eq. (B.5) of Appendix B and ϕ_i is a spin-orbital. By a unitary transformation, the matrix, A_{ij} can be diagonalized and $\gamma(1'|1)$ can be written in terms of diagonal matrix elements, n_i , and new orbitals $\tilde{\phi}_i$:

$$\gamma(1'|1) = \sum_i \tilde{\phi}_i^*(1') \tilde{\phi}_i(1) n_i. \quad (4.27)$$

The spin orbitals, $\tilde{\phi}_i$'s are called the *natural orbitals* (NO) and n_i is the occupation number of NO $\tilde{\phi}_i$.

The expectation value of the spin operator $\hat{S}_z = \sum_i^N \hat{S}_z(i) \delta(\vec{r} - \vec{r}_i)$, where $\hat{S}_z(i)$ is spin state ($\frac{1}{2}$ or $-\frac{1}{2}$) of i-th electron, can be written, using the one-particle density matrix,

$$\langle \hat{S}_z \rangle = \int_{1'=1} \hat{S}_z(1) \gamma(1'|1) d\tau(1) \quad (4.28)$$

Substituting $\gamma(1'|1)$ from Eq. (4.27) and Eq. (4.28) gives,

$$\langle \hat{S}_z \rangle = \int_{1'=1} \hat{S}_z(1) \sum_i n_i \tilde{\phi}_i^*(1') \tilde{\phi}_i(1) d\tau(1), \quad (4.29)$$

$$= \int \sum_i \frac{1}{2} \sigma_i n_i |\tilde{\phi}_i(1)|^2 d\tau(1), \quad (4.30)$$

where σ_i gives the spin state (+1 or -1) for up or down spin and n_i is the occupation number of the i -th spin-orbital.

From Eq. (4.30), we define a spin density, $s(\vec{r})$, in terms of NO's as

$$s(\vec{r}) = \sum_i \frac{1}{2} \sigma_i n_i |\tilde{\phi}_i(\vec{r})|^2. \quad (4.31)$$

As seen from Eq. (4.31), a physical quantity such as the local spin density can be represented by a simple form using NO's. In HF-SCF calculations, MO's are the same as NO's and the n_i are either 0 or 1. But in MCSCF or CI calculations, they are not (and the n_i 's are in general a fractional number between 0 and 1). Knowledge of the natural orbitals and occupation numbers allows us to calculate the spin density and thus the form factor. In our MCSCF calculation using the COLUMBUS code[colu88], the NO's are not available for up and down (α and β) electrons separately, directly from the code. Therefore we have developed appropriate programs to convert the MO's to NO's by constructing the matrix A_{ij} for α and β electrons separately. The details of developing the programs are described in Appendix B.

4.3 Theoretical form factor

The spin density of a molecule or a cluster can be rewritten from Eq. (4.31),

$$s(\vec{r}) = S_z \frac{1}{n} \sum_j^{occ} n_j \sigma_j |\phi_j(\vec{r})|^2, \quad (4.32)$$

0
0

T
A
by

where $\phi_j(\vec{r})$ is now the j -th natural orbital (NO) obtained from the HF or MCSCF calculations; $n = n_\uparrow - n_\downarrow$ where n_\uparrow (n_\downarrow) is sum of the occupation numbers of up(down) spin natural orbitals, so that $n = 1$ for a doublet spin state and $n = 2$ for a triplet state. When mean field theory (MFT) for the antiferromagnetic crystal is assumed, S_z is 1/2 for a doublet cluster state and 1 for a triplet cluster state.

We made an *ansatz* that the total spin density in the antiferromagnetic (AF) ordered crystal is given by the sum of contributions associated with each magnetic ion (or each of our clusters)

$$S(\vec{r}) = \sum_{\vec{n}} e^{i\vec{q}_A \cdot \vec{n}} s(\vec{r} - \vec{n}), \quad (4.33)$$

where \vec{n} is a lattice vector associated with the chemical unit cell, and \vec{q}_A is a particular AF wave vector: $e^{i\vec{q}_A \cdot \vec{n}}$ is $+1(-1)$ at up(down)-spin sites \vec{n} .

The experimentally measurable quantity from the neutron Bragg scattering is the Fourier transform of the magnetic moment density per unit cell, $g\mu_B S(\vec{r})/N$, (N is the number of unit cells) ;

$$\begin{aligned} m(\vec{q}) &= g\mu_B \frac{1}{N} \int S(\vec{r}) e^{-i\vec{q} \cdot \vec{r}} d\vec{r} \\ &= g\mu_B \frac{1}{N} \sum_{\vec{n}} e^{i\vec{q}_A \cdot \vec{n}} \int s(\vec{r} - \vec{n}) e^{-i\vec{q} \cdot \vec{r}} d\vec{r} \\ &= g\mu_B \frac{1}{N} \sum_{\vec{n}} e^{-i(\vec{q} - \vec{q}_A) \cdot \vec{n}} \int s(\vec{r}) e^{-i\vec{q} \cdot \vec{r}} d\vec{r}. \end{aligned} \quad (4.34)$$

The sum $\sum_{\vec{n}} e^{-i(\vec{q} - \vec{q}_A) \cdot \vec{n}}$ gives the Bragg peaks which are localized at the general AF wave vectors \vec{q}_A . The variation of the intensity of the Bragg peaks is controlled by

$$\begin{aligned} m(\vec{q}_A) &= g\mu_B \int s(\vec{r}) e^{-i\vec{q}_A \cdot \vec{r}} d\vec{r} \\ &= g\mu_B S_z f(\vec{q}_A), \end{aligned} \quad (4.35)$$

where $f(\vec{q})$ is the form factor defined from Eq. (4.35) and given by

$$f(\vec{q}) = \frac{1}{S_z} \int s(\vec{r}) e^{i\vec{q}\cdot\vec{r}} d\vec{r}. \quad (4.36)$$

In our cluster calculation, each natural orbital (NO) for a cluster is a linear combination of basis functions such as

$$\phi(\vec{r}) = \sum_k \chi_k^M(\vec{r}) + \sum_j \sum_l \chi_l^{L_j}(\vec{r}), \quad (4.37)$$

where χ_k^M is a basis function centered at the metal and $\chi_l^{L_j}$ is a basis function centered at the j -th ligand. The subscripts, k and l label the individual basis functions for the metal and the ligands respectively (for simplicity, we dropped the index j associated with the NO's in Eq. (4.36)). The probability density associated with the NO, $|\phi(\vec{r})|^2$ becomes

$$\begin{aligned} |\phi(\vec{r})|^2 = & \sum_{k,k'} \chi_k^M \chi_{k'}^M + 2 \sum_{k,l} \sum_i \chi_k^M \chi_l^{L_i} + \sum_{i,l} \sum_{i',l' \neq i,l} \chi_l^{L_i} \chi_{l'}^{L_{i'}} \\ & + \sum_i \sum_l \chi_l^{L_i} \chi_l^{L_i} \end{aligned} \quad (4.38)$$

Again for simplicity, the basis function χ is assumed to include its NO coefficient. When the i -th ligand is shared by two nearby magnetic metal ions such as Cu^{2+} 's with antiparallel spins in the CuO_2 plane, the contributions to $f(\vec{q})$ from the last term of Eq. (4.38) are cancelled by each other at $\vec{q} = \vec{q}_A$. This leads to the well-known covalent reduction in the form factor as discussed in Chap.3.

When we take account of the spin fluctuations beyond the mean field theory (MFT), S_z in Eq. (4.35) becomes the average value of the spin in the Heisenberg model, $\langle S_z \rangle_{\text{Heis}}$, instead of the MFT value (1 for Ni and 1/2 for Cu) [kapl92] (see Chap. 2). Thus we now have the magnetic moment density, $m(\vec{q}_A)$, in terms

of $\langle S_z \rangle_{Heis}$ which includes the quantum spin fluctuation effect, and $f(\vec{q}_A)$ which differs from the mean field value by the covalence discussed in Chap. 2:

$$m(\vec{q}_A) = g\mu_B \langle S_z \rangle f(\vec{q}_A). \quad (4.39)$$

4.4 Cluster and environment

4.4.1 Cluster

In all our cluster calculations, we have taken the basic cluster to consist of one central metal and 6 or 5 surrounding ligand ions, $(MX_{6(5)})$ cluster, $M = \text{Ni}$ or Cu and $X = \text{F}$ or O . The geometry of the cluster, $(MX_{6(5)})$, was taken from the structure of each compound, thus it has an octahedral symmetry for KNiF_3 and NiO , tetragonal symmetry for La_2NiO_4 , La_2CuO_4 , $\text{Sr}_2\text{CuO}_2\text{Cl}_2$, and still lower symmetry for $\text{YBa}_2\text{Cu}_3\text{O}_6$.

In order to construct molecular orbitals for a cluster, Wachters' [wach70] basis set, denoted as (13s9p5d), was used for Ni and Cu. For F, O, and Cl, we used Huzinaga [huzi71] basis sets with additional diffuse p orbital, which denoted as (9s6p). These basis sets, (13s9p5d) and (9s6p), are contracted to [7s3p2d] and [3s3p] respectively (see Ref.[levi91] for basis set denotation and contraction). The basis set (14s11p6d) for Ni with additional diffuse functions suggested by P.J. Hay [hay77] is also used to see how sensitive the calculations are to adding the diffuse basis functions for the metal ion. These two basis sets, (14s11p6d) and (13s9p5d) give the same form factor and charge density (difference is less than 1.5 %), even though Mulliken charge values are different. (See Appendix C for further discussion of this point.) Thus we present the results of the form factor with basis set (13s9p5d) for Ni and Cu.

4

E

n

p

tl

va

n

le

le

4.4.2 Point charge model

In order to generate the Madelung potential around a cluster, the point charge model was employed. We used Evjen's method [evje67] to carry this out. Formal ionic charges (for example in KNiF_3 , +2, -1 and +1 point charges for Ni^{2+} , F^- and K^+ respectively) were assigned to the atomic positions and fractional charge values on the boundary were taken such as to make the whole system charge neutral. For fractional charges, first we set up a cube as a Madelung cage, which contains point charges at the atomic positions. Then if we count each ion on a surface of the cube as being half in the cube, each one on an edge as being a quarter inside, and each one at a corner as being one-eighth inside, the total charge within the cube is zero.

This Evjen's method was reported to work well in the electronic structure calculation of perovskite and fcc structure materials like KNiF_3 and NiO [sous93].

4.4.3 Effective core potential(ECP)

For a more realistic treatment of the extra cluster environment, we replaced the nearby point charges by effective core potential (ECP), which enables us to incorporate Pauli repulsion between the electrons in the cluster and the environment.

ECP was originally developed to reduce the computational effort in generating the valence electron wave function in an atom, by doing calculations only for those valence electrons, instead of doing all electron calculations. The core-valence interaction is represented by an effective core potential acting on the valence electrons. In our calculation, we used ECP to generate a potential seen by the electrons of a cluster arising from the nearby extra-cluster ions. Here we review

how ECP is generated as a product of Gaussian function and polynomials following Ref. [wadt85].

The generation of effective core potentials (ECP's) begins with numerical Hartree-Fock orbitals. From HF orbitals, nodeless pseudo-orbitals are generated. Then a numerical potential is rigorously obtained from the pseudo-orbitals and then fitted to an analytic form. The underlying procedure consists of three major steps as discussed below.

(1) Set up the pseudo-orbitals, $\tilde{\phi}_l$'s, which are smooth and nodeless, from HF orbitals ϕ_l . The valence pseudo-orbital, $\tilde{\phi}_l(r)$, is chosen to behave as closely as possible to the original valence HF orbital, $\phi_l(r)$, in outer region of the atom, i.e. the valence region of the atom,

$$\begin{aligned}\tilde{\phi}_l(r) &= \phi_l(r) & r \geq r_c, \\ &= r^b f(r) & 0 \leq r < r_c,\end{aligned}\tag{4.40}$$

where r_c is chosen to be close to the outermost maximum of ϕ_l , and $f(r)$ is a polynomial and b is an integer constant depending on the angular momentum l of the orbital.

(2) Determine the angular dependence potential U_l requiring $\tilde{\phi}_l$ to be a solution of the Schrödinger equation in the field of U_l plus the Coulomb (\hat{J}) and exchange (\hat{K}) operators, \tilde{V}_{val} , arising from only the valence pseudo-orbitals

$$\left[-\frac{1}{2} \frac{d^2}{dr^2} + \frac{l(l+1)}{2r^2} - \frac{Z}{r} + U_l(r) + \tilde{V}_{val} \right] \tilde{\phi}_l(r) = \epsilon_l \tilde{\phi}_l(r),\tag{4.41}$$

$$\tilde{V}_{val} = \sum_i a_i \hat{J}(\tilde{\phi}_i) - b_i \hat{K}(\tilde{\phi}_i).\tag{4.42}$$

From Eq. (4.41), U_l can be determined in terms of $\tilde{\phi}_l$ and $\tilde{\phi}_l''$,

$$U_l(r) = \epsilon_l - \frac{l(l+1)}{2r^2} + \frac{Z}{r} + \frac{\tilde{\phi}_l''}{2\tilde{\phi}_l} - \frac{\tilde{V}_{val}\tilde{\phi}_l}{\tilde{\phi}_l}.\tag{4.43}$$

(3) From the numerical potentials $U_l(r)$ in Eq. (4.43), the product of r^2 and $U_l(r)$ is fitted to the analytic form as

$$\sum_k d_k r^{n_k} \exp[-\zeta_k r^2], \quad (4.44)$$

where $n_k = 0, 1, \text{ or } 2$. The parameters, d_k and ζ_k are optimized using least squares procedure. In general, those parameters to be used to generate ECP's are listed in the literature.

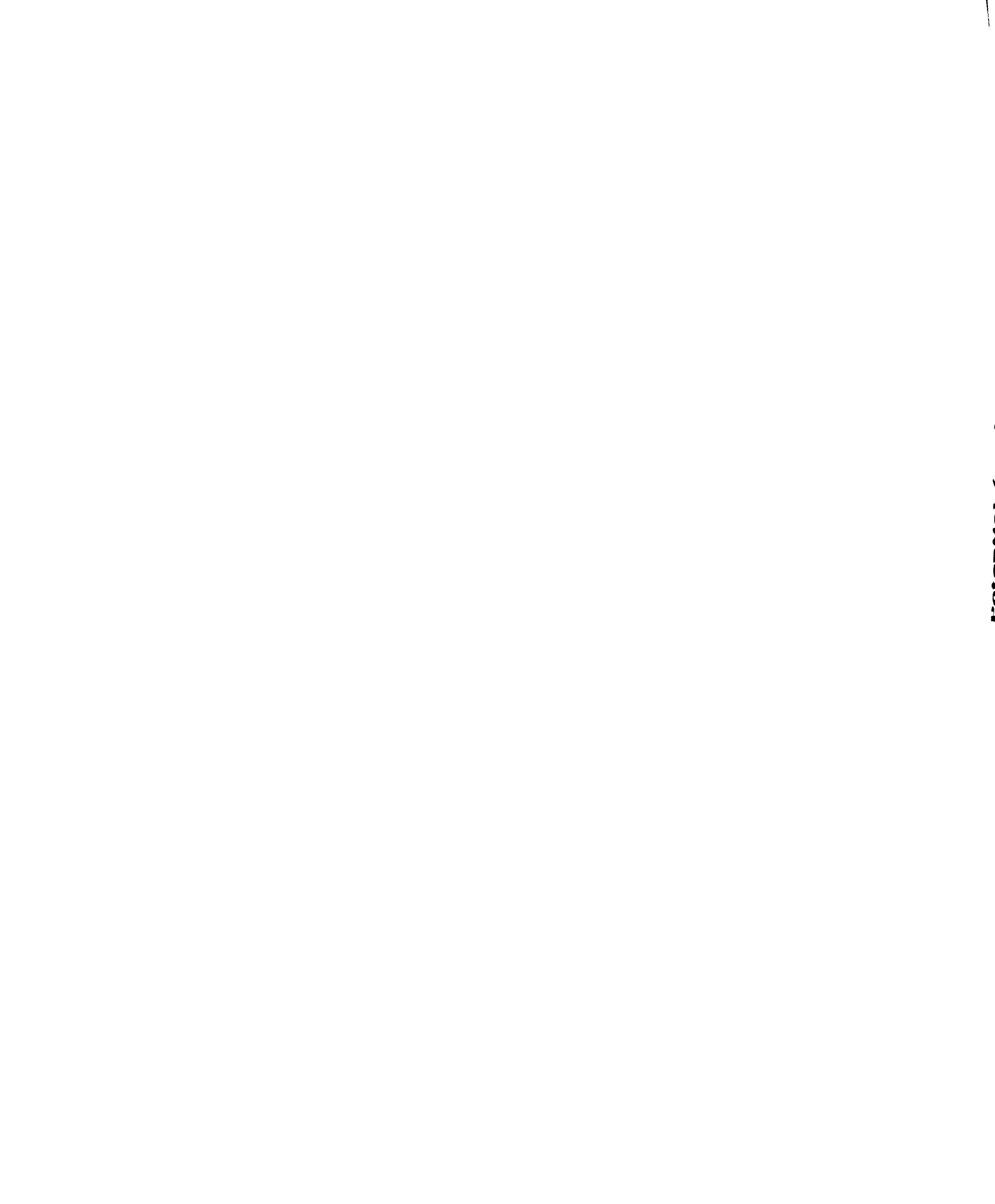
The total potential is represented as

$$U(r) = U_L(r) + \sum_{l=0}^{L-1} [U_l(r) - U_L(r)] \hat{P}_l, \quad (4.45)$$

where \hat{P}_l is core projection operator as $\hat{P}_l = |l \rangle \langle l|$, and L is one greater than the highest angular momentum quantum number of any core orbital.

In Fig. 4.1, the s, p, d and f effective core potentials of the La^{3+} ion are plotted as examples of the numerical ECP's obtained by the above procedure and listed in Ref. [wadt85]. In the figure, the potential $U_l(r) - Z_v/r$ has been plotted, where $Z_v = (Z - Z_{core})$. Thus $Z_v = 3$ for La^{3+} ECP. The plotted ECP's are compared with the point charge potential, $-3/r$, to show the difference between them. The electrons of the cluster experience this difference when the point charges are replaced by ECP's in our calculations.

As seen in Fig. 4.1, the valence electrons (or the electrons in the cluster in our calculation) with s or p angular momentum (with respect to the center of the La^{3+} ion) experience strong repulsion, while the valence electrons with d and f angular momentum experience attraction at small r . (r is the distance from La^{3+} ion center.) At large r , all the potentials behave as the point charge potential, $-3/r$.



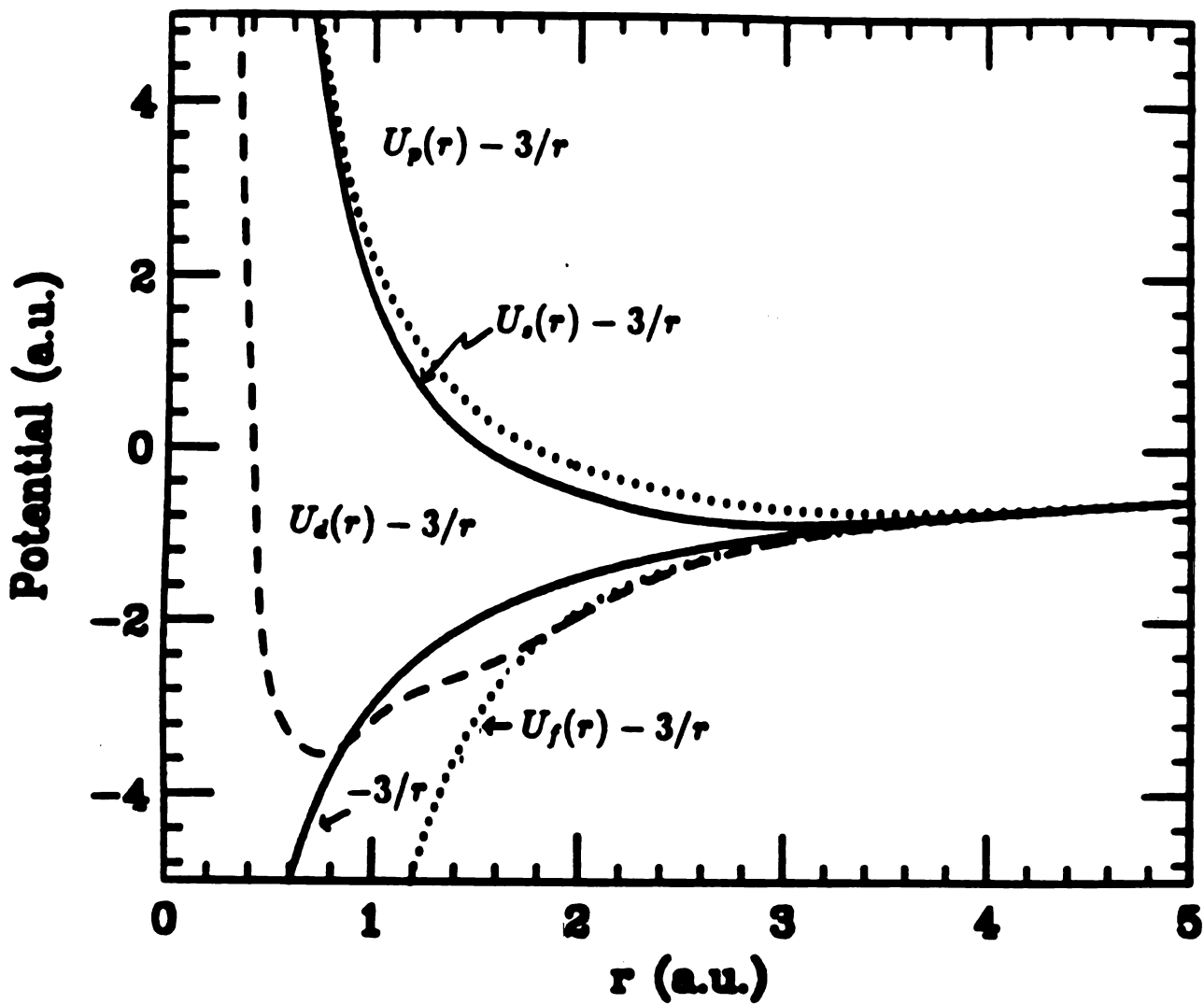


Figure 4.1: The s, p, d and f effective core potentials for La^{3+} are plotted in the form, $U_i(r) - 3/r$. These potentials behave as the point charge potential, $-3/r$ in the large r region.

Chapter 5

Neutron scattering form factor of the nickel compounds

5.1 Introduction

Since we decided to carry out a more realistic calculation of the neutron scattering form factor using *ab initio* methods, we first studied the weakly covalent anti-ferromagnets KNiF_3 and NiO to test our cluster model calculations, and then we applied the same method to La_2NiO_4 . Several *ab initio* cluster calculations have been done in KNiF_3 [elli68, mosk70, soul71, wach72] and NiO [bagu77, jans88]. However, most of these works were concerned with the excitation energies rather than the ground state wave function, which is needed to obtain the neutron form factor. The only cluster calculation of the form factor was carried out for KNiF_3 [elli68] more than 20 years ago, and was considered by the authors to be too crude to even compare with the experiment. Other attempts, which had been made to get the theoretical form factor using the free ion Ni^{2+} , wave function didn't give good agreement [shar76] with experiment. This paucity of work on the theoretical form factor motivated us to carry out cluster calculations using the techniques of *ab initio* quantum chemistry which have developed rapidly during the past two

decades [kap194]. We followed a standard procedure, namely the basic cluster was chosen to contain one Ni^{2+} ion and its 6 nearest neighbor ligands (F^- ion or O^{2-} ion respectively), and the rest of the lattice was taken into account by employing the point charge model explained in Sec. [4.4.2]. Corrections to the point charge model in the form of limited Pauli repulsion were also considered by taking ECP of the nearest extra-cluster cations.

In this chapter, I discuss the results of the cluster calculations for KNiF_3 , NiO and La_2NiO_4 carried out with both RHF and UHF methods [chan94]. Then I compare our theoretical results with experiment in these nickel compounds. Especially for KNiF_3 , where absolute experimental values of Bragg scattering are available, we could estimate the quantum spin fluctuations by fitting the theoretical values to the experimental values.

5.2 KNiF_3

KNiF_3 is an antiferromagnetic insulator and is considered to be an ideal compound to test theory vis-a-vis the experiments from several points of view[huch70]. It is well-known that pure stoichiometric samples of this cubic perovskite structure material can be prepared even at low temperature. The magnetic structure of KNiF_3 is known as simple cubic G-type[scat61]. In the G-type structure, a particular magnetic ion is coupled antiferromagnetically to its six nearest magnetic neighbors. (The magnetic ions form a simple cubic structure.)

In neutron scattering experiments, the nuclear diffraction intensities are governed only by the known nuclear scattering lengths. Therefore, by comparison, these nuclear peaks may be used to obtain the magnetic cross section on an ab-

solute basis [huch70]. The magnetic form factor measurement, in other words the measurement of magnetic peak intensities for more than one Bragg peak, was carried out by two groups [huch70, scat61]. The later experiment by Hutchings and Guggenheim [huch70] gives absolute values of the intensities of the magnetic peaks. Therefore we have chosen Hutchings and Guggenheim's experiment to compare with our theoretical calculations.

5.2.1 Experimental form factor

We have determined the form factor from the measured intensities of neutron powder diffraction in KNiF₃ in Ref. [huch70]. Hutchings and Guggenheim measured the Bragg peak intensities at 4.2 K. The lattice parameter of the chemical(nuclear) unit cell shown in Fig. 5.1 is $a_o = 4.00\text{\AA}$. But the lattice parameter of the antiferromagnetic unit cell is doubled from that of the nuclear unit cell and is $2a_o = 8.00\text{\AA}$. The magnetic peaks are indexed according to the magnetic unit cell.

Experimentally, one can determine $g < S_z > f(\vec{q}_M)$ from the ratio of nuclear and magnetic Bragg peak intensities . This quantity is related to several experimentally measured quantities by the equation (see Ref. [huch70])

$$\begin{aligned} \{g < S_z > f(\vec{q}_M)\}^2 &= \frac{I_M z_N F_N^2}{I_N v_n^2} \frac{v_m^2}{z_M F_M^2 N_M^2} \left(\frac{2mc^2}{e^2\gamma} \right)^2 \\ &\times \frac{\exp\{-2\bar{B}(\sin\Theta_N/\lambda)^2\} \sin\Theta_M \sin 2\Theta_M}{\exp\{-2\bar{B}(\sin\Theta_M/\lambda)^2\} \sin\Theta_N \sin 2\Theta_N} \end{aligned} \quad (5.1)$$

Here I_M and I_N are magnetic and nuclear peak intensities and the subscripts, M and N stand for magnetic and nuclear Bragg peaks respectively. \bar{B} is an average temperature parameter, and v_m and v_n are the volumes of magnetic

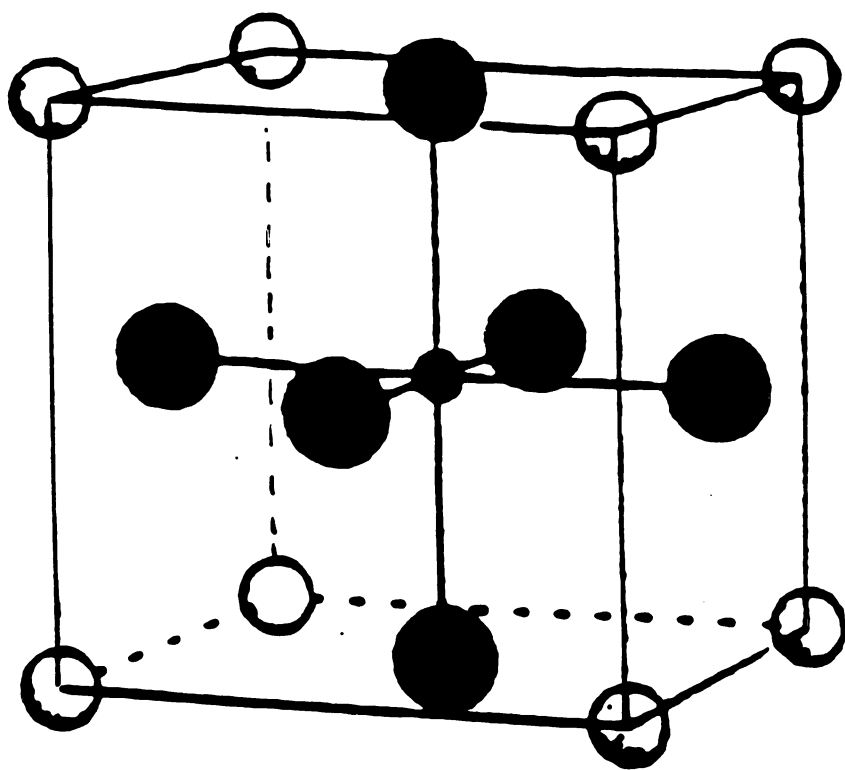


Figure 5.1: Crystal structure of KNiF_3 . The small (solid) circle is Ni^{2+} ion, and the middle-sized (empty) circles are K^+ ions, and the big (solid) circles are O^{2-} ions. The $(\text{NiF}_6)^{4-}$ cluster consists of the solid circles.

Table 5.1: Experimental values of $\langle S_z \rangle f(\vec{q}_M)$ in KNiF_3

magnetic peak index	$\langle S_z \rangle f(\vec{q}_M)$
(111)	0.783
(311)	0.672
(331)	0.552

and nuclear unit cells respectively ($v_m = 8v_n$). \vec{q}_M are the antiferromagnetic Bragg-peak wave vectors, called \vec{q}_A earlier in this thesis. The other parameters of Eq. (5.1) are structure parameters depending on the peak index. Hutchings and Guggenheim [huch70] measured 3 magnetic Bragg peaks, $(111)_M$, $(311)_M$ and $(331)_M$ and they also measured the nuclear $(200)_N$ peak which is well separated from nearby magnetic peaks. Thus we chose I_{200} as a reference nuclear peak to calculate the magnetic form factor $f(\vec{q}_M)$ in Eq. (5.1). We calculated the quantities, $[g \langle S_z \rangle f(\vec{q}_M)/F_{200}]^2$ for the 3 magnetic Bragg peaks using $F_{111} = F_{311} = F_{331} = 8$, $N_{111}^2 = N_{311}^2 = N_{331}^2 = \frac{2}{3}$, $z_{111} = 8$, $z_{311} = 24$, $z_{331} = 24$ and $z_{200} = 6$. Here $\left(\frac{2m_e c^2}{e^2 \gamma}\right)^2 = 0.2695 \times 10^{-4} \text{ \AA}$ and Θ 's can be obtained from Fig. 1 in Ref. [huch70] as $\Theta_{111} = 7.0^\circ$, $\Theta_{311} = 13.5^\circ$, $\Theta_{331} = 17.75^\circ$ and $\Theta_{200} = 8.25^\circ$. The quantity, $[g \langle S_z \rangle f(\vec{q}_M)/F_{200}]$ now involves no unknowns and so has only random experimental error. F_{200} was determined from scattering lengths as $F_{200} = b_{Ni} + (b_F - b_K)$ and was given as $F_{200} = 1.218(\pm 0.020) \text{ Cm}^{-12}$ in the same reference. Taking $g = 2.29(\pm 0.02)$ from Ref. [huch70], we obtained the values of $\langle S_z \rangle f(\vec{q}_M)$ which are listed in Table 5.1.

The quantity, $\langle S_z \rangle f(\vec{q}_M)$ is governed by quantum spin fluctuations(QSF) and covalence(COV) simultaneously as we discussed in Chap. 2. But Hutchings and Guggenheim's interpretation of the quantity, $\langle S_z \rangle f(\vec{q}_M)$, is different

from ours. They took $f(\vec{q}_M)$ at the first Bragg peak $(111)_M$ from Alperin's NiO form factor and then interpreted $\langle S_z \rangle$ to include both QSF and COV effects assuming $f(\vec{q}_M)$ is normalized to 1 when extrapolated to $|\vec{q}_M| = 0$. According to Hubbard-Marshall theory [hubb65], the antiferromagnetic form factor shouldn't be normalized to 1 when extrapolating to $|\vec{q}_M| = 0$ because of COV as discussed in Chap.3. If we knew $f(\vec{q}_M)$ which includes COV, then $\langle S_z \rangle$ should be interpreted as $\langle S_z \rangle_{Heis}$ as discussed in Chap. 2. We have therefore calculated the form factor $f(\vec{q}_M)$ and scaled our calculated values to give the best fit to the experimental quantity $\langle S_z \rangle f(\vec{q}_M)$ which then gives us $\langle S_z \rangle_{Heis}$ directly. This is compared with the spin wave theory later in Sec. 5.2.4.

5.2.2 $(\text{NiF}_6)^{4-}$ cluster

The $(\text{NiF}_6)^{4-}$ cluster in perovskite KNiF_3 has octahedral symmetry as shown in Fig. 5.1 . The distance between Ni^{2+} and F^- was taken as 2.00\AA . RHF and UHF Self-Consistent-Field (SCF) calculations on this cluster, were performed with the COLUMBUS code[colu88] and the Gaussian 92 code [g92] respectively using contracted Gaussian basis sets. All the electrons of the cluster, 86 electrons, are explicitly included in these *ab initio* calculations.

Huzinaga [huzi71] basis sets (9s6p) with additional diffuse p function are used for F. The basis set for Ni is Wachters' [wach70] basis (13s9p5d). The basis set (14s11p6d) for Ni with additional diffuse functions suggested by Hay [hay77] is also included to see how sensitive the calculations are to adding the diffuse basis functions. These two basis sets, (14s11p6d) and (13s9p5d) give the same form factor and charge density (difference is less than 1.5 %), so we present the figures of the form factor obtained with the basis set (13s9p5d) of Ni (see Appendix C

Table 5.2: Madelung potential value at the origin of the cluster in KNiF_3

number of point charges ^a	potential (eV)
82	-21.25
192	-21.16
482	-21.05
784	-20.98
1434	-20.96

^aThis number of charge does not include the cluster itself.

for further discussion of this point).

5.2.3 Environment

For the rest of the system outside the cluster, the point charge model is employed according to Evjen's method [evje67] discussed in Sec.[4.4.2] We took 482 point charges to obtain the Madelung potential for NiF_6^{4-} in KNiF_3 , after establishing a reasonable convergence in the value of the potential at the center of the cluster (variation within less than 0.2 %) shown in Table 5.2.

It should be noted that 482 point charges correspond to 64 chemical unit cells. The potential value generated by 482 point charges in KNiF_3 by Evjen's procedure is known to give an almost constant difference from the exact Madelung sum even rather far from the origin of the cluster for the perovskite KNiF_3 [sous93]. The constant difference of the Madelung potential does not affect, of course, the motion of an electron in the potential. We found that the calculated form factor hardly changed by increasing number of point charges beyond the 64 unit cells. The crystal field splitting of d electron of Ni^{2+} are discussed in Appendix [D] also

hardly changed either.

For a more realistic treatment of the environment effect in KNiF_3 , the point charges which originally represented the 8 nearest neighbor K^+ 's were replaced by Effective Core Potentials (ECP)[wadt85] in Sec.[4.4.3]. This enabled us to incorporate Pauli repulsion between electrons in the F^- 's of the cluster and those in neighboring K^+ 's. The effect of this replacement on the form factor of KNiF_3 was found to be negligible so we do not present the calculation including K^+ ECP.

5.2.4 Comparison with experiment

The theoretical AF form factor values from RHF and UHF are compared with the experimental values of Hutchings and Guggenheim [huch70] in Fig. 5.2-(a),(b). The experimental values of the product, $\langle S_z \rangle f(\vec{q}_M)$ were taken from Table 5.1.

The calculated form factor values are multiplied by the factor $\langle S_z \rangle$ to fit the experimental data. The UHF results in Fig 5.2-(b) differ slightly from the RHF results in Fig 5.2-(a), but this small difference helped to obtain a near perfect agreement between the UHF results and the experiment. The best fit to the experiment in Fig. 5.2-(b) gives $\langle S_z \rangle = 0.90$ which can be directly compared with the result of spin wave theory for the simple cubic lattice $\langle S_z \rangle_{\text{spinwave}} = 0.92$ [ande52]. The covalent reduction in KNiF_3 was found to be 0.95 in UHF calculations. (See Eq. (2.68) for the definition of the covalence reduction factor.) We conclude that the theoretical results for the magnetic moment density $m(\vec{q}_A)$ in terms of covalence and spin fluctuation effect (Eq. (4.39)), agree very well with the experimental data in KNiF_3 .

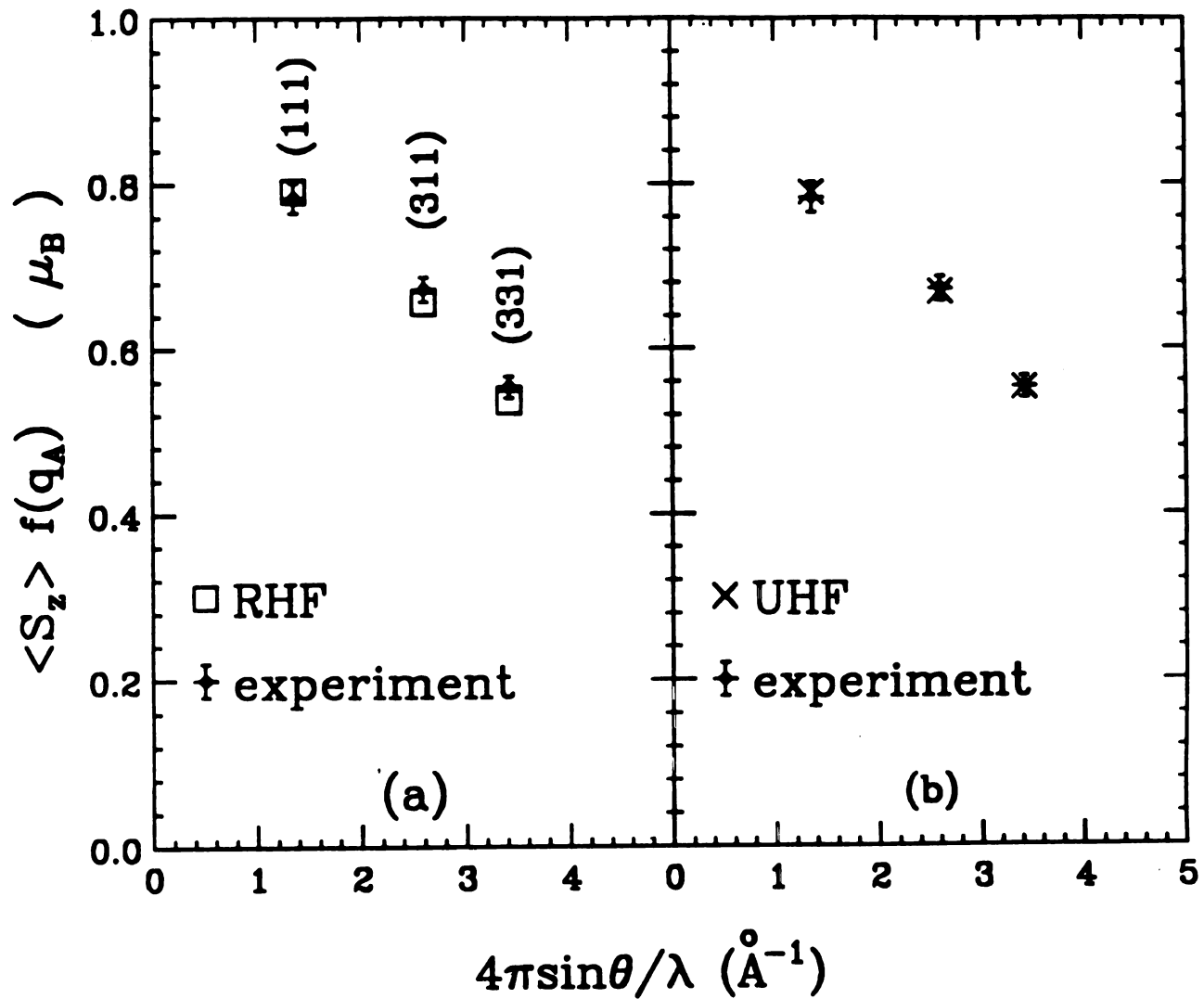


Figure 5.2: The calculated (a)RHF and (b)UHF form factor are compared with Hutchings and Guggenheim' experiment [huch70] in KNiF₃.

5.3 NiO

After the success of *ab initio* cluster methods in calculating the neutron form factor in KNiF_3 , we decided to apply the same procedure to NiO before proceeding to La_2NiO_4 . NiO had been studied for a long time both theoretically and experimentally for various physical properties. But no calculation of the magnetic form factor was available with *ab initio* or any other sophisticated theoretical methods even though experiments had been done by Alperin more than 30 years ago[alpe61]. The form factor of NiO has been measured at many Bragg peaks [alpe61] while in KNiF_3 , experiments were available for only 3 Bragg peaks[huch70]. In fact the Bragg peaks over a broad range of $|q|$ can give detailed information about the spin distribution in $|\vec{r}|$ space. Thus NiO is an excellent case to test our cluster method.

Just like KNiF_3 , NiO is an antiferromagnetic(AF) insulator with $T_N = 525\text{K}$. It has the rock-salt structure as shown in Fig. 5.3 with $a_o = 4.16\text{\AA}$.

The Ni^{2+} ions along the line Ni-O-Ni have antiparallel spins while the nearest neighboring Ni^{2+} ion spins are parallel. The spins of magnetic ions are aligned in the (111) plane forming a ferromagnetic sheet and each (111) ferromagnetic sheet is antiparallel to the adjacent (111) sheets[mart67]. The AF unit cell has the lattice parameter $2a_o = 8.32\text{\AA}$ with a fcc structure and its volume is 8 times the volume of the chemical unit cell. The Bragg peaks in NiO are indexed by that magnetic unit cell.

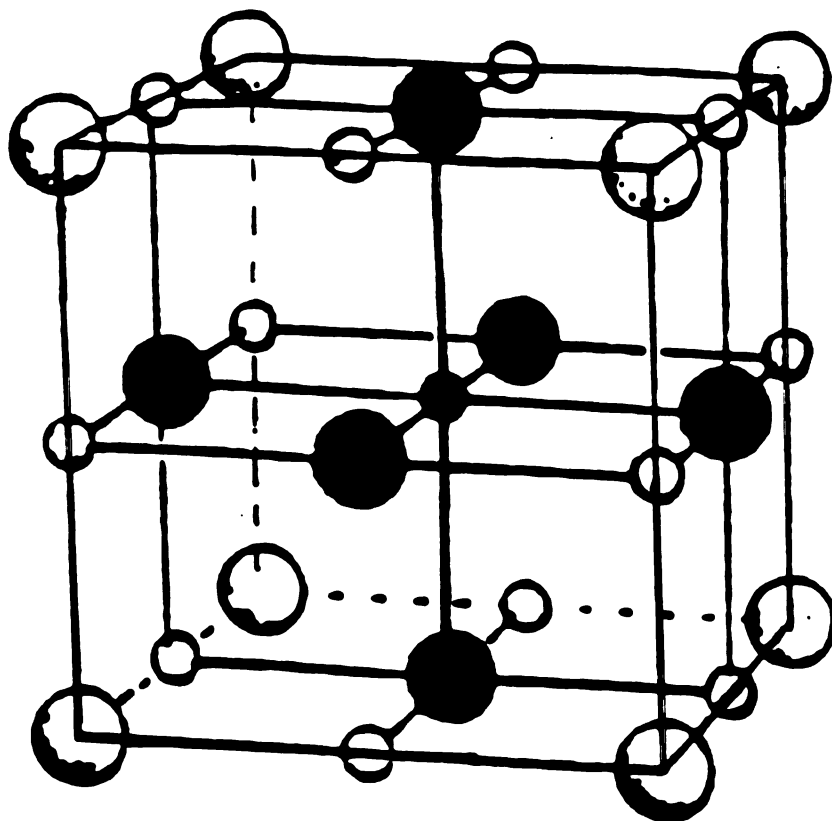


Figure 5.3: Crystal structure of NiO. The small circles are Ni²⁺ ions and the big circles are O²⁻ ions. The (NiO₆)¹⁰⁻ cluster consists of the solid circles.

Table 5.3: Madelung potential value at the origin of the cluster in NiO

number of point charges ^a	potential (eV)
118	-24.26
326	-24.19
722	-24.20
1324	-24.20

^aThis number of charge does not include the cluster itself.

5.3.1 Cluster

The $(\text{NiO}_6)^{10-}$ cluster was chosen: it has octahedral symmetry as shown in Fig. 5.3. The distance between Ni and O is 2.08\AA . All the 86 electrons of the $(\text{NiO}_6)^{10-}$ cluster were taken into account in the RHF and UHF calculations. COLUMBUS [colu88] and Gaussian 92[g92] codes were used for the RHF and the UHF respectively. Wachters' basis set (13s9p5d) for Ni[wach70] was used as in KNiF_3 and Huzinaga basis sets (9s6p) for O [huzi71] with an additional diffuse p function were used. The Mulliken charge for NiO was found to be very sensitive to the choice of the basis set for Ni. But physically significant quantities, the form factor and charge densities hardly changed from basis set (13s9p5d) to (14s11p6d). The apparent puzzle indicated by these results is discussed and resolved in Appendix C.

5.3.2 Environment

The point charge model by Evjen's method in Sec.(4.4.2) was taken for the rest of the system outside the cluster. 722 point charges within 64 chemical unit cells were taken to produce the Madelung potential in the region of the $(\text{NiO}_6)^{10-}$

cluster. The potential value at the center of the cluster is listed in Table (5.3) and as can be seen in the table, the potential is well-converged by 722 point charges. Evjen's method with 722 point charges (even 336 point charges) in a fcc structure like NiO was found to be a good approximation to the exact Madelung potential in the electronic structure calculations [sous93]. Since the effect by adding ECP was found to be negligible in KNiF₃, we did not incorporate ECP in the NiO case.

5.3.3 Comparison with experiment

The theoretical AF form factor values from RHF and UHF are compared with Alperin's single-crystal experimental values [alpe61] in Fig. 5.4 and Fig. 5.5-(a),(b).

The absolute values of $\langle S_z \rangle f(\vec{q}_A)$ are not available from Alperin's experiment; the experimental values were scaled by 0.93 to give the best fit to our UHF results, particularly in the small $|\vec{q}_A|$ region. The experimental Bragg scattering data in NiO extends to a larger region of $|\vec{q}_A|$ compared to that in KNiF₃. In the Fig. 5.5-(a), we compare our UHF results with the scaled experimental values. The UHF results agree very well with the experiment for the first three Bragg peaks and are consistently somewhat lower than the experiment for the larger $|\vec{q}_A|$ values. However, the bumpiness of the data is traced rather well by our theoretical calculations, which results from the asphericity of the spin density around each Ni. The overall agreement between the UHF results and the experiment in Fig. 5.5-(a) is reasonable.

An additional contribution to the form factor comes from the orbital motion of the electrons. This contribution was found to be appreciable only for large $|\vec{q}|$

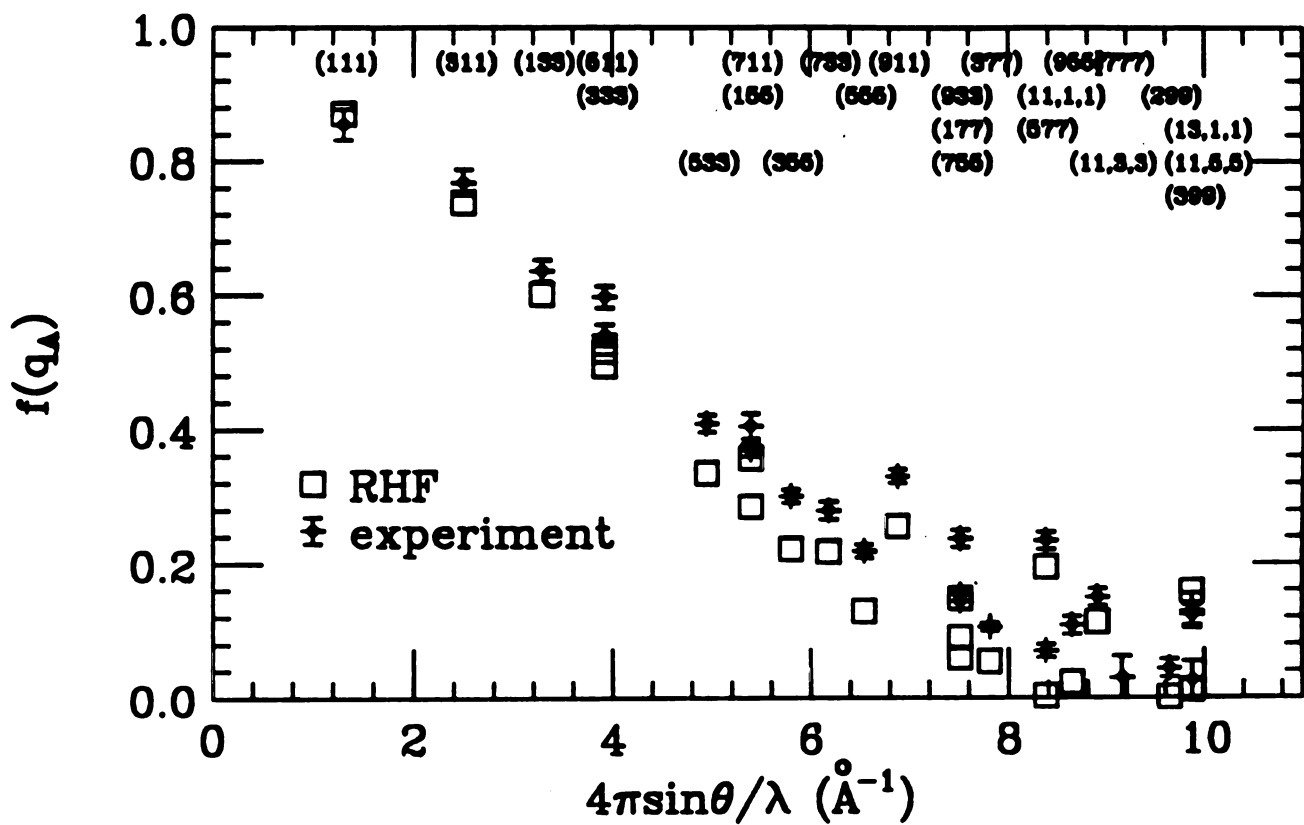


Figure 5.4: The calculated RHF form factor is compared with Alperin's experiment [alpe61] in NiO.

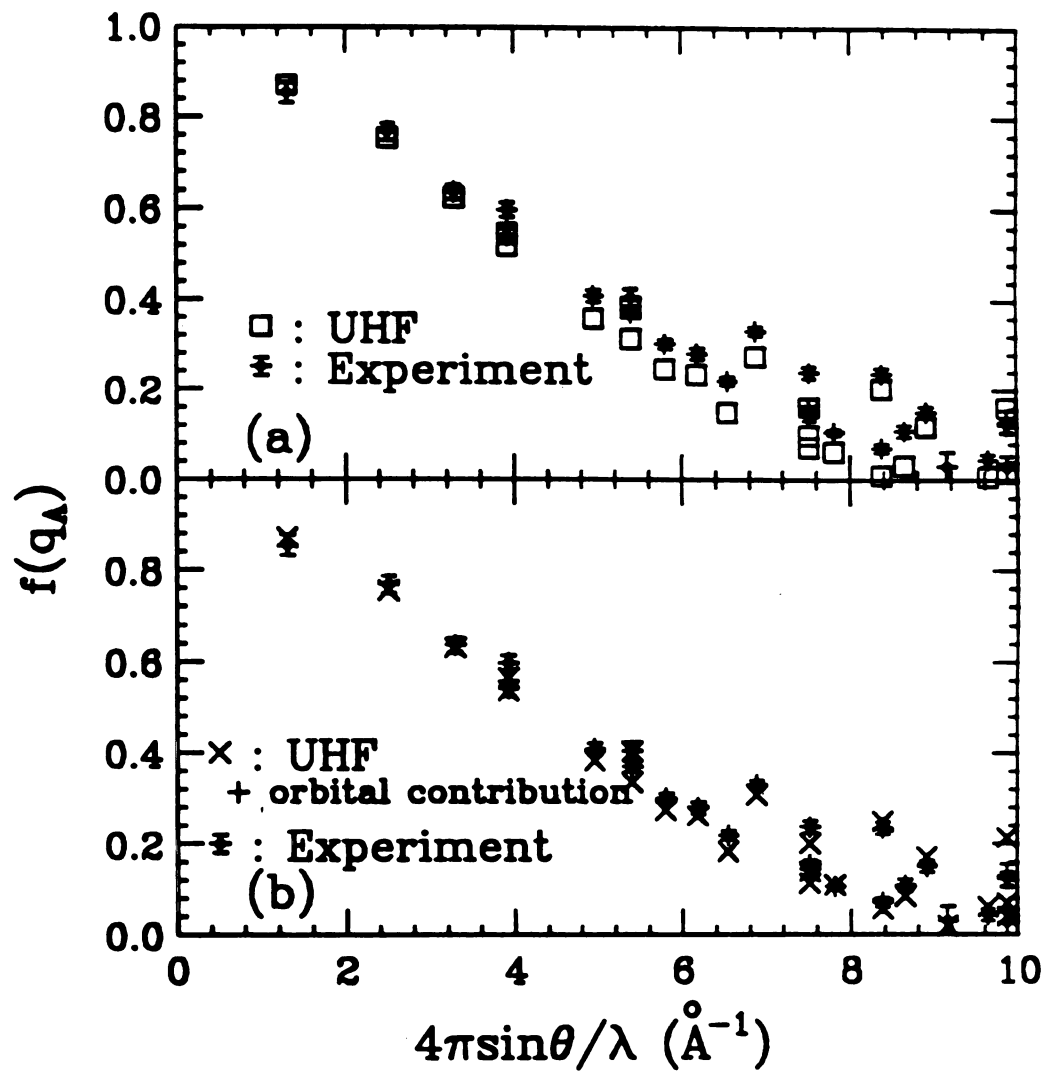


Figure 5.5: The calculated (a) UHF form factor, and (b) UHF form factor with orbital contribution from Khan et. al.[khan81], are compared with Alperin's experiment[alpe61] in NiO.

in Ref. [khan81, blum61]. We took the orbital contribution for NiO from the work of Khan et. al. who made a spherically averaged estimation of this contribution using the ionic Ni²⁺ wave function [khan81]. This orbital contribution is negligible in the small q region, so we do not expect it to be important in our discussion of the KNiF₃ results, where the experimental data are available only for small q. For larger q, the orbital contribution in NiO helps to give a better fit with the experiment, as shown in Fig. 5.5-(b). The small discrepancy between the calculated and the experimental values in Fig. 5.5-(b) might arise from the error involved in the spherically averaged estimation of the orbital contribution. With the inclusion of the orbital contribution to the form factor, we conclude that the results in Fig. 5.5-(b) are in very good agreement with experiment.

Unfortunately, we could not determine $\langle S_z \rangle_{Heis}$ from Alperin's experiment by scaling the calculated form factor as we did in KNiF₃, because the experiment [alpe61] gave only the relative form factor values. However we found a later experiment by Fender et. al. [fend68] who measured only one magnetic peak, but who gave information which allowed a determination of the absolute intensities; the ratios of intensities for the (111), (222), and (400). From the intensity ratio, they determined $\left(\frac{F_{111}}{F_{222}}\right)_{exp}^2$ which can be written in terms of the scattering lengths, b_{Ni} and b_O ,

$$\left(\frac{F_{111}}{F_{222}}\right) = \left(\frac{1}{4}\right) \frac{32p}{32(b_{Ni} - b_O)}. \quad (5.2)$$

Here (111) and (222) refer to the magnetic peak and nuclear peak respectively. $p = (e^2\gamma/2mc^2)gSf$ where γ is the magnetic moment of the neutron, g is the Landé factor, f is the magnetic form factor and S can be interpreted as $\langle S_z \rangle_{Heis}$. Using the values, $b_{Ni} = 1.03 \times 10^{-12}cm$, $b_O = 0.577 \times 10^{-12}cm$ and $g = 2.23$ from

the same reference and taking the magnetic form factor f_{111} from our UHF cluster calculation as $f_{111} = 0.871$, we obtained $\langle S_z \rangle_{Heis} = 0.88$. We also estimated $\langle S_z \rangle_{Heis}$ as 0.87 from $\left(\frac{F_{111}}{F_{400}}\right)_{exp}^2$ given in the same reference. Considering the spin wave value, $\langle S_z \rangle_{Heis} = 0.92$, for Type II AF fcc structure as appropriate for NiO[coll72], our theoretical estimate, $\langle S_z \rangle_{Heis} = 0.88 \pm 0.01$ appears to be quite reasonable. In our UHF calculation for NiO, the covalence reduction factor in Eq. (2.68) was found to be 0.91. Considering the covalence reduction factor in KNiF₃, 0.95, we conclude that NiO is more covalent than KNiF₃. This is physically reasonable because the O²⁻ wave functions are more diffuse compared to F⁻ wave functions.

5.4 La₂NiO₄

Now we apply our *ab initio* cluster method to calculate the form factor of La₂NiO₄. The procedures of the cluster calculation are very similar to those of NiO. The main difference between the clusters NiO and in La₂NiO₄ is the structure of the cluster and the surrounding point charges. The cluster for La₂NiO₄ is tetragonal while the cluster for NiO is octahedral.

Recently La₂NiO₄ has received special attention since it is isostructural with La₂CuO₄ which is the parent of a high T_C superconductor. It also exhibits a structure distortion from tetragonal to orthorhombic at $\sim 700K$ similarly to La₂CuO₄. However, La₂NiO₄ shows another structural transition from orthorhombic to low-temperature tetragonal structure(LTT) at $\sim 70K$ [land89]. Also doped La₂NiO₄ has been found not to be a superconductor.

The crystal structure of La₂NiO₄ is shown in Fig. 5.6. Wang et. al. [wang92]

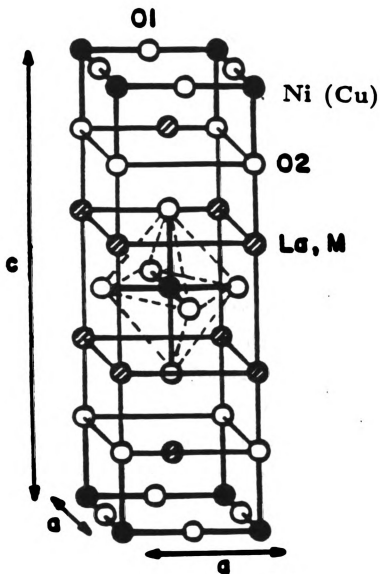


Figure 5.6: Crystal structure of La_2NiO_4 . La_2CuO_4 has the isostructure of La_2NiO_4 (Ni^{2+} ions are replaced by Cu^{2+} ions). The contents of the $(\text{NiO}_6)^{10-}$ cluster are connected by the dotted lines.

measured the form factor at $15K$ where La_2NiO_4 is in the LTT phase. We followed their indexing for magnetic Bragg peaks for La_2NiO_4 .

Several values of the Néel temperature, T_N , in La_2NiO_4 have been reported in the literature. T_N was reported to be 650K in Ref. [land89] and 330K in Ref. [naka95] even for stoichiometric La_2NiO_4 , as the authors of the latter paper claimed. T_N is very sensitive to oxygen content in La_2NiO_4 : $\text{La}_2\text{NiO}_{4+0.05}$ shows $T_N = 70K$ in Ref. [aep88]. Although the value of T_N is controversial, the temperature, $15K$, where Wang et. al.[wang92] measured the form factor, is well below any of the T_N values.

5.4.1 Cluster

The tetragonal cluster, $(\text{NiO}_6)^{10-}$, was taken for La_2NiO_4 with distances between Ni-O as 1.95\AA in the NiO_2 plane and 2.21\AA along the apical axis. Wachters' basis set (13s9p5d) for Ni[wach70] and Huzinaga basis sets (9s6p) for O [huzi71] with an additional diffuse p function were used as in NiO. All 86 electrons in the $(\text{NiO}_6)^{10-}$ cluster were taken into account in our RHF and UHF calculations. The COLUMBUS[colu88] and Gaussian 92[g92] codes were used for RHF and UHF respectively.

5.4.2 Environment

We took 552 point charges to simulate the crystalline environment around the cluster in La_2NiO_4 . These 552 point charges for La_2NiO_4 are within 27 unit cells which is denoted as PC333 in table 1 of Ref. [mart91]. The deviation from the exact Madelung sum is listed in the same table. We noted that this number of point charges for La_2NiO_4 does not give a constant difference from the Madelung

sum; however it did not seem to affect the form factor. Increasing the number of point charges, from PC333 (27 unit cells) to PC553 (75 unit cells) in the notation of Martin's paper, hardly changed the form factor.

Although the point charge model was found to be good enough to generate the Madelung potential for KNiF_3 or NiO , we speculated that the point charge model might not be appropriate for La_2NiO_4 . The calculated form factor with different ECP environments is shown in Fig. 5.7. Since the nearest neighbors of the cluster, La^{3+} 's, are quite close to the apical oxygens, a point charge, $+3e$, for La^{3+} might attract the electrons of the apical oxygens too strongly. The Mulliken population analysis from our cluster calculations on La_2NiO_4 showed that more charges were assigned to the apical oxygens than the planar oxygens, which is consistent with the above picture. Bare point charges are of course, more attractive than real ions. One way to reduce this strong attraction by the La^{3+} in a realistic way is to introduce an effective core potential (ECP) for these nearby La^{3+} ions. As a first step to include ECP, we replaced the eight nearest neighbor $+3e$ point charges by La^{3+} ECP's which is denoted as ECP1. It did change the form factor as shown in Fig. 5.7 and Mulliken charge of the apical oxygen was reduced. As a second step, denoted as ECP2, we replaced two more $+3e$ point charges, right above and below the apical oxygens by La^{3+} ECP in addition to the 8 La^{3+} ECP's considered above. This procedure including 10 La^{3+} ECP's also changed the form factor and reduced Mulliken charge of the apical oxygen. Then we replaced the 4 point charges of $+2e$ with Ni^{2+} ECP [sabe80] for neighboring Ni^{2+} ions, noted as ECP3. Changing from ECP2 to ECP3 hardly changed the form factor.

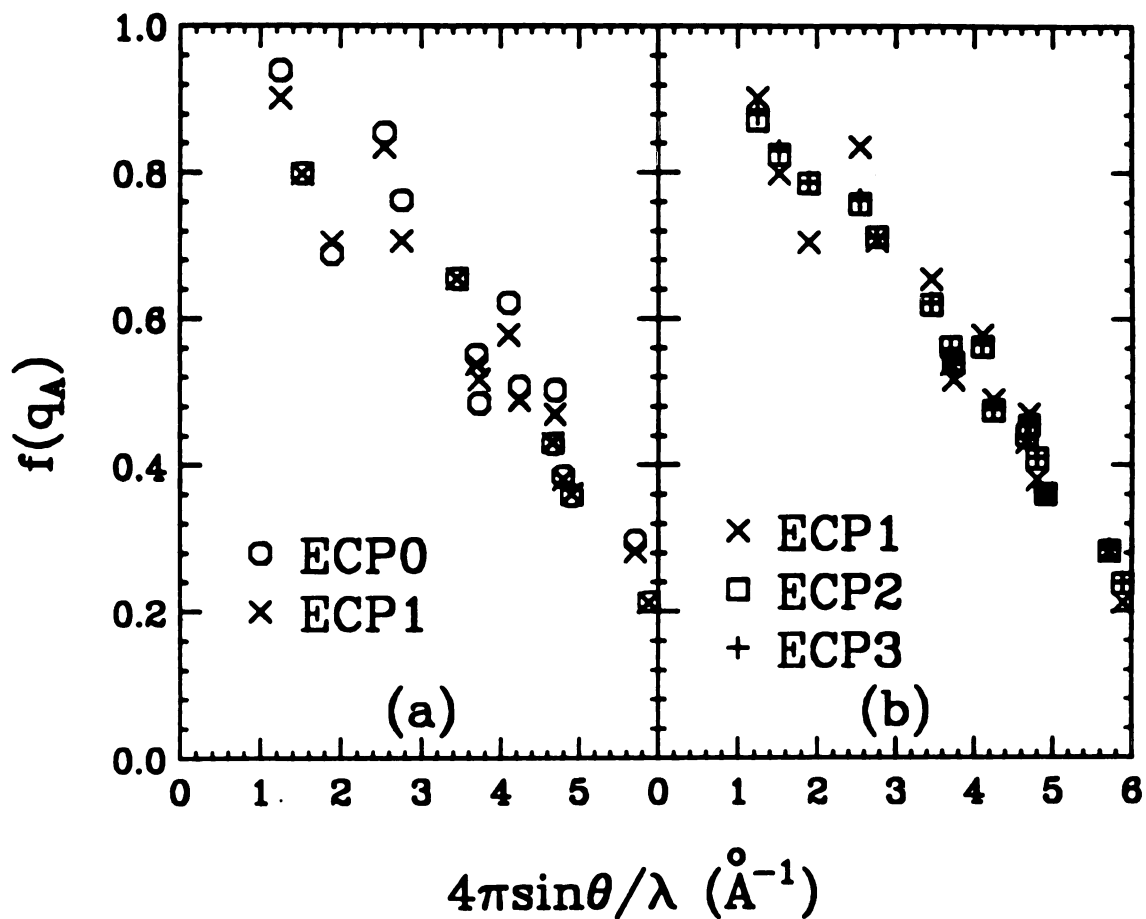


Figure 5.7: The calculated UHF form factor of La_2NiO_4 with different ECP environment were compared. In ECP0, only point charge distribution is considered, i.e. no ECP incorporated. In ECP1, ECP2, and ECP3, (8 La^{3+}), (10 La^{3+}), and (10 La^{3+} + 4 Cu^{2+}) point charges are replaced by the appropriate ECP's respectively.

5.4.3 Comparison with experiment

The theoretical AF form factor values with ECP1 environment from RHF and UHF are compared with the experimental values of Wang et. al.'s [wang92] in Fig. 5.8. Both RHF and UHF results in Fig. 5.8 disagree seriously with the experiment. Especially, the experimentally observed plateau at small q values is not reproduced in either calculations or other ECP environments shown in Fig. 5.7.

The effect of the spin fluctuations is only to scale the calculated values by a constant factor; we clearly can not reproduce the shape of the form factor with this type of scaling.

The plateau at small q in the measured form factor was seen not only in La_2NiO_4 but also in La_2CuO_4 [frel88]. If we assume that this plateau characterizes the covalence effect on the spin density through the Ni-ligand cross terms, it appears that our present cluster model has failed to describe this covalence effect in La_2NiO_4 , in contrast to the success in KNiF_3 and NiO .

5.5 Summary

The remarkably good agreement between our UHF results and the experiment in KNiF_3 and NiO indicates that the UHF cluster method, with a simple point charge model, well describes the form factor for these rather highly ionic materials. For KNiF_3 , where the absolute experimental values are available, we found that the experimental data support our previous theoretical studies [kapl92], namely the magnetic moment density $m(\vec{q}_A)$ is affected by both the covalence and the quantum spin fluctuations. Furthermore, the reduction due to the spin fluctuations agrees well with the spin wave theory. For NiO , we conclude that the

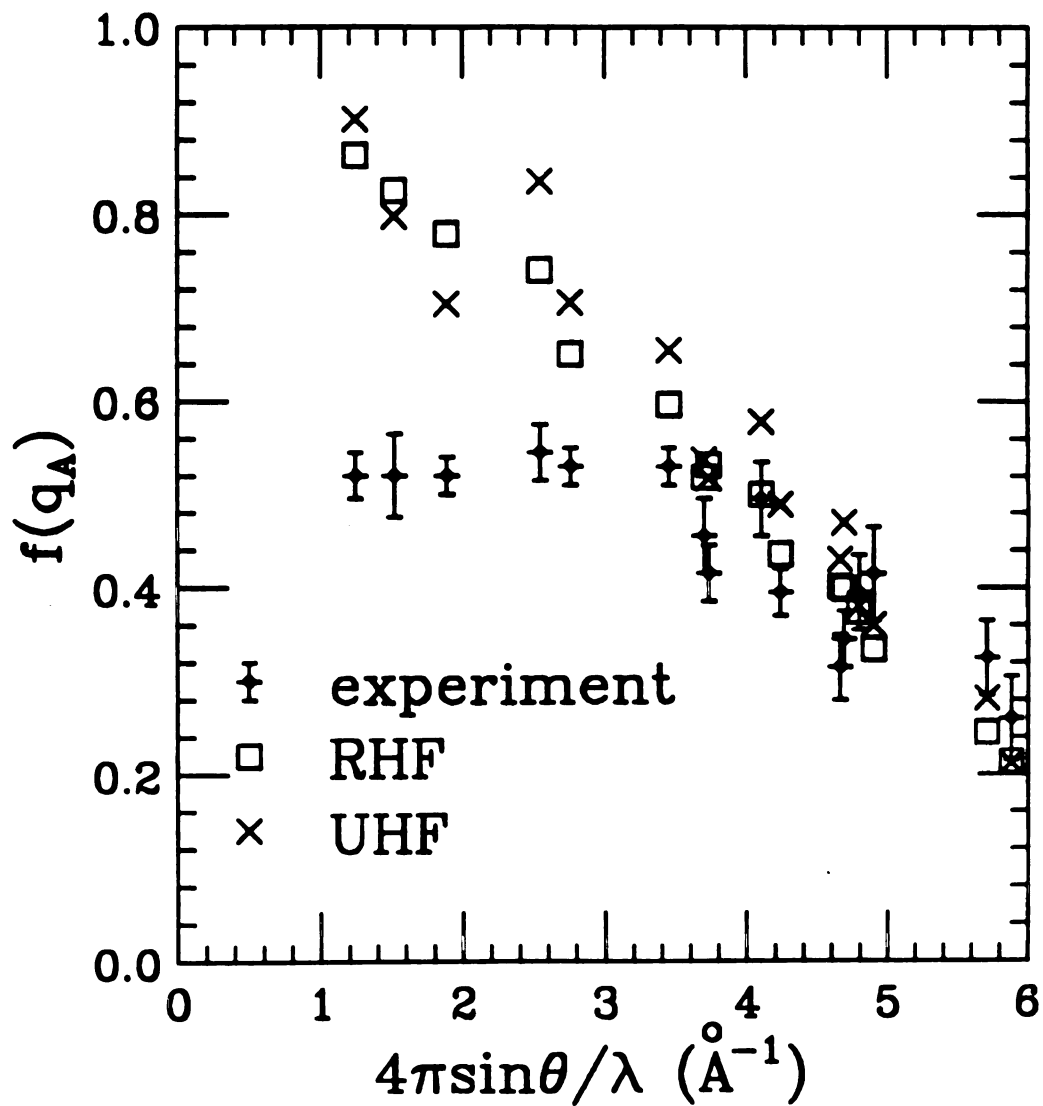


Figure 5.8: The calculated RHF and UHF form factor are compared with Wang et. al.'s experiment[wang92]. These calculation have been done with ECP1 environment in the text.

calculated values of $m(\vec{q}_A)$ which include an approximate evaluation of the rather small orbital contribution are in excellent agreement with the experiment. For further improvement in the theoretical results, we need to use a more accurate calculation of the orbital contribution (in the larger $|\vec{q}|$ region). We also estimated $\langle S_z \rangle_{Heis}$ for NiO using our calculated form factor and found it to be close to the spin wave value.

The covalent reduction of the ordered moment as defined in [kapl92, maha93, hubb65] is found to be 0.95 and 0.91 for KNiF_3 and NiO, respectively. These values were obtained from the UHF calculations using the basis set (13s9p5d) for Ni. When we used the basis set (14s11p6d) which includes diffuse basis functions for Ni, we found slightly different values, 0.92 and 0.88 for KNiF_3 and NiO, respectively. We understand that when the diffuse basis functions in Ni give appreciable density on the ligands, a simple subtraction of the $\chi(\vec{r})^2$ terms in Eq. (4.38) and the appendix of Ref. [maha93] leads to a different value of the ordered moment. Thus the ordered moment defined in Refs. [kapl92, maha93, hubb65] depends on the choice of the basis set like the Mulliken charge population discussed in Appendix C. The ordered moment is defined to be determined by propagating the cluster spin density along AF ordering in the crystal and integrating the spin density in the Wigner-Seitz cell in real space. But it needs enormous numerical calculation. However the estimation of covalence by the above method, i.e. via the subtraction of the $\chi(\vec{r})^2$ terms, can be a reasonable way if a compound is ionic and the basis set is chosen properly. We believe the values from the basis set (13s9p5d) are more reasonable in the view of the reasonable Mulliken charges of that basis set.

In La_2NiO_4 , the result of the essentially similar cluster method completely

failed to capture even the essential qualitative feature of the form factor experimentally. The difference between the clusters in NiO and La_2NiO_4 is structure and environment. The AF ordering is 2-dimensional in La_2NiO_4 while it is 3-dimensional in NiO. Therefore the magnetic moment of the apical oxygens is canceled by AF ordering in NiO but not in La_2NiO_4 . The form factor of La_2NiO_4 seems very sensitive to the spin density of the apical oxygen because it shows a noticeable change by replacing nearby point charges by La^{3+} ECP. The simple cluster with point charge plus ECP might be inadequate for La_2NiO_4 . We applied a similar cluster method to La_2CuO_4 and the difference between Ni and Cu will be discussed in Chap. 6. The failure in La_2NiO_4 is also discussed further in Chap. 6.

Chapter 6

Neutron scattering form factor of the cuprate compounds

6.1 Introduction

In this chapter we discuss our *ab initio* calculations of the form factor in the cuprate compounds, La_2CuO_4 , $\text{Sr}_2\text{CuO}_2\text{Cl}_2$ and $\text{YBa}_2\text{Cu}_3\text{O}_6$. We followed the same approach as in our earlier work on nickel compounds in discussed in Chap. 5 because of our success in KNiF_3 and NiO in comparing our calculations with very detailed and extensive experimental data. Although problems with La_2NiO_4 still remain as discussed in Sec. [5.4], we believe a comparison between $(\text{NiO}_6)^{10-}$ and $(\text{CuO}_6)^{10-}$ clusters might give some insight into the difference between Ni and Cu compounds and possibly the source of the trouble in the nickelate.

We have carried out both RHF and UHF calculations on the clusters $(\text{CuO}_6)^{10-}$, $(\text{CuO}_4\text{Cl}_2)^{8-}$ and $(\text{CuO}_5)^{8-}$ for La_2CuO_4 , $\text{Sr}_2\text{CuO}_2\text{Cl}_2$ and $\text{YBa}_2\text{Cu}_3\text{O}_6$, respectively. The ions outside the cluster are treated as point charges, except that nearby external ions are replaced by effective core potentials (ECP) similar to La_2NiO_4 . We also extended our calculation method beyond Hartree-Fock (HF) to include correlation corrections via the multi-configuration self-consistent field

method (MCSCF).

In addition to the cluster form factor, we have also calculated the Cu^{2+} ion form factor using various methods, RHF, UHF, MCSCF and CI. These calculations of the ionic form factor enabled us both to study the effect of covalence (by comparing with cluster form factor) and to evaluate the reliability of estimating the correlation effect using MCSCF and configuration interaction (CI) methods.

In this Chapter, I discuss the result of calculation of the Cu^{2+} ion with various methods. Then I address the methods and results of our cluster calculations and compare the results with experiment on $\text{YBa}_2\text{Cu}_3\text{O}_6$, La_2CuO_4 and $\text{Sr}_2\text{CuO}_2\text{Cl}_2$. I conclude the chapter comparing the result of the cuprates with the corresponding nickelates.

6.2 Cu^{2+} ion

Since MCSCF results of the clusters, $(\text{CuO}_6)^{10-}$ and $(\text{CuO}_5)^{8-}$, indicated that $d-d$ intra-atomic correlation of Cu^{2+} in the cluster was most important (as discussed in the later sections), one might assume that the correlation effects in a free Cu^{2+} ion are similar to those in the $(\text{CuO}_6)^{10-}$ and $(\text{CuO}_5)^{8-}$ clusters. Accordingly, we decided to study in detail correlation effects in the free Cu^{2+} with various levels of approximation. We have carried out UHF and single- and double-substitution CI (CISD) calculations using Gaussian 92 [g92]. Two levels of CISD have been carried out and will be denoted as CISD1 and CISD2 respectively. We correlated only the 3d electrons in CISD1 and 3s, 3p and 3d electrons in CISD2. In addition, RHF and MCSCF calculations for the Cu^{2+} ion have been carried out with COLUMBUS [colu88]. In this case, MCSCF allowed only the 3d electrons

to be correlated similar to CISD1. When we say that we correlate $3d$ electrons, that means we choose $3d$ -dominant occupied molecular orbitals (MO) and other virtual (empty) MO's to build determinants in the configuration state functions (see Chap. 4).

To check the sensitivity of the form factor to the choice of basis set for the Cu^{2+} ion, the basis set (14s11p6d) with additional diffuse functions suggested by Hay [hay77] was used instead of the (13s9p5d) basis set. These two basis sets, (14s11p6d) and (13s9p5d) contracted to [8s4p3d] and [7s3p2d] respectively, gave almost the same ion form factor. Therefore we present only the results with the basis set (13s9p5d) for the Cu^{2+} ion. (See Appendix C for details about choosing different basis sets.)

6.2.1 Ionic form factor

We have calculated the form factor from the ionic wavefunction obtained by RHF, UHF, MCSCF, CISD1 and CISD2 for the \vec{q} values corresponding to the Bragg peaks in $\text{YBa}_2\text{Cu}_3\text{O}_6$ which Shamoto et. al.[sham93] measured for two families, $(1/2, 1/2, k)$ and $(3/2, 3/2, k)$. This notation refers to a tetragonal structure, (a, a, c) , taking a along the line between the nearest neighbor Cu^{+2} and c along the apical axis.

The RHF and UHF results are compared in Fig. 6.1-(a) and the UHF and MCSCF results are shown in Fig. 6.1-(b). The form factors from CISD1 and CISD2 were found to be almost same as the MCSCF results, so here we present the latter only. Total energies of the Cu^{2+} ion obtained with these various methods are listed in Table 6.1. The lowering in the total energy due to correlation is about 5 eV and does not depend strongly on the environment.

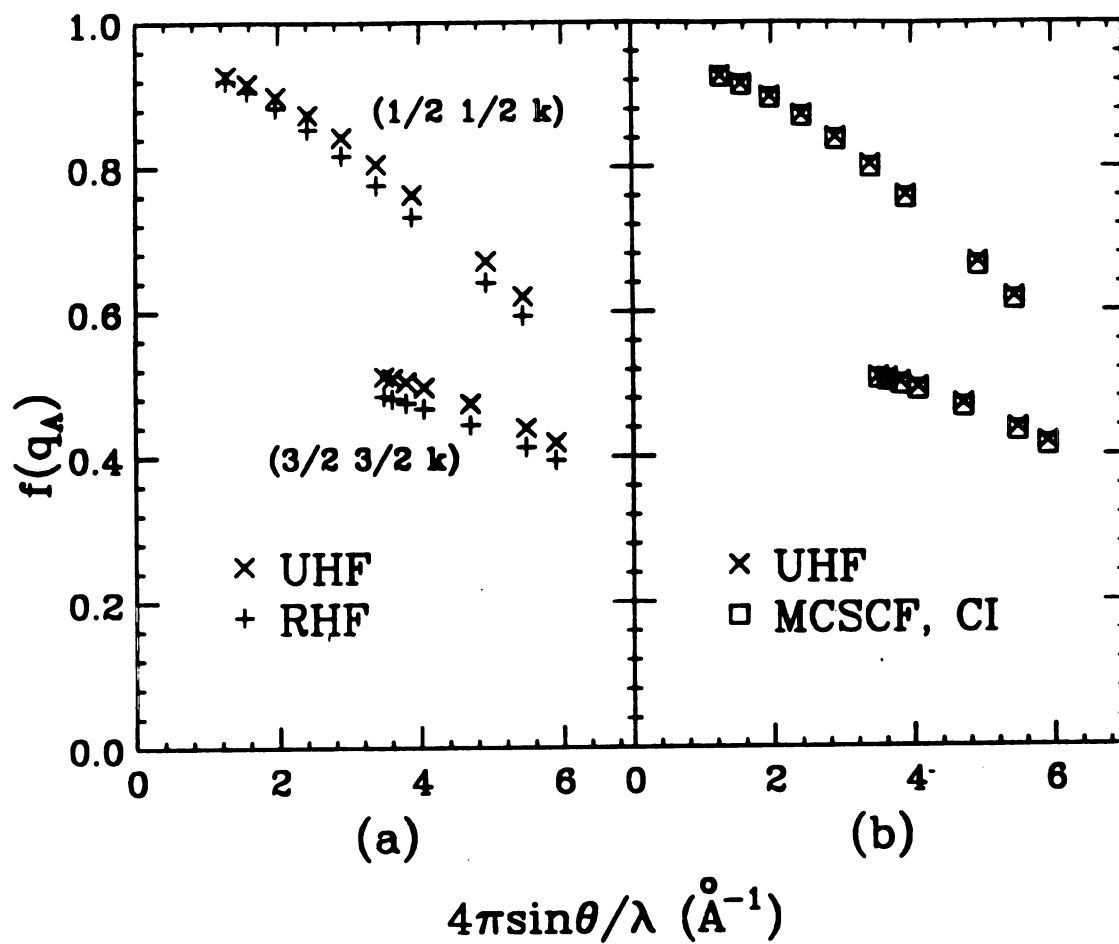


Figure 6.1: The calculated ionic form factor with RHF, UHF and MCSCF methods.

Table 6.1: Total energies (eV) relative to the RHF values of various calculations for Cu^{2+} ion; It is noted that the RHF energy value includes the nuclear repulsion amongst the environmental point charges as well as between the ion nucleus and the point charges.

	free Cu^{2+} ion	Cu^{2+} ion with point charges ^a
RHF	0.0 ^b	0.0 ^c
UHF	-0.011	-0.013
MCSCF	-2.414	-2.514
CISD1	-3.031	-3.088
CISD2	-5.403	-5.454

^aPoint charges correspond to the atomic positions of $\text{YBa}_2\text{Cu}_3\text{O}_6$

^bRHF energy = -1638.01987633 (a.u.) (1 a.u.=27.2114 eV)

^cRHF energy = -1886.85744701 (a.u.)

The differences between the RHF and UHF form factors are noticeable except for the first few points (at small $|\vec{q}|$) in Fig. 6.1-(a). When we considered the contribution to the form factor from each atomic orbital, we found the difference between RHF and UHF mainly came from the spin density of the paired electrons due to core polarization in UHF (including the t_{2g} electrons). At small $|\vec{q}|$, corresponding to large $|\vec{r}|$, the form factor picks up mainly the spin density from the 3d orbitals. Thus the contribution from the core polarization of 3s and 3p to the form factor is negligible in the small $|\vec{q}|$ region. This explains the result that the difference at small $|\vec{q}|$ is smaller than at large $|\vec{q}|$.

We found that the MCSCF form factor hardly changed from the UHF results as seen in Fig. 6.1-(b). However, as shown in the Table 6.1, although the total energy value changed by only about 0.01 eV from RHF to UHF, it changed by more than 2 eV due to the correlation effect involved in MCSCF and CISD. That is, the core polarization associated with UHF affects the form factor (i.e. the

spin density) appreciably but not the energies, while correlation effects included in MCSCF, CISD1 or CISD2 hardly affect the form factor, at least in Cu^{2+} ion.

We have calculated the form factor for the Cu^{2+} ion with point charge distributions of $\text{YBa}_2\text{Cu}_3\text{O}_6$ using RHF, UHF, MCSCF, CISD1 and CISD2. The form factor also hardly changed from the free Cu^{2+} ion value in all the methods listed above. The MCSCF form factors for the two cases are compared in Fig. 6.2. The trend of the energy changes in Table 6.1 is very similar to that of the free Cu^{2+} ion. Thus the crystal field as simulated by the point charge distribution has very little effect on both the form factor and the total energy.

6.3 $\text{YBa}_2\text{Cu}_3\text{O}_6$

The experimental situation regarding the ordered moment in $\text{YBa}_2\text{Cu}_3\text{O}_6$ is controversial [kap194]. There are discrepancies between the moment values obtained by two different groups, Refs. [jurg89, burl88] and Refs. [tran88L, tran88B], although not so severe as in La_2CuO_4 (as discussed in Sec. 6.4). The ordered moment, μ , and T_N in $\text{YBa}_2\text{Cu}_3\text{O}_{6+x}$ were found to be essentially constant for $0 \leq x \leq 0.20$ by both the groups [jurg89, tran88B], and the value of T_N agreed very well. The ordered moment μ was found to be $0.64 \pm 0.03\mu_B$ for the single crystal [jurg89] with $x = 0.0$ and 0.15 , compared to $0.66 \pm 0.07\mu_B$, $0.46 \pm 0.05\mu_B$, and $0.50 \pm 0.05\mu_B$ for $x = -0.06$, $x = -0.01$, and 0.15 in Ref. [tran88B]. Recently a detailed experimental study of the neutron scattering form factor was reported for $\text{YBa}_2\text{Cu}_3\text{O}_{6.15}$ by Shamoto et. al.[sham93]. They found the Néel temperature to be $410 \pm 3\text{K}$ which is close to the value of T_N for undoped $\text{YBa}_2\text{Cu}_3\text{O}_6$ [jurg89, tran88B, rebe89]. Since T_N and μ showed a linear dependence on each

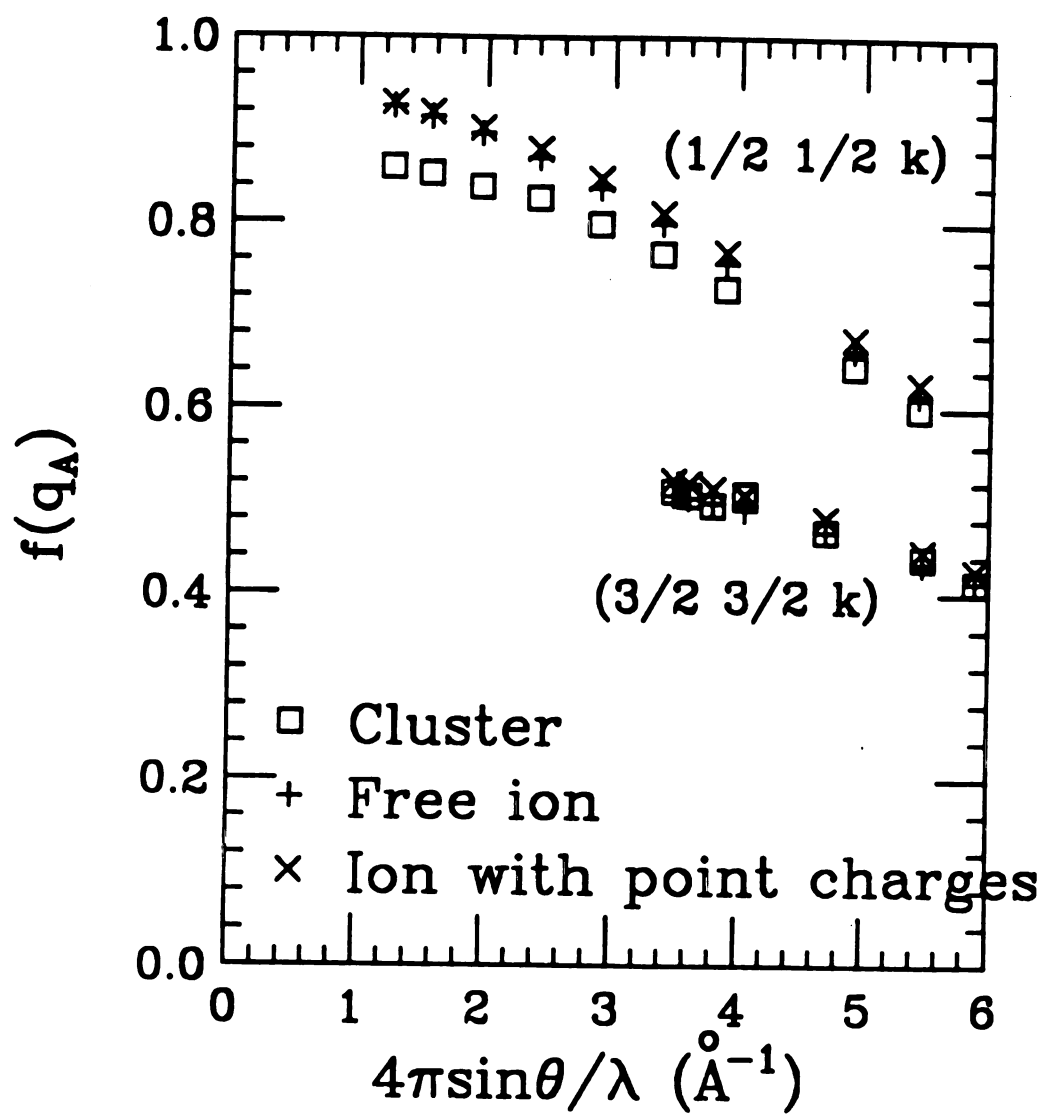


Figure 6.2: Comparison of form factor of free Cu^{2+} ion, Cu^{2+} ion with point charge distribution of $\text{YBa}_2\text{Cu}_3\text{O}_8$, and $(\text{CuO}_5)^{4-}$ cluster form factor.

other and both were found to change very little from $x = 0.0$ to $x = 0.15$ for $\text{YBa}_2\text{Cu}_3\text{O}_{6+x}$, one expects the form factor of $\text{YBa}_2\text{Cu}_3\text{O}_{6.15}$ to be close to that of $\text{YBa}_2\text{Cu}_3\text{O}_6$. Also, from Burlet et. al.'s experiment [bur188], it appears that the relative form factor values at different reflections are insensitive to small changes in the oxygen content. Therefore, as with La_2CuO_4 , we will compare the shape of the calculated magnetic form factor vs. momentum transfer, $|\vec{q}|$, with the experiment even though the sample is not stoichiometric, since the absolute value or overall scale factor is uncertain.

The structure of $\text{YBa}_2\text{Cu}_3\text{O}_6$ is quite complicated as shown in Fig. 6.3. The Cu^{2+} magnetic ions are antiferromagnetically coupled in the 2-dimensional CuO_2 plane, but these Cu^{2+} ions are not at the center of inversion. Moreover the CuO_2 plane has a double-layered structure. The spins are aligned in the CuO_2 plane but the precise direction within the plane has not been determined [tran88B, tran88L].

6.3.1 Cluster

We have chosen the six atom $(\text{CuO}_5)^{8-}$ cluster in a tetragonal structure to represent $\text{YBa}_2\text{Cu}_3\text{O}_6$. Similar clusters have been used by Sulaiman et. al. [sula90] for calculating the hyperfine properties at the Cu^{2+} site in this system. The cluster electronic wave functions have been calculated using RHF and UHF procedures. RHF and UHF calculations were performed with the COLUMBUS code [colu88] and the Gaussian 92 code [g92] respectively, using contracted Gaussian basis sets. Wachters' [wach70] basis (13s9p5d) sets for Cu and Huzinaga [huzi71] basis sets (9s6p) with additional diffuse p function for O were used. All 77 electrons in the $(\text{CuO}_5)^{8-}$ cluster were explicitly included in these *ab initio* calculations keeping the total spin $S = 1/2$.

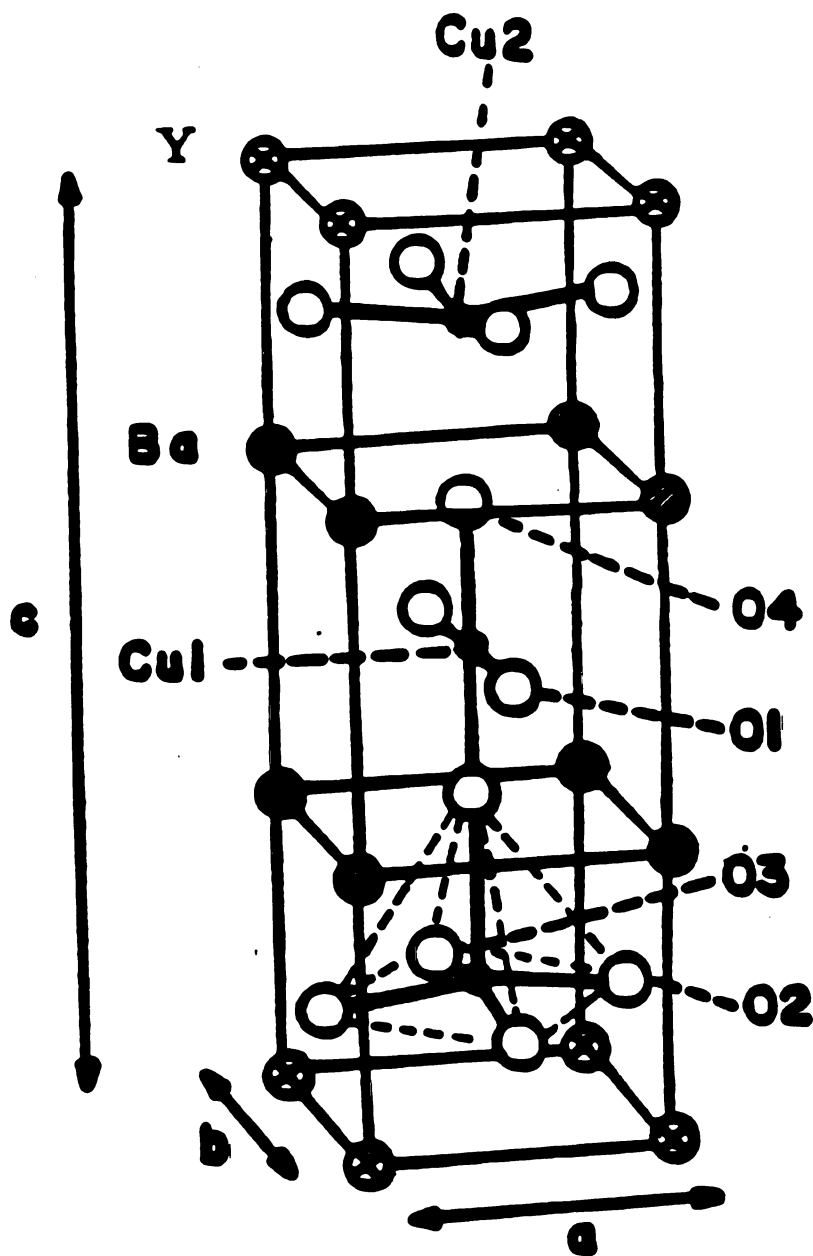


Figure 6.3: Crystal structure of $\text{YBa}_2\text{Cu}_3\text{O}_6$. The contents of the $(\text{CuO}_5)^{6-}$ cluster are connected by the dotted lines.

Since we want to compare our calculated form factor with the experimental results of Shamoto et. al. [sham93], we have used the values of the lattice parameters given by them to obtain the positions of the atoms in the cluster and the environmental point charges. Therefore the Cu-O distance in the CuO_2 plane, where there is a small buckling, was taken as 1.94\AA and the distance between Cu-O along the apical axis was taken to be 2.44\AA .

In addition to RHF and UHF calculations, we have also performed MCSCF calculations using the Columbus code[colu88] to investigate correlation effects. In order to calculate the form factor, which is proportional to the Fourier transform of the spin density, we have developed programs to obtain the natural orbitals associated with spin up and down electrons separately (see Sec. 4.2.3).

In the MCSCF calculations for the $(\text{CuO}_5)^{8-}$ cluster, each doubly occupied d -dominant orbital was correlated with one virtual orbital. This yields 354 configurations. In principle, MCSCF[shep88] allows the d electrons in Cu to correlate amongst themselves and with the p electrons in the ligand. It also allows $p - p$ correlation within the ligands. However, the result of this correlation calculations suggests that $d - d$ correlations are most important.

6.3.2 Environment

We took 8 unit cells for $\text{YBa}_2\text{Cu}_3\text{O}_6$ as the environment, which gave 516 point charges around the $(\text{CuO}_5)^{8-}$ cluster. For a more realistic environment, the point charges which had originally represented the nearest neighboring 4 Y^{3+} 's and 4 Ba^{2+} 's were replaced by effective core potentials (ECP)[wadt85]. The UHF result of this procedure was reported in earlier work in Ref. [kapl94]. Here we extended our ECP by replacing the neighboring 4 Cu^{2+} ions in the CuO_2 plane by Cu^{2+} ECP

[mart]. Introducing these ECP's enabled us to incorporate Pauli repulsion effect particularly between electrons in the O^{2-} ions of the cluster and those belonging to the neighboring extra-cluster ions.

6.3.3 Calculated form factor

The calculated value of the form factor for $(CuO_5)^{8-}$, according to Eq. 4.36 in Sec. 4.3, is not a real number anymore because of the lack of inversion symmetry of the cluster wave function itself. In order to compare the calculated form factor with the experiment, we have to recover the inversion symmetry of the form factor. To recover the inversion symmetry of the system, we consider two nearby CuO_2 planes which form a bilayer structure. Now, the Y^{3+} ion in the middle of the two layers is a center of the symmetry as shown in Fig. 6.4.

We can write the spin density, $\tilde{\rho}_s(\vec{r})$, associated with two Cu^{2+} ions, Cu1 and Cu2 (see Fig. 6.4), which has anti-inversion symmetry with respect to the central Y.

$$\tilde{\rho}_s(\vec{r}) = \rho(\vec{r}) - \rho(-\vec{r} + 2\vec{R}) \quad (6.1)$$

where $\rho(\vec{r})$ and $\rho(-\vec{r} + 2\vec{R})$ are the cluster spin densities associated with Cu1 and Cu2 respectively and \vec{R} is the vector connecting Cu1 and central Y. The minus sign between them indicates the spins of Cu1 and Cu2 are antiferromagnetically ordered. The full form factor is $\tilde{f}(\vec{q})$ which is the Fourier transform of $\tilde{\rho}_s(\vec{r})$.

$$\begin{aligned} \tilde{f}(\vec{q}) &= \int (\rho(\vec{r}) - \rho(-\vec{r} + 2\vec{R})) e^{i\vec{q}\cdot\vec{r}} d\vec{r} \\ &= 2ie^{i\vec{q}\cdot\vec{R}} Im (f_c(\vec{q})e^{-i\vec{q}\cdot\vec{R}}) \end{aligned} \quad (6.2)$$

where $f_c(\vec{q}) = \int \rho(\vec{r})e^{i\vec{q}\cdot\vec{r}} d\vec{r}$, the complex form factor which we can calculate from our cluster wave function of $(CuO_5)^{8-}$ associated with a single ion, Cu1.

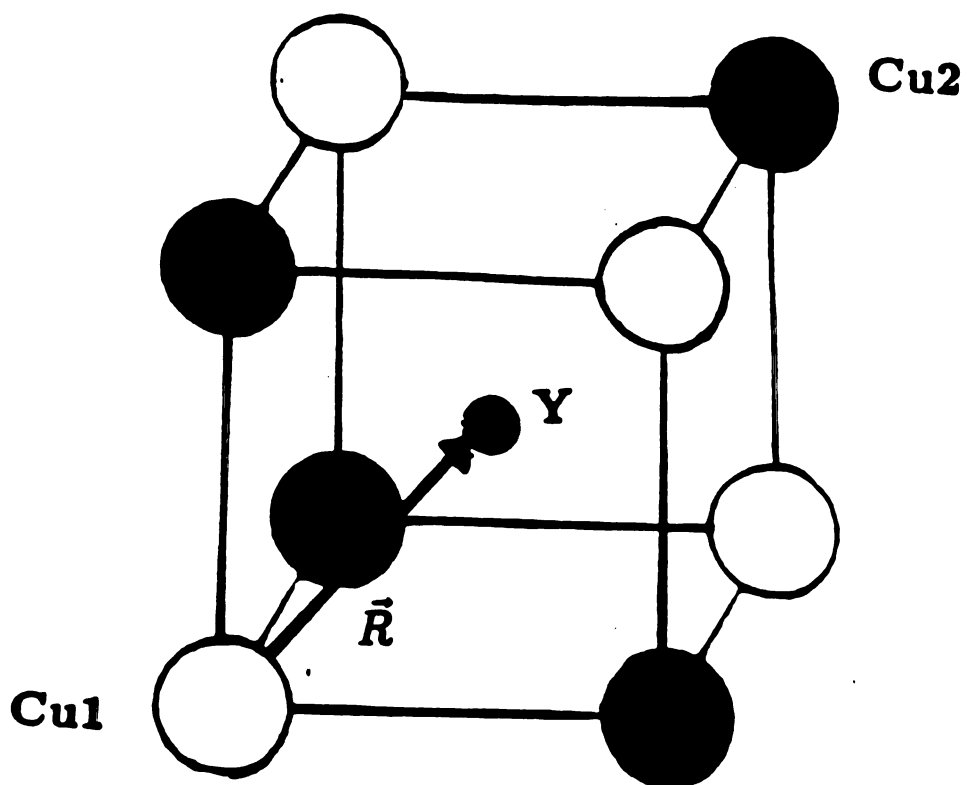


Figure 6.4: Bilayer structure of CuO_2 planes in $\text{YBa}_2\text{Cu}_3\text{O}_6$. The small shaded circle is Y^{3+} . The big circles are Cu^{2+} ions (the solid and empty circles represent antiparallel spins).

An observable quantity is the absolute value of $\tilde{f}(\vec{q})$, which is given as

$$|\tilde{f}(\vec{q})| = 2 \left| \text{Im} \left(f_c(\vec{q}) e^{-i\vec{q} \cdot \vec{R}} \right) \right| \quad (6.3)$$

In the experiment, Shamoto et. al.[sham93] determined the magnetic structure factor F_M from the integrated intensities of the magnetic Bragg peaks. From their equation, the square of F_M is proportional to

$$|F_M|^2 \propto \mu^2 f^2(\vec{q}) g^2(\vec{q}) \quad (6.4)$$

where they call μ the magnetic moment, $f(\vec{q})$ is the magnetic form factor, and $g(\vec{q})$ is a bilayer structure factor, $g(\vec{q}) = 2 \sin(\vec{q} \cdot \vec{R})$. Because Shamoto et. al. took the form factor as the Cu^{2+} ionic form factor, their form factor is real and does not include any covalence effect. When we compare our calculation with the experiment, we have to compare $|\tilde{f}(\vec{q})|$ in Eq. (6.3) with the corresponding experimental value which is given as

$$|\tilde{f}(\vec{q})| = 2 f(\vec{q}) |\sin(\vec{q} \cdot \vec{R})|. \quad (6.5)$$

From Eqs. (6.3) and (6.5), the calculated form factor, to be compared with experiment, can be written as

$$f(\vec{q}) = \frac{\left| \text{Im} \left(f_c(\vec{q}) e^{-i\vec{q} \cdot \vec{R}} \right) \right|}{|\sin(\vec{q} \cdot \vec{R})|} \quad (6.6)$$

This is a form factor associated with one Cu^{2+} ion.

The calculated form factors from RHF, UHF and MCSCF $(\text{CuO}_5)^{-8}$ cluster spin densities are compared in Fig. 6.5-(a),(b). In Fig. 6.5-(a), the UHF form factor is flatter than that of RHF in the small $|\vec{q}|$ region and the UHF form factor lies above the RHF form factor at large $|\vec{q}|$. These trends of RHF-UHF form factor differences also occurred in the previous cluster calculations on nickel compounds

Table 6.2: Comparison of total energies (eV) of clusters

	$(\text{CuO}_5)^{8-}$ in $\text{YBa}_2\text{Cu}_3\text{O}_6$	$(\text{CuO}_6)^{10-}$ in La_2CuO_4
RHF	0.0 ^a	0.0 ^b
UHF	-0.042	-0.044
MCSCF	-2.693	-2.655

^aRHF energy = -2257.23425980 (a.u.) (1 a.u.=27.2114 eV)

^bRHF energy = -2389.44155671 (a.u.)

discussed in Chap. 5. Considering the spin density in the \vec{r} -space, we found more spin density on the O sites in the CuO_2 plane in UHF than in RHF. This explains why the UHF is flatter at small $|\vec{q}|$: more spin density on the O's in the CuO_2 plane is canceled out due to AF ordering. As in the Cu^{2+} case, the difference at large q is mainly due to core polarization.

In Fig. 6.5-(b), we can see that the MCSCF form factor differs little from the UHF result. The UHF values lie above the MCSCF values except at the first few Bragg peaks. This is similar to the result in the Cu^{2+} ion as seen in Fig. 6.1-(b). However the difference between UHF and MCSCF is slightly larger in the cluster than in the free ion. It seems to indicate that existence of some correlation (although very small) between d electrons in Cu and p electrons in O which does not exist in the free ion. We also found less spin density at the O sites in the plane in MCSCF compared to UHF. It makes the MCSCF values at small $|\vec{q}|$ similar to the RHF values. Our calculation suggests that the correlation effect makes the spin density more localized near the Cu site.

The total energy values of RHF, UHF and MCSCF for the cluster are listed in Table 6.2. It shows that the correlation energy of the cluster in MCSCF is

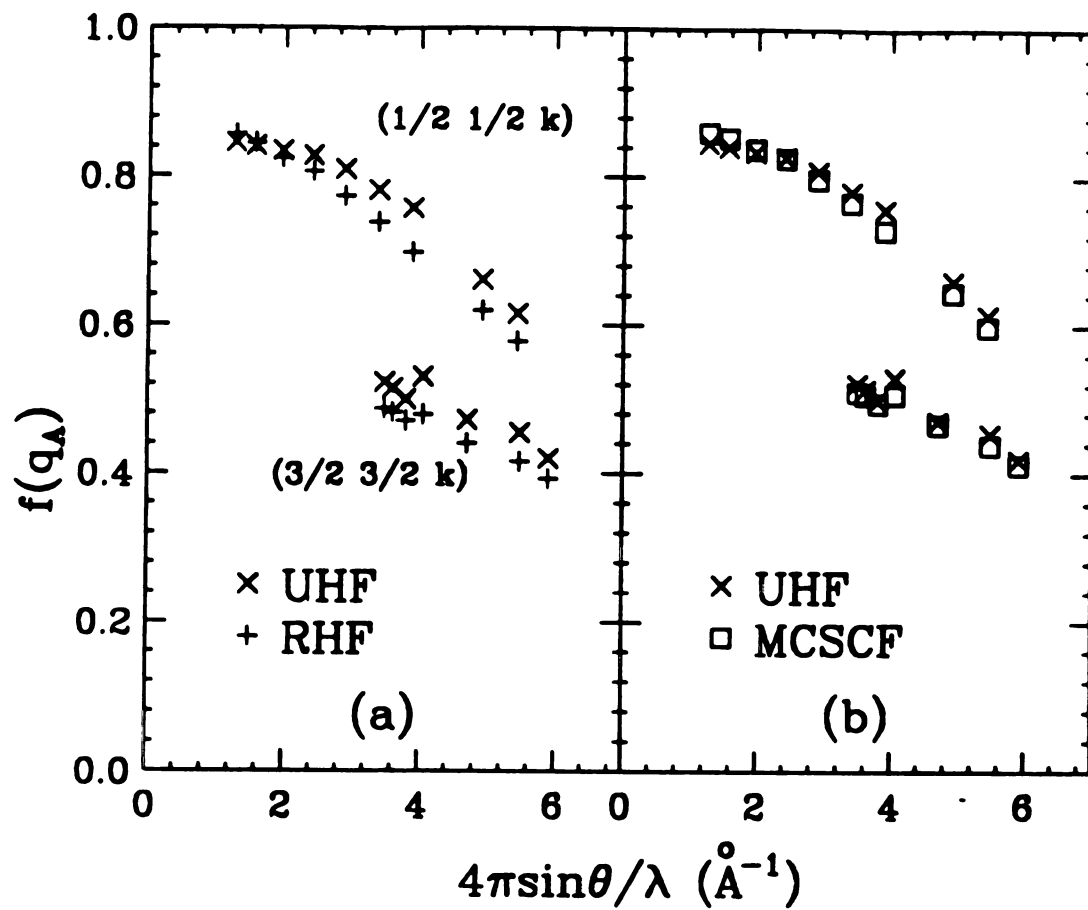


Figure 6.5: The calculated $\text{YBa}_2\text{Cu}_3\text{O}_6$ form factor with RHF, UHF and MCSCF methods.

similar to that of free Cu^{2+} ion in Table 6.1. The form factor for free Cu^{2+} hardly changed from MCSCF to CISD2; thus one might expect that the form factor of CISD for the cluster is similar to that of MCSCF. Accordingly, we expected our MCSCF to be a good approximation to find the correlation effect on the form factor without doing extended CI calculations for the cluster. However a recent work on the cluster of La_2CuO_4 by Martin and Hay [mart93] using extended CI calculations contradicts this expectation: it gave the Mulliken charge values which were quite different from RHF results. This will be discussed further at the end of this chapter.

We compare the MCSCF form factors for the cluster, the free ion and the ion with point charge distributions in Fig. 6.2. The cluster form factors are certainly lower than the ion form factors at small $|\vec{q}|$, the slope of the cluster form factor being flatter than that for the ion. This is a manifestation of the *covalence*. In the cluster, the electrons in O are allowed to hop to the Cu sites. It means that spin density can be transferred from Cu to O. When an O is shared by two antiferromagnetically ordered Cu's, the transferred spin density at the O site doesn't give any contribution to the form factor at the AF wave vectors. It reduces the form factor values at small $|\vec{q}|$ and also leads to the covalent reduction of the magnetic moment at the Cu site. However, at large $|\vec{q}|$, the covalent effect is hardly seen, especially in the 2nd family $(3/2, 3/2, k)$. It is because the form factor at large $|\vec{q}|$ probes the spin density at small $|\vec{r}|$, so it is insensitive to the spin density near the O sites.

6.3.4 Comparison with experiment

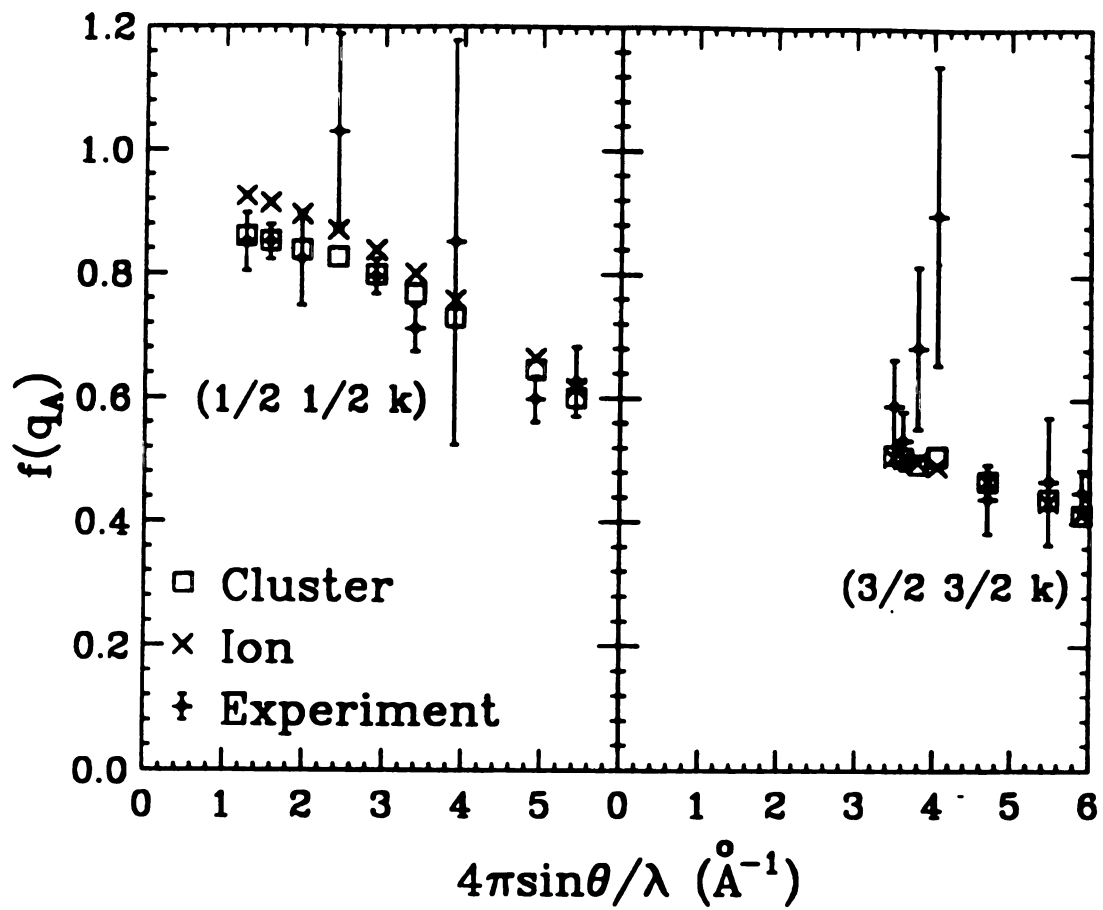


Figure 6.6: The calculated ionic and cluster form factors were compared with experiment [sham93] in $\text{YBa}_2\text{Cu}_3\text{O}_6$.

We compare the MCSCF form factors with the experiments for $\text{YBa}_2\text{Cu}_3\text{O}_6$ in Fig. 6.6. Because of the uncertainty in determining the absolute values of the ordered moments in the present experimental results as mentioned in the introduction part of this section, we again compare the *shape* of the form factor rather than the absolute values. Thus the experimental values are scaled to give the best fit to the calculated MCSCF values. Fig. 6.6 compares the MCSCF form factor for the ion and the cluster with the experiment of Shamoto et. al. [sham93]. From Fig. 6.6, we see that the shape of the calculated cluster form factor agrees with experiment except at the few points which have large error bars for both the families, $(1/2, 1/2, k)$ and $(3/2, 3/2, k)$. When we compare the ionic form factor with the experiment as Shamoto et. al. [sham93] did, it also gives a reasonable agreement. Even though we see the covalence effect by comparing the ionic and cluster form factor, the difference between them is within experimental error. In order to see the covalence effect in the form factor, a more accurate experiment is needed, at least according to this calculation.

From the experimental and theoretical study of the two families of Bragg peaks, $(1/2, 1/2, k)$ and $(3/2, 3/2, k)$, one sees that the slope of the form factor of a given family is nearly flat. These small changes in a family indicate that the spin density is mainly confined to the CuO_2 plane. This is confirmed by studying the spin density of the cluster in the real space, \vec{r} . Also, we found a very small amount of *negative* spin density on the apical O site. This negative spin density can be understood as the result of the exchange interaction between the oxygen p electrons and the unpaired d electron (with positive spin) in the UHF and MCSCF methods. (The result follows from the fact that the exchange interaction, which is attractive, occurs only between parallel-spin electrons.)

6.4 La_2CuO_4

Even though La_2CuO_4 has been extensively studied since La_2CuO_4 was known as a parent of the high T_C superconductor, the experiment on La_2CuO_4 still has uncertainty, since preparation of a pure stoichiometric sample of La_2CuO_4 is difficult and observable physical quantities such Néel temperature and structure transition temperature strongly depend on the oxygen content. La_2CuO_4 is isostructural to La_2NiO_4 , shown in Fig. 5.6. It is known that La_2CuO_4 is tetragonal at high temperatures and undergoes an orthorhombic distortion at lower temperature. The transition temperature varies from 450K to 530K depending on the oxygen vacancies (y) in $\text{La}_2\text{CuO}_{4-y}$ [vakn87].

Different values of the Néel temperature, T_N , and the ordered moment, μ , were reported in different works: 185K and $0.30 \mu_B$ [frel88], and 250K and $0.40 \mu_B$ [yang87] respectively. Yamada et. al. measured T_N and the ordered moments on samples of $\text{La}_2\text{CuO}_{4-y}$ with different y values; they found that higher T_N corresponded to higher moment and reported 289K and $0.60 \mu_B$ as the maximum values of these two quantities in a particular sample [yama87]. Finally, Keimer et. al. reported a Néel temperature of 325K in their sample of La_2CuO_4 , believed to be very close to stoichiometric [keim92]. From Yamada et al.'s results one expects this sample to have a larger μ (unfortunately Keimer et al. didn't measure the ordered moment in their samples).

The experimental form factor measurement for more than one Bragg peak was reported by only two groups [frel88, vakn87], as far as we know. Other experiments measured only one Bragg peak to determine the ordered moment by using the form factor of K_2CuF_4 as discussed in Chap. 1. However their samples seem far

from stoichiometric judging from their low Néel temperature; 187K in Freltoft et. al.[frel88] and 220K in Vaknin et. al.[vakn87]. Nevertheless, we will compare our results with the later experiment of Freltoft et al.[frel88], in the hope that the *shape* might not be sensitive to stoichiometry. Some indication, that this might be true, was given Burlet et. al.'s experiment in $\text{YBa}_2\text{Cu}_3\text{O}_6$ [bur188]. Another form factor measurement in a powder sample by Vaknin et. al.[vakn87], was claimed to be a preliminary result by Freltoft et. al.[frel88] who measured the form factor in a single crystal sample later. Thus we compare our result with the later experiment, those of Freltoft et. al. [frel88].

6.4.1 Cluster

The cluster electronic wave functions for a $(\text{CuO}_6)^{10-}$ in La_2CuO_4 have been calculated using RHF, UHF and MCSCF procedures. We took our cluster as a Cu ion and 6 ligand O ions in the appropriate tetragonal geometry with distances between Cu-O as 1.89\AA in the CuO_2 plane and 2.41\AA along the apical axis. We ignored small orthorhombic distortion in our cluster calculation since we found that a small distortion hardly changed the wave functions.

RHF and UHF calculations were performed with the COLUMBUS code[colu88] and the Gaussian 92 code [g92] respectively, with the same basis sets in $\text{YBa}_2\text{Cu}_3\text{O}_6$ calculation. All the 87 electrons of the $(\text{CuO}_6)^{10-}$ cluster, considering $S = 1/2$, were included explicitly in the *ab initio* calculations.

To investigate correlation effects beyond HF, an MCSCF calculation with COLUMBUS[colu88] was performed for the $(\text{CuO}_6)^{10-}$ cluster similarly to $\text{YBa}_2\text{Cu}_3\text{O}_6$. The result of MCSCF with 354 configuration state functions in $(\text{CuO}_6)^{10-}$ indicated that d-d correlation was most dominant, similar to the re-

sult in MCSCF for $\text{YBa}_2\text{Cu}_3\text{O}_6$.

6.4.2 Environment

We took a 552 point-charge environment outside the $(\text{CuO}_6)^{10-}$ cluster. The positions of the point charges were determined from Cava et. al. [cava87]. The point charge environment is PC333 corresponding to 27 unit cells, the same as in La_2NiO_4 in Sec. 5.4. Beyond the simple point charge model, we first replaced the neighboring point charges by ECP's[wadt85]. The procedure of replacing point charges by ECP's in La_2CuO_4 is the same as in La_2NiO_4 ; denoted as ECP1 (8 La^{3+} ECP's), ECP2 (10 La^{3+} ECP's) and ECP3 (10 La^{3+} and 4 Cu^{2+} ECP's).

6.4.3 Calculated form factor

The theoretical form factors were calculated from RHF, UHF and MCSCF for the two families of the Bragg peaks in La_2CuO_4 , $(1/2, 1/2, k)$ and $(3/2, 3/2, k)$, similar to $\text{YBa}_2\text{Cu}_3\text{O}_6$ in tetragonal notation. The calculated form factors in Fig. 6.7-(a),(b) show the covalent effect as a plateau at small $|\vec{q}|$. The overall changes from RHF to UHF in Fig. 6.7-(a) and from UHF to MCSCF in Fig. 6.7-(b) are very similar to the results in $\text{YBa}_2\text{Cu}_3\text{O}_6$.

The total energy values of RHF, UHF and MCSCF are listed in Table 6.2 and the energy differences are also similar to those of $\text{YBa}_2\text{Cu}_3\text{O}_6$. The theoretically calculated form factors of La_2CuO_4 and $\text{YBa}_2\text{Cu}_3\text{O}_6$ were found to be quite similar despite a rather big difference between the basic clusters (one of the apical O's is missing in $\text{YBa}_2\text{Cu}_3\text{O}_6$). We can understand the similarity of the results by realizing that the spin density originates, mainly, from a $d_{(x^2-y^2)}$ orbital, which is rather disconnected from the apical O's.

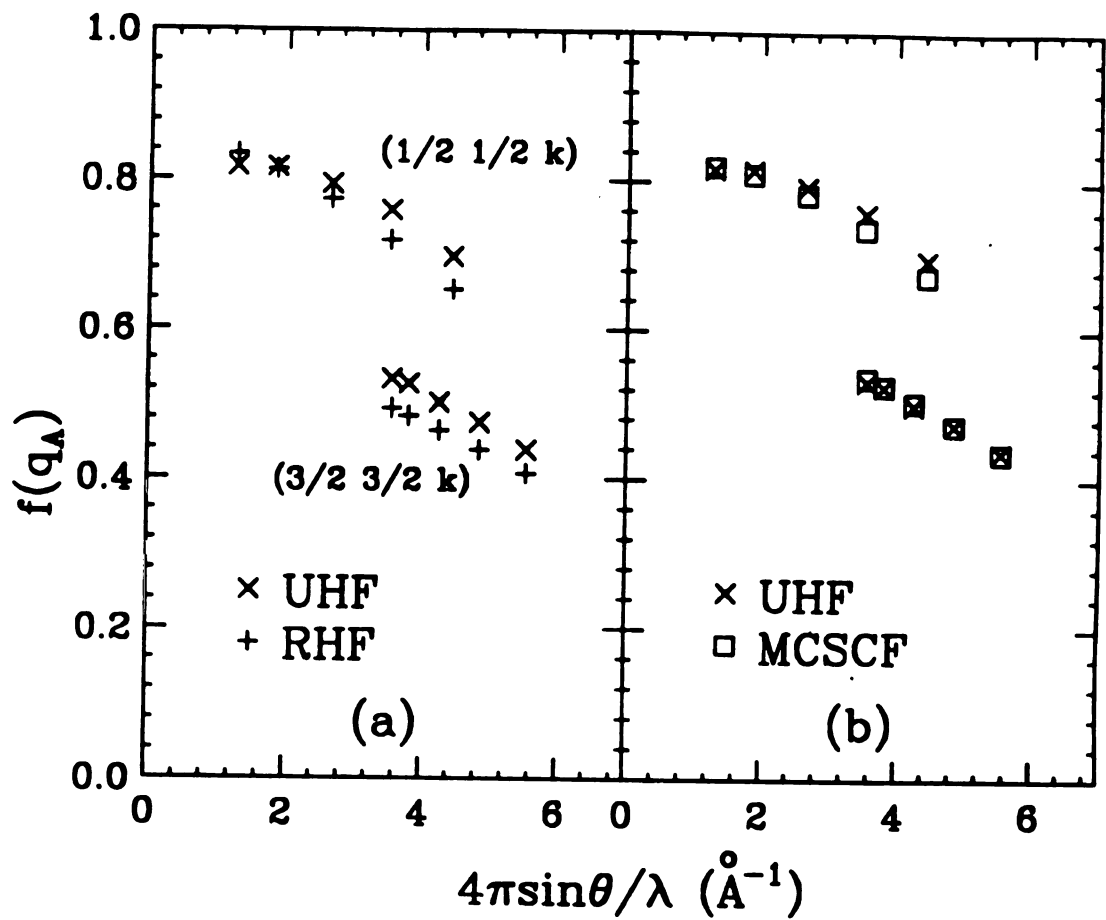


Figure 6.7: The calculated La_2CuO_4 form factor with RHF, UHF and MCSCF methods.

For La_2CuO_4 , we found the form factor changed when we replaced nearby point charges by ECP's, by roughly 5 %. Replacing a positive point charge by a corresponding ECP seems to suppress the spin density of the nearby O sites because ECP for a positive ion is less attractive to the electrons in the O's than the positive point charge. This effect is noticeable especially when two +3 point charges at the positions of La^{3+} 's right above and below the apical oxygens of the cluster of La_2CuO_4 were replaced by La^{3+} ECPs. In our paper[kap194], where we included only the nearest La^{3+} ECP's (of which there are 8) (ECP1), we had found more spin density in the apical oxygen sites than in ECP3. The effect of reducing the spin density at the oxygen sites by additional ECP's was also found when we replaced 4 more point charges by Cu^{2+} ECP in the CuO_2 plane in La_2CuO_4 and later in $\text{YBa}_2\text{Cu}_3\text{O}_6$. However, the Cu^{2+} ECP replacement caused very little change in the spin density. The general suppression of the spin density at the O sites resulted in smaller covalent reduction of the ordered moment defined in Sec. 2.4. In addition to the effect from ECP, MCSCF also resulted in reducing the spin density at the O sites in the CuO_2 plane, from the UHF result.

6.4.4 Comparison with experiment

For La_2CuO_4 , we compare the MCSCF form factors for the ion and the cluster with Freltoft et. al.'s experiment[frel88]. Because of the uncertainty in determining the absolute values of the ordered moments in the present experimental results for La_2CuO_4 as mentioned in Sec. 6.4, we compared the *shape* of the form factor. Thus the experimental values are scaled to give the best fit to the calculated MCSCF values. One should note that the notation in Ref. [frel88] for the Bragg peaks is different from our tetragonal notation because they used an orthorhombic

conventional notation. Fig. 6.8 shows that the cluster form factor agrees better with the experiment than the ionic form factor. The form factor of La_2CuO_4 also shows the plateau in the experiment as well as the cluster calculation.

6.5 $\text{Sr}_2\text{CuO}_2\text{Cl}_2$

We applied our cluster method to $\text{Sr}_2\text{CuO}_2\text{Cl}_2$, which has a tetragonal structure, similar to La_2CuO_4 , but the LaO layers in La_2CuO_4 are replaced by SrCl. Since the apical oxygens in La_2CuO_4 are replaced by Cl, the study of the form factor of $\text{Sr}_2\text{CuO}_2\text{Cl}_2$ can give us some insight into the magnetic moment of the out-of-plane oxygen sites,

$\text{Sr}_2\text{CuO}_2\text{Cl}_2$ is known to be antiferromagnetically ordered at $\sim 250\text{K}$ and the spins are aligned along the line connecting next nearest neighbor Cu-Cu as found by Vaknin et. al.[vakn90].

The experimental form factor was measured by two groups, Ref. [wang90] and Ref. [vakn90], and their experimental form factor agreed with each other within experimental error. They measured the form factor at 15K[wang90] and 10K[vakn90] where $\text{Sr}_2\text{CuO}_2\text{Cl}_2$ still has a tetragonal structure while La_2CuO_4 transforms from the tetragonal to orthorhombic structure below 540 K. The experimentally measured form factor of $\text{Sr}_2\text{CuO}_2\text{Cl}_2$ by both the groups is similar to that of La_2CuO_4 [frel88]. Wang et. al. [wang90] compared their experiment with the Cu^{2+} ion form factor and with band theory calculations, but neither of them agreed with experiment. Later in this chapter, we compare our cluster calculation with Wang et. al.'s to see the difference between their band calculation and our cluster calculation of the form factor.

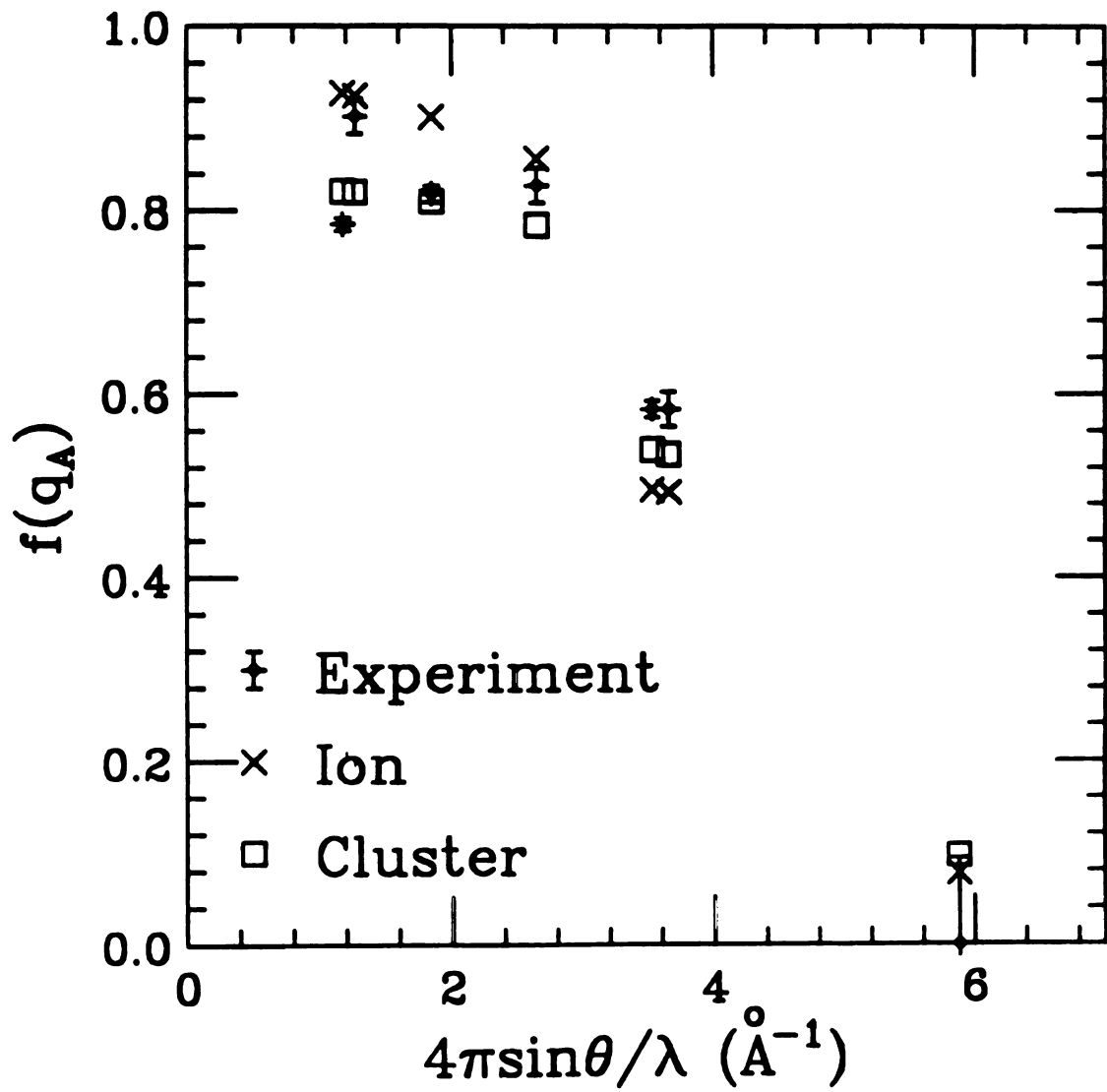


Figure 6.8: The calculated ionic and cluster form factors were compared with experiment [frel88] in La_2CuO_4 .

6.5.1 Cluster

The $(\text{CuO}_4\text{Cl}_2)^{8-}$ cluster is similar to the $(\text{CuO}_6)^{10-}$ cluster except the two apical oxygens in $(\text{CuO}_6)^{10-}$ are replaced by Cl^+ 's. The distance between Cu-O in the CuO_2 plane is 1.99\AA and the distance between Cu-Cl along the apical axis is 2.86\AA . The same basis sets for Cu, (13s9s5d)[wach70], and for O, (9s6p)[huzi71], as in $(\text{CuO}_6)^{10-}$ were used for $(\text{CuO}_4\text{Cl}_2)^{8-}$. The basis set for Cl was also taken from Ref. [huzi71] with an additional diffuse p orbital as (9s6p). All 103 electrons in $(\text{CuO}_4\text{Cl}_2)^{8-}$ were treated via UHF calculations using Gaussian 92 code[g92].

6.5.2 Environment

The point charges within 27 unit cells were taken via Evjen's method discussed in in Sec. 4.4.2, as in La_2CuO_4 . The positions of point charges were determined from Vaknin et. al. [vakn90]. Beyond the point charge model, the same ECP environment, ECP3 (10 Sr^{2+} 's ECP and 4 Cu^{2+} 's ECP), as in La_2CuO_4 was taken except that the La^{3+} ECP in La_2CuO_4 was replaced by the Sr^{2+} ECP [wadt85].

6.5.3 Comparison with experiment

The calculated UHF form factors are compared with the experimental results of Wang et. al.[wang90] and the ionic form factor in Fig. 6.9. The UHF result reproduced the plateau in the small q region as seen in the experiment [wang90]. Compared to the band calculation (LDA) carried out by Wang et. al.[wang90], or the free Cu^{2+} ion calculation, our *ab initio* cluster results seem to agree much better with the experiment, thus providing a good justification of our method.

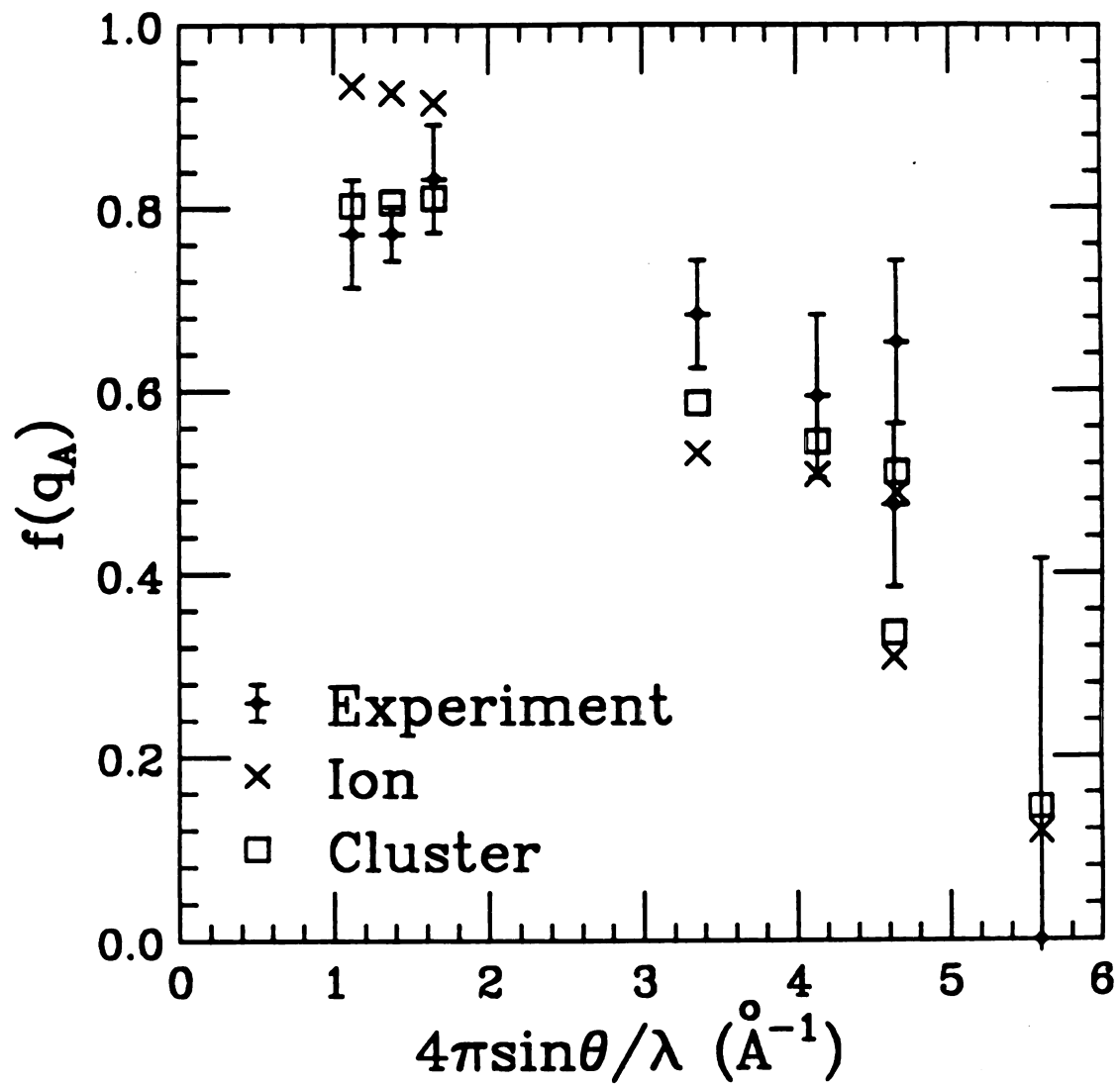


Figure 6.9: The calculated ionic and cluster form factors were compared with experiment [wang90] in $\text{Sr}_2\text{CuO}_2\text{Cl}_2$.

Table 6.3: Covalence factors obtained from the cluster calculations defined in Eq. (2.68).

	MCSCF (ECP3)	UHF (ECP3)	UHF (ECP1)
YBa ₂ Cu ₃ O ₆	0.85	0.81	0.78
La ₂ CuO ₄	0.84	0.80	0.75

The calculated and experimental form factors of Sr₂CuO₂Cl₂ are similar to that in La₂CuO₄, showing a plateau in the small q region. It indicates that replacing the apical oxygen by Cl hardly affects the spin density in general and in particular the out of plane spin density is negligible. The spin density in the layered cuprate materials seems to be primarily confined in the CuO₂ plane.

6.6 Conclusions

From the study of the form factor of YBa₂Cu₃O₆, La₂CuO₄, and Sr₂CuO₂Cl₂, we conclude that the calculated shapes of the neutron form factor agree reasonably well with experiments for these cuprate materials. For La₂CuO₄ and Sr₂CuO₂Cl₂, the cluster form factor agrees with the experiments much better than the ionic form factor. Within a family of \vec{q} values when only q_z increases, the slope is nearly flat. That lead us to conclude that the spin density of the cuprate material is confined in mainly the CuO₂ plane. We have also improved our calculated results including correlation effects via MCSCF and introducing additional ECP's. Unfortunately, the changes in the form factor by these efforts lie within the experimental errors.

The cluster results when compared to the ionic form factor clearly shows the

covalence effect. The covalence factors, calculated by using Eq.(2.68) in Sec. 2.4, are listed in the Table 6.3. The covalence factor is sensitive to the ECP environment because replacing the point charges by ECP, changes the spin density at the planar oxygen as well as at the apical oxygen. The covalence factor is determined by how much spin density is at the planar oxygen sites since the spin density at these oxygen sites is canceled by AF ordering. We also found that the covalence factor has changed by including correlation effects via MCSCF. However, our MCSCF calculations, which are limited to 354 configuration state functions, might not be good enough to give accurately the effect of correlation on the covalence factor. MCSCF gave less covalence than UHF, which is anti-intuitive, i.e. we expected that including correlation should lead to more covalence. Moreover from an analysis of the Mulliken charge, Martin and Hay [mart93] found more covalence in their CI calculation compared to our MCSCF, while our RHF results agree with theirs. In order to study the covalence effect *more accurately*, we have to expand our MCSCF calculation to include more configuration state functions. This will be a next step following this thesis work.

The *ab initio* cluster method appears to work rather well in the form factor calculation for the cuprate system. Then the question is, why the same method failed so badly to reproduce the experimental form factors for La_2NiO_4 , which is isostructural to La_2CuO_4 . The main difference between La_2NiO_4 and La_2CuO_4 is the different spin states of Ni^{2+} and Cu^{2+} . In the ground state of the $(\text{NiO}_6)^{10-}$ cluster, two molecular orbitals, which have e_g symmetry such as $d_{x^2-y^2}$ and $d_{3z^2-r^2}$, are singly occupied. Thus the spin density in $(\text{NiO}_6)^{10-}$ is 3-dimensional while the spin density in $(\text{CuO}_6)^{10-}$ is 2-dimensional. This explains why replacing apical La^{3+} point charges by ECP changed the form factor values in La_2NiO_4 , by about

10%, more compared to La_2CuO_4 where this change is about 5%). Unfortunately there is only one measurement of the form factor for La_2NiO_4 which showed a dramatic flattening, i.e. a big plateau in the small $|q|$ region, which was not seen in the form factor of other nickel compounds such as KNiF_3 and NiO . We have investigated several possibilities to explain the observed plateau, such as a mixing of the singlet and triplet spin states on each site [kapl94] and other configurations for the ground state such as one t_{2g} and one e_g state are singly occupied rather than the two e_g 's. But these attempts failed to reproduce the observed shape of the form factor. An extensive correlation calculation on the cluster might resolve this problem. Also another experiment is needed to confirm the observed strange form factor seen in La_2NiO_4 [wang91].

Appendix A

Perturbation calculation of the contribution of the 4-spin hamiltonian $\hat{\mathcal{H}}^{(4)}$

$\mathcal{H}^{(4)}$ can be written in terms of spin operators [taka77]

$$\begin{aligned}
 \mathcal{H}^{(4)} = & \frac{1}{U^3} \left\{ \sum_{i<j} 4t_{ij}^4 (1 - 4\vec{S}_i \cdot \vec{S}_j) + \sum_{i<k} t_{ij}^2 t_{jk}^2 (4\vec{S}_i \cdot \vec{S}_k - 1) \right. \\
 & + \sum_{loop} t_{ij} t_{jk} t_{kl} t_{li} [80(\vec{S}_i \cdot \vec{S}_j)(\vec{S}_k \cdot \vec{S}_l) \\
 & + 80(\vec{S}_j \cdot \vec{S}_k)(\vec{S}_l \cdot \vec{S}_i) - 80(\vec{S}_i \cdot \vec{S}_k)(\vec{S}_j \cdot \vec{S}_l) \\
 & - 4(\vec{S}_i \cdot \vec{S}_j) - 4(\vec{S}_j \cdot \vec{S}_k) - 4(\vec{S}_k \cdot \vec{S}_l) - 4(\vec{S}_l \cdot \vec{S}_i) \\
 & \left. - 4(\vec{S}_i \cdot \vec{S}_k) - 4(\vec{S}_j \cdot \vec{S}_k) + 1 \right\} \quad (\text{A.1})
 \end{aligned}$$

If we take the spin-up sublattice, the spin operators in the *Holstein-Primakoff representation* are given by

$$S_j^\dagger = \sqrt{2S} \left(1 - \frac{a_j^\dagger a_j}{2S} \right)^{1/2} a_j, \quad (\text{A.2})$$

$$S_j = a_j^\dagger \sqrt{2S} \left(1 - \frac{a_j^\dagger a_j}{2S} \right)^{1/2}, \quad (\text{A.3})$$

$$S_j^z = S - a_j^\dagger a_j. \quad (\text{A.4})$$

In spin wave approximation [matt65, kitt63], the above spin operators can be expanded in powers of $(1/S)$ as

$$\begin{aligned} S_j^\dagger &\approx \sqrt{2S} \left(1 - \left(\frac{1}{S} \right) a_j^\dagger a_j \right) a_j, \\ S_j &\approx \sqrt{2S} a_j^\dagger \left(1 - \left(\frac{1}{S} \right) a_j^\dagger a_j \right). \end{aligned} \quad (\text{A.5})$$

We introduce the spin operators in \vec{k} space as

$$\begin{aligned} a_j &= \frac{1}{\sqrt{N}} \sum_{\vec{k}} e^{-i\vec{k} \cdot \vec{R}_j} a_{\vec{k}}, \\ a_j^\dagger &= \frac{1}{\sqrt{N}} \sum_{\vec{k}} e^{i\vec{k} \cdot \vec{R}_j} a_{\vec{k}}^\dagger. \end{aligned} \quad (\text{A.6})$$

We then use Bogoliubov transformations which makes \mathcal{H}_o diagonal, i.e.,

$$\begin{aligned} a_{\vec{k}} &\rightarrow (\cosh u_{\vec{k}}) B_{\vec{k}} + (\sinh u_{\vec{k}}) B_{-\vec{k}}^\dagger, \\ a_{\vec{k}}^\dagger &\rightarrow (\cosh u_{\vec{k}}) B_{\vec{k}}^\dagger + (\sinh u_{\vec{k}}) B_{-\vec{k}}, \end{aligned} \quad (\text{A.7})$$

with $u_{\vec{k}} = u_{-\vec{k}} = u_{*\vec{k}}$ and requiring the condition, $\tanh 2u_{\vec{k}} = (1/Z) \sum_{\vec{\tau}} \cos(\vec{k} \cdot \vec{\tau})$.

Keeping the leading terms of $O(1/S)$ inside the square brackets, \mathcal{H}_o reduces to

$$\mathcal{H}_o = \left(\frac{4t^2}{U} \right) \frac{ZS^2}{2} \left[-N \left(1 + \frac{1}{S} \right) + \frac{2}{S} \sum_{\vec{k}} (n_{\vec{k}} + 1) \sqrt{1 - \gamma_{\vec{k}}^2} \right] \quad (\text{A.8})$$

where $n_{\vec{k}} = B_{\vec{k}}^\dagger B_{\vec{k}}$ and $\gamma_k = (1/Z) \sum_{\vec{\tau}} e^{i\vec{k} \cdot \vec{\tau}}$.

$\mathcal{H}^{(4)}$ can be separated into two parts, diagonal terms and off-diagonal terms,

as

$$\mathcal{H}^{(4)} = V_{dia} + V_{off} \quad (\text{A.9})$$

where

$$\begin{aligned}
V_{dia} = & \frac{t^4}{U^3} \left[3N + 48S^2 \left\{ N\left(1 + \frac{1}{S}\right) - \frac{2}{S} \sum_{\vec{k}} \left(n_{\vec{k}} + \frac{1}{2}\right) \sqrt{1 - \gamma_{\vec{k}}^2} \right\} \right. \\
& + 8S^2 \left\{ N - \frac{1}{S} \sum_{\vec{k}} (a(\vec{k})n_{\vec{k}} + c(\vec{k})) \right\} \\
& + 8S^2 \left\{ N - \frac{1}{S} \sum_{\vec{k}} (f(\vec{k})n_{\vec{k}} + h(\vec{k})) \right\} \\
& + 80S^4 \left\{ 2 \left(N\left(1 + \frac{2}{S}\right) - \frac{4}{S} \sum_{\vec{k}} \left(n_{\vec{k}} + \frac{1}{2}\right) \sqrt{1 - \gamma_{\vec{k}}^2} \right) \right. \\
& \left. \left. - \left(N - \frac{2}{S} \sum_{\vec{k}} (a(\vec{k})n_{\vec{k}} + c(\vec{k})) \right) \right\} \right], \tag{A.10}
\end{aligned}$$

and

$$\begin{aligned}
V_{off} = & \frac{t^4}{U^3} \left[-8S^2 \sum_{\vec{k}} \frac{1}{S} \left\{ (b(\vec{k}) + g(\vec{k})) (B_{\vec{k}}^\dagger B_{-\vec{k}}^\dagger + B_{-\vec{k}} B_{\vec{k}}) \right\} \right. \\
& \left. + 80S^4 \sum_{\vec{k}} \frac{2}{S} \left\{ b(\vec{k}) (B_{\vec{k}}^\dagger B_{-\vec{k}}^\dagger + B_{-\vec{k}} B_{\vec{k}}) \right\} \right]. \tag{A.11}
\end{aligned}$$

For 2-dimensional system, relevant to our cuprate and related systems,

$$\begin{aligned}
a(\vec{k}) &= 2(\mu_{\vec{k}}^2 + \nu_{\vec{k}}^2)(1 - \cos \vec{k} \cdot \vec{\tau}_x \cos \vec{k} \cdot \vec{\tau}_y), \\
b(\vec{k}) &= 2\mu_{\vec{k}}\nu_{\vec{k}}(1 - \cos \vec{k} \cdot \vec{\tau}_x \cos \vec{k} \cdot \vec{\tau}_y), \\
c(\vec{k}) &= 2\nu_{\vec{k}}^2 - 2\mu_{\vec{k}}^2 \cos \vec{k} \cdot \vec{\tau}_x \cos \vec{k} \cdot \vec{\tau}_y, \\
f(\vec{k}) &= (\mu_{\vec{k}}^2 + \nu_{\vec{k}}^2)(2 - \cos 2\vec{k} \cdot \vec{\tau}_x - \cos 2\vec{k} \cdot \vec{\tau}_y), \\
g(\vec{k}) &= \mu_{\vec{k}}\nu_{\vec{k}}(2 - \cos 2\vec{k} \cdot \vec{\tau}_x - \cos 2\vec{k} \cdot \vec{\tau}_y), \\
h(\vec{k}) &= 2\nu_{\vec{k}}^2 - \mu_{\vec{k}}^2(\cos 2\vec{k} \cdot \vec{\tau}_x + \cos 2\vec{k} \cdot \vec{\tau}_y), \tag{A.12}
\end{aligned}$$

where the relation $\mu_{\vec{k}}^2 - \nu_{\vec{k}}^2 = 1$ holds.

The expectation value of the site spin operator, S_j^z , is given by

$$\langle S_j^z \rangle = \langle \Psi | S_j^z | \Psi \rangle, \quad (\text{A.13})$$

where Ψ is the ground state of the Hamiltonian in Eq. (2.58). $\Psi = \Psi_o + \delta\Psi$, where Ψ_o is the ground state of \mathcal{H}_o , $\Psi_o = |0\rangle$, i.e. the zero magnon state, and $\delta\Psi$ is the perturbed eigenstate associated with $\mathcal{H}^{(4)}$, then we have

$$\delta\Psi = \sum_{l''} \frac{\langle 0 | \mathcal{H}^{(4)} | l'' \rangle}{E_o^0 - E_{l''}^0} | l'' \rangle, \quad (\text{A.14})$$

where $|l''\rangle$ are the two magnon states and E^0 's are the eigenvalues of \mathcal{H}_o . Here $\langle 0 | \mathcal{H}^{(4)} | l'' \rangle$ has non-zero contribution from only the V_{off} part of $\mathcal{H}^{(4)}$.

We obtain $\langle S_j^z \rangle$ up to the first correction as

$$\langle S_j^z \rangle = \langle \Psi_o | S_j^z | \Psi_o \rangle + 2\langle \Psi_o | S_j^z | \delta\Psi \rangle \quad (\text{A.15})$$

For the square lattice with $S = 1/2$, the two terms in Eq. (A.15) are given

$$\begin{aligned} \langle \Psi_o | S_j^z | \Psi_o \rangle &\equiv \langle S_z \rangle_{\text{Heis}} \\ &= \frac{1}{N} \sum_{\vec{k}} \left(\frac{1}{2}\right) \frac{1}{\sqrt{1 - \gamma_k^2}}. \end{aligned} \quad (\text{A.16})$$

$$\begin{aligned} \langle \Psi_o | S_j^z | \delta\Psi \rangle &= \left(\frac{t^2}{U^2}\right) \frac{1}{4N} \sum_{\vec{k}} \frac{\gamma_k^2}{(1 - \gamma_k^2)^{3/2}} [8(1 - \cos\vec{k} \cdot \vec{\tau}_x \cos\vec{k} \cdot \vec{\tau}_y) \\ &\quad - (2 - \cos 2\vec{k} \cdot \vec{\tau}_x - \cos 2\vec{k} \cdot \vec{\tau}_y)], \end{aligned} \quad (\text{A.17})$$

where $\gamma_k = \frac{1}{2} \sum_{\vec{\tau}} e^{i\vec{k} \cdot \vec{\tau}} = \frac{1}{2} (\cos\vec{k} \cdot \vec{\tau}_x + \cos\vec{k} \cdot \vec{\tau}_y)$. We calculate the above summations numerically. After checking the convergency of our numerical calculations, we obtain $\langle S_z \rangle_{\text{Heis}} = 0.30362$ in Eq. (A.16) which agrees with Anderson's well-known result [ande52] and $2\langle \Psi_o | S_j^z | \delta\Psi \rangle = 1.2839(\frac{t^2}{U^2})$ in Eq. (A.17).

Appendix B

Construction of natural orbitals in MCSCF

In this appendix, I describe the development of the programs to construct natural orbitals (NO) in our MCSCF calculation.

The one particle density matrix is given by Eq. (4.23)

$$\gamma(1'|1) = N \int \psi^*(1', 2, \dots, N) \psi(1, 2, \dots, N) d\tau(2, \dots, N). \quad (\text{B.1})$$

Eq. (B.1) can be written with the determinants in the configuration state functions (CSF)'s of Eq. (4.19) and Eq. (4.20)

$$\gamma(1'|1) = N \sum_I \sum_J \sum_k \sum_l C_I^* C_J C_{kI}^* C_{lJ} \langle D_k^I | D_l^J \rangle_{2..N}. \quad (\text{B.2})$$

Let's define $I(I, J, k, l)$ as

$$\begin{aligned} I(I, J, k, l) &= \langle D_k^I | D_l^J \rangle_{2..N} \\ &= \int D_k^{I*} D_l^J d\tau(2..N) \end{aligned} \quad (\text{B.3})$$

Then $I(I, J, k, l)$ can be reduced to a form of

$$I(I, J, k, l) = \frac{1}{N} \sum_i \sum_j \phi_i^*(1') a_{ij}(I, J, k, l) \phi_j(1), \quad (\text{B.4})$$

where $a_{ij}(I, J, k, l)$ is determined from Eq. (B.3). The matrix A_{ij} is

$$A_{ij} = \sum_I \sum_J \sum_k \sum_l C_I^* C_J C_{kI}^* C_{lJ} a_{ij}(I, J, k, l) \quad (\text{B.5})$$

In order to construct A_{ij} , we have to find the non-zero contribution from $a_{ij}(I, J, k, l)$.

In an MCSCF calculation, only active molecular orbitals, which form configuration state functions, contribute non-diagonal terms in A_{ij} , so we can construct A_{ij} whose dimension is ($N_{active} \times N_{active}$) rather than ($NMO \times NMO$). ' NMO ' is the total number of molecular orbitals and ' N_{active} ' is the number of active molecular orbitals.

B.1 Development of programs

The construction of NO's consists of the following steps.

- (1) Read the determinants, D_k^I and D_l^J .

The information of CSF including the determinants and the CI coefficients can be read from the file generated by `mcpc.x` in COLUMBUS code[`colu88`].

- (2) Construct the one particle density matrix A_{ij} .

We can construct A_{ij} in the basis of active molecular spin orbitals by finding non-zero contribution of $I(I, J, k, l)$

A determinant, D_k^I , for N active electrons with N_{active} active molecular spin orbitals, is written as

$$D_k^I = |\phi_1(1)\phi_2(2)\dots\phi_i(\nu)\dots\phi_k(N)| \quad (\text{B.6})$$

where ν is the index for an electron and i, k are the indexes for molecular spin orbitals running between 1 and N_{active} .

When D_k^I and D_l^J are the same, $I(I, J, k, l)$ becomes

$$I(I, J, k, l) = \frac{1}{N} \sum_i^{\text{occ}} \phi_i^*(1') \phi_i(1) \quad (\text{B.7})$$

The other non-zero contribution to $I(I, J, k, l)$ comes only from the pair of determinants;

$$\begin{aligned} D_k^I &= |\phi_1(1)\phi_2(2)\dots\phi_i(\nu)\dots\phi_k(N)| \\ D_l^J &= |\phi_1(1)\phi_2(2)\dots\phi_j(\mu)\dots\phi_k(N)| \end{aligned} \quad (\text{B.8})$$

when $i = j$ but $\nu \neq \mu$, or when $i \neq j$ with $\nu = \mu$. Then

$$\begin{aligned} I(I, J, k, l) &= \frac{1}{N} (-1)^{(i+j)} \phi_i^*(1') \phi_j(1) \quad \text{for } i \neq j \\ &= \frac{1}{N} \phi_\nu^*(1') \phi_\mu(1) \quad \text{for } \nu \neq \mu \end{aligned} \quad (\text{B.9})$$

After summation on (I, J, k, l) in Eq. (B.5) and changing dummy indexes ν, μ to i, j we obtain the one-particle density matrix for active space

$$\gamma(1'|1) = \sum_i^{\text{Nactive}} \sum_j^{\text{Nactive}} \phi_i^*(1') \phi_j(1) A_{ij}. \quad (\text{B.10})$$

(3) Diagonalize A_{ij} and find eigenvalues and eigenvectors.

Eq. (B.10) can be written with a vector $\Phi = (\phi_1 \phi_2 \dots \phi_N)$ and a matrix $\mathbf{A} = A_{ij}$

$$\gamma(1'|1) = \Phi(1') \mathbf{A} \Phi^\dagger(1) \quad (\text{B.11})$$

If we chose a proper unitary matrix, \mathbf{C} and $\tilde{\Phi} = \Phi \mathbf{C}$, then $\gamma(1'|1)$ becomes

$$\gamma(1'|1) = \tilde{\Phi}(1') \mathbf{C}^\dagger \mathbf{A} \mathbf{C} \tilde{\Phi}^\dagger(1) \quad (\text{B.12})$$

where

$$\mathbf{C}^\dagger \mathbf{A} \mathbf{C} = \mathbf{N} \quad (\text{B.13})$$

where \mathbf{N} is a diagonal matrix whose elements, n_i 's, are called occupancy numbers.

Eq. (B.13) is reduced to the eigenvalue problem

$$\mathbf{AC} = \mathbf{CN}. \quad (\text{B.14})$$

(4) Construct NO's from the eigenvectors.

By solving the eigenvalue problem of the Eq. (B.14), we can construct NO's by $\tilde{\Phi} = \Phi\mathbf{C}$ from the active MO's.

In the procedure (3), A_{ij} can be separated to α_{ij} and β_{ij} for up-spin orbitals and down-spin orbital respectively because there is no spin cross term in A_{ij} . Then we can construct α -NO's and β -NO's separately in the procedure (4). From α -NO's and β -NO's, we can calculate the spin density.

The above procedures are integrated in the main program usually named as **norb_***.for** with the subroutine program, **density_sub.for**. Fig. B.1 shows the structure of the programs.

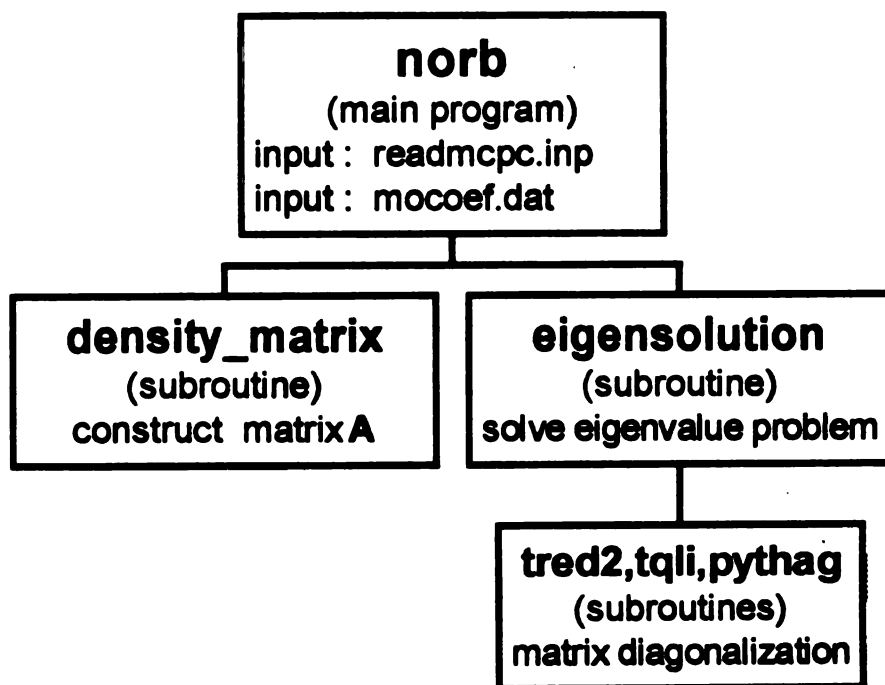


Figure B.1: Structure of program sets to construct NO's

Appendix C

Failure of the Mulliken Charge Population Analysis

In the UHF calculations of NiO and KNiF₃, we found the Mulliken charge values [levi91] obtained with diffuse basis functions in Ni (14s11p6d) to be quite different from the nominal charge values for the ionic material (see Table C.1). Particularly for NiO, the discrepancy is very large. These values (-0.21 for Ni and -1.63 for O) for NiO seem to contradict the assumption that NiO is highly ionic, which allows us to assign the nominal point charge values, +2 for Ni and -2 for O, when generating the Madelung potential. Therefore we performed the same cluster UHF calculations without diffuse basis functions in Ni (13s9p5d) to see how sensitive the Mulliken charge population was to the choice of basis functions. The Mulliken charge values without diffuse basis functions (13s9p5d) were found to be +1.75 for Ni and -1.95 for O, much closer to the nominal point charge values. (Similar values were obtained by Sulaiman et. al. [Saho90] in their cluster calculations of YBa₂Cu₃O₆ and La₂CuO₄).

Even though the results of the two calculations, with different basis sets, look so different in Mulliken charge analysis, we found that physically meaningful quan-

Table C.1: Mulliken charge population values for different basis sets for Ni

	NiO		KNiF ₃	
	Ni	O	Ni	F
(14s11p6d)	-0.21	-1.63	1.76	-0.96
(13s9p5d)	1.75	-1.96	1.86	-0.98

tities, such as the charge and the spin density, are essentially the same. Our understanding of how this is possible is the following. The diffuse functions in Ni (14s11p6d) are so diffuse that they spread over the neighboring oxygen sites and can mimic the diffuse function on the oxygens. We estimate that the approximately 1/3 of an electron per O assigned to the diffuse Ni orbitals are physically associated with the oxygen ions.

The Mulliken population values in KNiF₃ are rather stable with respect to the choice of basis sets and the calculated values are close to their ionic charges (+2 for Ni²⁺ and -1 for F⁻) even when we use the diffuse basis functions in Ni (see Table C.1). This is due to the fact that the F⁻ wave function is much more compact compared with the O²⁻ wave function so that the diffuse Ni functions are simply not appreciably occupied.

In summary, these results show that the Mulliken charges assigned to different ions (such as Ni, F, O etc.) depend not only on the choice of basis set but also on the type of ions in the cluster. (A similar problem was noted by Noell[noel82] and Bauschlicher and Bagus[baus84] for the transition metal complexes.) Therefore it sometimes may be misleading to use these charge assignments in describing physical quantities such as the electrostatic potential. As we just noted, our

NiO results give an extreme example: clearly the assignment to Ni of electrons in orbitals centered on Ni but so diffuse that most of their weight is at the Ni-O distance, is not sensible. The Mulliken assignment is much more sensible when the orbitals are not so diffuse. The charge density was in fact found to be essentially the same with or without these diffuse Ni functions, so it is clearly reasonable to prefer the Mulliken charges calculated without diffuse functions.

Appendix D

Crystal field splitting in KNiF_3 and NiO

In addition to the form factor, we have calculated the crystal field splitting in KNiF_3 and NiO in various calculation methods such as RHF, MCSCF, and CI. In this appendix, we briefly discuss our cluster calculation results of the crystal field splittings.

The atomic $3d$ orbitals of a transition metal ion like Ni^{2+} are degenerated if it is isolated. However a Ni^{2+} ion in KNiF_3 or NiO is subject to a crystal field of octahedral symmetry. The atomic $3d$ orbitals of a metal ion split, in the presence of such a field, into a triply degenerate t_{2g} level and a doubly degenerate e_g level. The e_g orbitals are higher in energy than the t_{2g} orbitals, and the difference between them is called $10Dq$ or the crystal field splitting. This $10Dq$ value is equivalent to the difference in one-electron energy between $t_{2g}^m e_g^n$ and $t_{2g}^{m-1} e_g^{n+1}$. For Ni^{2+} with 8 d -electrons, $10Dq$ is the energy difference between $t_{2g}^6 e_g^2$ and $t_{2g}^5 e_g^3$. Within the Hartree-Fock scheme for the cluster, $10Dq$ may be defined as the energy difference between two independently calculated N -electron states, ${}^3A_{2g}$ and ${}^3T_{2g}$ [elli68]:

$$10Dq = E_{{}^3T_{2g}} - E_{{}^3A_{2g}} \quad (\text{D.1})$$

Table D.1: $10Dq$ values for KNiF_3 and NiO (cm^{-1})

	KNiF_3	NiO
Experiment	6980 ^a	9114 ^b
RHF	5842	6363
MCSCF	6516	7114
CI	6224	6783

^aRef. [ferg64]

^bRef. [newm59]

Here ${}^3A_{2g}$ and ${}^3T_{2g}$ are the ground state and the first excited state, respectively, of the cluster, $(\text{NiF}_6)^{4-}$ or $(\text{NiO}_6)^{10-}$.

RHF, MCSCF and CI calculations had been carried out for octahedral $(\text{NiF}_6)^{4-}$ and $(\text{NiO}_6)^{10-}$ cluster with COLUMBUS[colu88] to get $10Dq$. We note that the $(\text{NiF}_6)^{4-}$ cluster calculations have been done with the nearest neighboring 8 K^+ ECP and 474 point charge environment while the $(\text{NiO}_6)^{10-}$ cluster calculations done with only 722 point charge environment.

The $10Dq$ value for KNiF_3 obtained by MCSCF agrees well with the experimental value within $\sim 7\%$ error. This is the best agreement with the experimental $10Dq$ using *ab initio* method for KNiF_3 as far as we know. For NiO , our best number from MCSCF is about 22% off from the experimental value even though we improved it from RHF to MCSCF.

Bibliography

- [aepp88] G. Aepli and D. J. Buttrey Phys. Rev. Lett. **61**, 203 (1988).
- [akim76] J. Akimitsu and Y. Ito, J. Phys. Soc. of Japan, **40** 1621 (1976)
- [alpe61] H.A. Alperin, Phys. Rev. Letters **2**, 55 (1961)
- [ande52] P. W. Anderson, Phys. Rev. **86**, 694 (1952)
- [bagu77] P.S. Bagus and U. Wahlgren, Molecular Phys. **33**, 641 (1977)
- [baus84] C.W. Bauschlicher, Jr. and P.S. Bagus, J. Chem. Phys. **81**, 5889 (1984)
- [blum61] M. Blume, Phys. Rev. **124**, 96 (1961)
- [burl88] P. Bulet, C. Vettier, M.J.G.M. Jurgens, J.Y. Henry, J. Rossat-Mignod, H. Noel, M. Potel, P. Gougeon and J.C. Levet, Physica C 153-155, 1115 (1988)
- [cava87] R.J. Cava, A. Santoro, D.W. Johnson, Jr. , and W.W. Rhodes, Phys. Rev. B **35**, 6716 (1987)
- [chak90] S. Chakravaty, in *High Temperature Superconductivity*, edited by K.S. Bedell, D. Coffey, D.E. Meltzer, D. Pines and J.R. Schriffer, Addison-Wesley, 1990, p136

- [chan94] Hyunju Chang, J.F. Harrison, T.A. Kaplan and S.D. Mahanti, *Phys. Rev. B* **49**, 15753 (1994)
- [chan91] Hyunju Chang, T. A. Kaplan, S. D. Mahanti and J. F. Harrison, *Bill. A. Phys. Soc.* **37** (1991)
- [coll72] M.F. Collins and V. K. Tondon *Canadian J. of Phys.* **50**, 2991 (1972)
- [colu88] COLUMBUS, R. Shepard, I. Shavitt, R. M. Pitzer, D. C. Comeau, M. Pepper, P. G. Szalay, R. Alrichs, F. B. Brown and J. G. Zhao, *Int'l Jrl. Quantum Chemistry*, S22, 149-165 (1988)
- [elli68] D. E. Ellis, A. J. Freeman and P. Ros, *Phys. Rev.* **176**, 688 (1968)
- [evje67] J. C. Slater, *Insulators, Semiconductors and Metals*, McGraw-Hill, New York, pp 215-220 (1967)
- [fend68] B.E.F. Fender, A.J. Jacobson and F.A. Wedgwood *J. Chem. Phys.* **48**, 990 (1968). , Private communication with Professor A. J. Jacobson to get correction to the expression of $\left(\frac{F_{111}}{F_{222}}\right)^2$.
- [ferg64] J. Ferguson, H.J. Guggenheim, and D. L. Wood *J. Chem. Phys.* **40**, 822 (1964).
- [frel88] T. Freltoft, G. Shirane, S. Mitsuda, J.P. Remeika, and A.S.Cooper, *Phys. Rev. B* **37**, 137 (1988)
- [g92] *Gaussian 92/DFT*, Revision F.3, M. J. Frisch, G. W. Trucks, H. B. Schlegel, P. M. W. Gill, B. G. Johnson, M. W. Wong, J. B. Foresman, M. A. Robb, M. Head-Gordon, E. S. Replogle, R. Gomperts, J. L. Andres, K. Raghavachari, J. S. Binkley, C. Gonzalez, R. L. Martin,

- D. J. Fox, D. J. Defrees, J. Baker, J. J. P. Stewart, and J. A. Pople, Gaussian, Inc., Pittsburgh PA, 1993.
- [gros89] M. Gross, E. Sanchez-Velasco and E. Siggia Phys. Rev. B **39**, 2484 (1989)
- [hay77] P.J. Hay, J. Chem. Phys. **66**, 4377 (1977)
- [hira74] K. Hirakawa and H. Ikeda, Phys. Rev. Lett. **33**, 374 (1974)
- [hubb65] J. Hubbard and W. Marshall, Proc. Phys. Soc. **86**, 561 (1965) ; W. Marshall and S. W. Lovesey, Theory of Thermal Neutron Scattering (Oxford Univ. Press, London, 1971).
- [huch70] M.T. Hutchings and H.J. Guggenheim, J.Phys. C **3**, 1303 (1970)
- [huzi71] S. Huzinaga, *Approximate Atomic Functions. Research Report* ; Division of Theoretical Chemistry, The Univ. of Alberta (1971)
- [hybe90] M. S. Hybertson, E. B. Stechel, M. Schluter, and D. R. Jennison, Phys. Rev. B **41**, 11068 (1990).
- [jans88] G.J.M. Janssen and W. C. Nieuwpoort , Phys. Rev. B **38**, 3449 (1988)
- [jans88a] G.J.M. Janssen and W. C. Nieuwpoort, Quantum Chemistry Symposium bf 22, p679 *Int. Journal of Quantum Chemistry* (1988)
- [jurg89] M.J. Jurgens, P. Burlet, C. Vettier, L.P. Regnault, J.Y. Henry, J. Rossat-Mignod, H. Noel, M. Potel, P. Gougeon and J.C. Levet, Physica B **156 & 157**, 846 (1989),
- [kapl91] T. A. Kaplan and S. D. Mahanti, J. Appl. Phys. **69**, 5382 (1991).

- [kapl92] T.A. Kaplan, S.D. Mahanti, Hyunju Chang, Phys. Rev. B **45**, 2565(1992)
- [kapl94] T.A. Kaplan, Hyunju Chang, S.D. Mahanti and J.F. Harrison, to appear in *Fundamental Materials Sciences : I*, Series Editor M.F. Thorpe, **Electronic Properties of Solids using Cluster Methods**, Edited by T.A. Kaplan and S.D. Mahanti, Plenum Press, New York, 1994
- [keim92] B. Keimer, A. Aharony, A. Auerbach, B.J. Birgeneau, A. Cassanho, Y. Endoh, R.W. Erwin, M.A. Kastner and G. Shirane, Phys. Rev. B **45**, 7430 (1992)
- [khan81] D.C. Khan, S.M. Kirtane, and K. Sharma, Phys. Rev. B **23**, 2697 (1981)
- [kitt63] C. Kittel *Quantum Theory of Solids*, John Wiley & Sons, (1963)
- [land89] G. H. Lander, P.J. Brown, J. Spalek and J. M. Honig Phys. Rev. B **40**, 4463 (1989).
- [levi91] I.N. Levine, *Quantum Chemistry*, 4th ed. ,Prentice Hall, (1991)
- [lowe78] J. P. Lowe, *Quantum Chemistry*, Academic Press, (1978)
- [maha93] S.D. Mahanti, T.A. Kaplan, Hyunju Chang, J.F.Harrison, J. Appl. Phys. **73**, (10) 6105 (1993)
- [mart67] D. H. Martin *Magnetism in Solids*, London Iliffe Books Ltd. (1967)
- [mart91] R.L. Martin, *Cluster Models for Surface and Bulk Phenomena*, NATO ASI Series, G. Pacchioni and P.S. Bagus eds. (1991)

- [mart93] R.L. Martin and P.J. Hay, J. Chem. Phys. **98**, 8680 (1993).
- [mart] R.L. Martin, private communication
- [matt65] D. C. Mattis *The Theory of Magnetism* Happer & Row Publishers, (1965)
- [mcwe89] R. McWeeny *Methods of molecular quantum mechanics* 2nd Ed. Academic Press, (1989)
- [mosk70] J. W. Moskodwitz, C. Hollister, C. J. Hornback and H. Basch, J. Chem. Phys. **53**, 2570 (1970).
- [naka95] K. Nakajima, K. Yamada, S. Hosoya, Y. Endoh, M. Greven, and R.J. Birgeneau, Z. Phys. B **96**, 479 (1995).
- [newm59] R. Newman and R. M. Chrenko, Phys. Rev. **114**, 1507 (1959).
- [noel82] J.O. Noell, Inorg. Chem. **21**, 11 (1982)
- [pick89] W. E. Pickett Rev. of Mod. Phys. **61**, 433 (1989).
- [rege88] J. D. Reger and A. P. Young, Phys. Rev. B **37**, 5978 (1988)
- [rebe89] L. Rebelsky, J.M. Tranquada, G. Shirane, Y. Nakazawa and M. Ishikawa, Physica C **160**, 197 (1989)
- [sabe80] N. H. Sabelli, L. R. Kahn and R. Benedek J. Chem. Phys. **73**, 6259 (1980). Their Ni²⁺ 2 ECP is spin dependent. In our form factor calculation, we tested both high and low spin ECP and the result turned out same. Thus we used high spin Ni²⁺ ECP here.

- [Saho90] N. Sahoo, Sigrid Markert, T.P. Das, and K. Nagamine, Phys. Rev. B **41**, 220 (1990)
- [scat61] V. Scatturin, L. Corliss, N. Elliot and J. Hastings Acta Cryst. **14**, 19 (1961)
- [sham93] S. Shamoto, M. Sato, J.M. Tranquada, B.J. Sternlieb, and G. Shirane, Phys. Rev. B **48**, 13817 (1993)
- [shar76] J.K. Sharma and D.C. Khan, Phys. Rev. B **14**, 4184 (1976)
- [shep88] R. Shepard, I. Shavitt, R. M. Pitzer, D. C. Comeau, M. Pepper, P. G. Szalay, R. Alrichs, F. B. Brown and J. G. Zhao, Int'l Jrl. Quantum Chemistry, S22, 149-165 (1988)
- [soul71] T.F. Soules, J. W. Richardson and D. M. Vaught, Phys. Rev. B **3**, 2186 (1971).
- [sous93] C. Sousa, J. Casanovas, J. Rubio, and F. Illas, J. Computational Chem. **14**, 680 (1993)
- [sula90] S.B. Sulaiman, N. Sahoo, T.P. Das, O. Donzelli, E. Torikai, and K. Nagamine, Phys. Rev. B **44**, 7028 (1991)
- [taka77] M. Takahashi, J. Phys. C: Solid State Phys., **10**, 1289 (1977)
- [towl94] M.D. Towler, N.L. Allan, N.M. Harrison, V.R. Saunders, W.C. Mackrodt and E. Aprà, Phys. Rev. B **50**, 5041 (1994).
- [tran88B] J.M. Tranquada, A.H. Moudden, A.I. Goldman, P. Zolliker, D.E. Cox, G. Shirane, S.K. Sinha, D. Vaknin, D.C. Johnston, M.S. Al-

- varez, A.J. Jacobson, J.T. Lewandowski and J.M. Newsman, Phys. Rev. B **38**, 2477 (1988),
- [tran88L] J.M. Tranquada, D.E. Cox, W. Kunnmann, H. Moudden, G. Shirane, M. Suenaga, P. Zolliker, D. Vaknin, S.K. Sinha, M.S. Alvarez, A.J. Jacobson, D.C. Johnston, Phys. Rev. Lett. **60**, 156 (1988)
- [tran89] J.M. Tranquada and G. Shirane, Physica C 162-164, 849(1989)
- [vakn87] D. Vaknin, S.K. Sinha, D.E. Moncton, D.C. Johnston, J.M. Newsam, C.R. Safinya, and H.E. King, Jr., Phys. Rev. Lett. **58**, 2802 (1987)
- [vakn90] D. Vaknin, S. K. Shiha, C. Stassis, L. L. Miller, and D. C. Johnston, Phys. Rev. B **41**, 1926 (1990).
- [wach70] A. J. H. Wachters, J. Chem. Phys. **52**, 1033 (1970)
- [wach72] A. J. Wachters and W. C. Nieuwpoort , Phys. Rev. B **5**, 4291 (1972)
- [wadt85] W. R. Wadt and P. J. Hay, J. Chem. Phys. **82**, p270, p284, and p299 (1985)
- [wang90] X. L. Wang, L. L. Miller, J. Ye, C. Stassis, B. N. Harmon, D. C. Johnston, A. J. Schultz and C.-K. Loong, J. Appl. Phys. **67**, 4524 (1990).
- [wang91] Xun-Li Wang, C. Stassis, D.C. Johnston, T.C. Leung, J. Ye, B.N. Harmon, G.H. Lander, A.J. Schultz, C.-K. Loong and J.M. Honig, J. Appl. Phys. **69**, 4860 (1991).

- [wang92] Xun-Li Wang, C. Stassis, D.C. Johnston, T.C. Leung, J. Ye, B.N. Harmon, G.H. Lander, A.J. Schultz, C.-K. Loong and J.M. Honig, *Phys, Rev. B* **45**, 5645 (1992)
- [yama87] K. Yamada, E. Kudo, Y. Endoh, Y. Hidaka, M. Oda, M. Suzuki and T. Murakami, *Solid State Comm.* **64**, 753 (1987)
- [yang87] B.X. Yang, Setsuo Mitsuda, Gen Shirane, Yasuo Yamaguchi, Hiroshi Yamauchi and Yasuhiko Syono, *J. of Phys. Soc. Japan* **56**, 2283 (1987)

MICHIGAN STATE UNIV. LIBRARIES



31293014103109